N 70 33737
CR 66981

NASA Grant NRG 34-002-073

FINAL REPORT:

THE PIEZORESISTIVE EFFECT IN ELECTRON IRRADIATED SILICON AND ITS APPLICATION TO THE IMPROVEMENT OF SEMICONDUCTOR STRAIN GAGES

June 1, 1970

CASE FILE
COPY

DEPARTMENT OF ELECTRICAL ENGINEERING
NORTH CAROLINA STATE UNIVERSITY
RALEIGH, NORTH CAROLINA

SDL-15-NRG 34-002-073

NASA Grant NRG 34-002-073

FINAL REPORT:

THE PIEZORESISTIVE EFFECT IN ELECTRON IRRADIATED SILICON AND ITS APPLICATION TO THE IMPROVEMENT OF SEMICONDUCTOR STRAIN GAGES

June 1, 1970

by

C. D. Loggins Jr.

M. A. Littlejohn

Semiconductor Device Laboratory
Department of Electrical Engineering
North Carolina State University
at
Raleigh, North Carolina

TABLE OF CONTENTS

TABLE OF CONTENTS (continued)

LIST OF TABLES

LIST OF FIGURES

LIST OF FIGURES (continued)

LIST OF FIGURES (continued)

1. INTRODUCTION

The application of mechanical stress to silicon changes its resistivity. This phenomenon is called piezoresistivity. The amount by which the resistivity is changed is influenced first of all by the type of stress, the magnitude of the stress, and the orientation of the stress relative to the crystal lattice axes of the silicon sample. The temperature of the silicon and the numbers and types of defect states in its forbidden energy band are other parameters whose values directly affect this stress-induced resistivity change.

Piezoresistivity, as manifested by silicon, is a tensor prpperty. However, this thesis will not be concerned with the tensor aspect of piezoresistivity. Here piezoresistivity will be defined as that scalar quantity which is equal to the fractional change in resistivity due to an applied stress divided by that applied stress. Piezoresistivity is largest in silicon for stresses applied in a $<100>$ lattice direction, that is for a stress applied parallel to one of the crystal lattice axes. Silicon's gage factor, which is proportional to the piezoresistivity, is nearly two orders of magnitude larger for this orientation than that of a metal, since for a metal the gage factor is due only to a change in the geometry of the sample with stress.

Due to its large gage factor, silicon is frequently used as a material in the fabrication of strain transducers. However, the resistivity and gage factor of presently available silicon are highly temperature dependent making silicon transducers unsuitable for many

applications. All past efforts to significantly improve these undesirable characteristics have failed. Experimental results indicate that in extrinsic silicon it is impossible to simultaneously minimize the temperature variations of both quantities and retain a large gage factor.

Recent studies of silicon strain gages which have been irradiated with high-energy electrons have shown a substantial improvement in the temperature characteristics of the gages. This work has revealed that the variation of resistivity with temperature is reduced by irradiation in p-type silicon gages, and that in n-type gages the temperature variation of both the resistivity and the gage factor are reduced. The improvement in the thermal characteristics of the gages was accompanied by only a small decrease in the magnitude of the gage factor.

The effect of the irradiation on the gages is understood in a qualitative sense. It is known that the irradiation produces an acceptor level in the band gap of the silicon and that this level can greatly influence the majority carrier concentration. This level, which is usually called the A-center, makes the number of conduction band electrons in n-type silicon significantly increase with temperature for temperatures near 300°K. This offsets somewhat the increase in resistivity due to the inherent decrease of electron mobility with temperature.

However, these reported results do not fit any of the existing models for piezoresistivity. In fact, some results of measurements on unirradiated silicon are not in agreement with the present theories.

In general these models for piezoresistivity predict a linear dependence on strain and a monotonic decrease with increasing temperature. Piezoresistivity in irradiated silicon exhibits a more complex behavior than this. For example, for certain orientations of irradiated silicon the piezoresistivity exhibits a maximum as the temperature is increased. For other orientations the piezoresistivity has been observed to change from a positive to a negative quantity at approximately $0^{\circ}F$. Likewise for unirradiated silicon the existing theories for piezoresistivity neglect the contributions due to relaxation time changes with stress, and thus underestimate the piezoresistivity. Departures from linearity with strain and inverse temperature have been observed in unirradiated silicon.

A need for a thorough study of piezoresistivity in electron-irradiated silicon is apparent and it is to such a study that this thesis is addressed. This study includes an experimental phase in which data is obtained on n-type irradiated silicon as well as a theoretical phase in which a mathematical model is developed that fits the experimental results. The goal of this research is a better understanding of the influence that defect states and relaxation times have on the piezoresistivity of semiconductors.

2. LITERATURE REVIEW

The study of piezoresistive phenomena in silicon and germanium has yielded rich rewards in terms of knowledge of their energy band structures and transport properties. Such studies were initiated by Smith (1954), who used uniaxial extension to determine the piezoresistance coefficients of silicon and germanium. The results of his measurements, which were made at room temperature on silicon and germanium rods of several orientations, showed that n-type silicon rods oriented parallel to one of the crystal lattice's <100> axes exhibited an exceptionally large piezoresistivity. For germanium the piezoresistivity of rods oriented parallel to the <110> lattice direction was larger than that for germanium rods of other orientations. This anisotropy in piezoresistivity observed by Smith did not agree with a simple one-valley conduction band model, leading him to suspect that the conduction bands of silicon and germanium were more complex than this classical picture.

Smith's results were, in fact, in agreement with a theory later developed by Herring (1955) in which transport in a semiconductor with a simple many-valley conduction band was studied. Herring's theory predicted a piezoresistivity which was linear with strain and inverse temperature, and enunciated the two first order effects contributing to piezoresistivity in a many-valley semiconductor. These two first order effects are the population transfer effect, and the change in relaxation time due to the effect of stress on intervalley scattering. Population transfer with stress forms the basis for all the published models of piezoresistivity. However, the effect of stress on

intervalley scattering is not included in these models. The influence on piezoresistivity of defect states in the forbidden energy band gap near the Fermi energy is also omitted in the earliest theories of piezoresistivity. From Smith's data and a study of magnetoresistivity Herring deduced that silicon was a many-valley semiconductor with valleys situated on the six $<100>$ lattice axes.

Useful formulas for the piezoresistivity of silicon and germanium were first published by Herring and Vogt (1956). These likewise predicted a piezoresistivity linear with strain and inverse temperature. Also discussed for the first time was the important concept of a tensor relaxation time. The limitation of Herring's and Vogt's formulation for piezoresistivity, which was made for the limit of zero strain, is that it underestimates the magnitude of piezoresistivity due to a neglect of the effect of stress on intervalley scattering.

In order to obtain deformation potential constants for use in mobility theory, Morin et al. (1957) studied piezoresistivity in n-type and p-type silicon and germanium. Using compressive uniaxial stresses on the order of 5×10^7 dynes/cm^2, data was obtained on silicon samples for the temperature range 20°K-350°K. A departure of the piezoresistivity of silicon from the predicted $1/T$ variation was observed and discussed by the authors. They concluded that this departure was due to the effect of stress on intervalley scattering. One arsenic-doped germanium sample studied by Morin et al. had a piezoresistivity which decreased anomalously at low temperatures. The authors were unable to explain this unexpected behavior.

However, Fritzsche (1959) was able to explain the anomalous behavior of arsenic-doped germanium. He attributed this behavior to the detailed splitting with strain of the lowest donor state of arsenic. Fritzsche thus recognized that defect states in the band gap of a semiconductor can have a great influence on piezoresistivity. Defect state influence was included in his model for the piezoresistivity of germanium, which he formulated to higher orders in strain than was done in the earlier theories. Although he studied germanium while this thesis will be concerned with silicon, a conclusion can be drawn from Fritzsche's work which is relevant to the present study. The conclusion is that detailed knowledge of the splitting of electrically active states near the Fermi level is necessary in order to predict piezoresistivity.

Much of the literature on piezoresistivity in silicon and germanium has been reviewed and the important results summarized and tabulated by Cresswell and Muss (1967). Also to be found in this publication are the mathematical tools needed to calculate piezoresistivity for a general lattice direction in a many-valley semiconductor like silicon and germanium.

Piezoresistivity measurements made on electron-irradiated silicon have recently been reported by Gross (1967). Gross found that the piezoresistivity for the irradiated samples he studied behaved in a manner totally different from that of unirradiated samples. The classical 1/T variation of piezoresistivity was not observed. Instead, some of the samples exhibited a piezoresistivity having a parabolic-like temperature dependence. This unusual behavior points

out the inadequacy of existing formulations for the piezoresistivity of silicon and calls for a more general theoretical treatment of this phenomenon.

3. CONDUCTION BAND ELECTRON CONCENTRATION

3.1 Introduction

The electrical conductivity of an n-type silicon sample is affected by an applied stress through both a stress-induced change in the number of electrons in a particular conduction band minimum (i.e. population transfer), and a stress-induced change in the relaxation times of a conduction electron due to the effect of stress on inter-valley scattering. The latter of these two effects is discussed in chapter 4, while the former is analyzed in this chapter.

This chapter will first of all deal with the effect of stress on the conduction band energies of the six conduction band minima of silicon. This is followed by a discussion of the phosphorus donor energy level in silicon. Irradiation-produced defects are then described, and the stress-induced splitting of the energy levels of these defects is evaluated. Finally, equations are developed which may be solved to yield the values of the Fermi energy in both the stressed and unstressed situations, assuming that the various impurity concentrations and their energy levels are known. The effect of stress on the concentration of electrons in each individual conduction band minimum may be determined once these Fermi energies are known.

3.2 Effect of Uniaxial Stress on the Conduction Band Minima of Silicon

The application of a uniaxial stress to a crystal changes the interatomic spacing of the constituent atoms of the crystal. In silicon the cubic symmetry of its unit cell is removed by all except $\langle 111 \rangle$ stresses. Due to this loss of symmetry, each of the six

conduction band minima, all of which have the same energy E_{c_o} in the absence of stress, shift in energy. These energy shifts can be calculated using the results of Herring's and Vogt's (1956) deformation potential theory for many-valley semiconductors. According to Herring and Vogt, the shift ΔE_i in the energy of the i^{th} conduction band minimum is equal to

$$\Delta E_i = E_{c_i} - E_{c_o} = \sum_{j=1}^{6} \Xi_j^{(i)} e_j , \tag{3.1}$$

where E_{c_i} is the stressed conduction band energy. The $\Xi_j^{(i)}$ ($j = 1$ to 6) are deformation potential constants. The e_j are strain components, referred to the crystallographic axes and indexed in the usual manner (see Appendix 10.1). Due to symmetry restrictions on the $\Xi_j^{(i)}$, for silicon it is found that all the $\Xi_j^{(i)}$ can be expressed in terms of two constants Ξ_d, and Ξ_u. The shifts of the six conduction band minima of silicon, in terms of these two constants, have the values (see Kanda (1967))

$$\Delta E([100], [\bar{1}00]) = \Delta E_1 = \Xi_d e + \Xi_u e_1 \tag{3.2a}$$

$$\Delta E([010], [0\bar{1}0]) = \Delta E_2 = \Xi_d e + \Xi_u e_2 \tag{3.2b}$$

$$\Delta E([001], [00\bar{1}]) = \Delta E_3 = \Xi_d e + \Xi_u e_3 \tag{3.2c}$$

where $e = e_1 + e_2 + e_3$ = hydrostatic strain. The quantities in parentheses ([100], [010], etc.) identify the location of the minima in $\vec{k}$-space.

Wortman (1964) has shown that these equations are not completely general in that an additional term must be added to equations 3.2 when the strain has shear components. For the stress levels used in this thesis, the shear strains are always less than 0.2 percent. The error resulting from using equations 3.2 to calculate the conduction band shifts for shear strains of this magnitude is less than 4 percent, and is probably smaller than the error due to the uncertainty in the knowledge of the values of the deformation potentials Ξ_d and Ξ_u. For this reason, the effect of shear components of strain on the ΔE_i will be neglected.

Because this thesis is concerned with the piezoresistivity of relatively low resistivity n-type silicon, all the conductivity will be assumed to be due to extrinsic conduction band electrons and the effect of valence band holes and intrinsic electrons on the conductivity will be neglected. It will be further assumed that the shifts in the energies of the impurities in the forbidden energy band gap (such as the phosphorus donors, the A-center acceptors, and the E-center acceptors) due to the hydrostatic strain ($e = e_1 + e_2 + e_3$) are the same as the shift in energy of the conduction band minima due to the hydrostatic strain. Thus it will be assumed that an energy level (e.g. conduction band energy) is merely split by stress and that there is no relative energy shift between the conduction band and the impurities in the forbidden energy band gap due to the hydrostatic strain. Since only energy differences are involved in calculating the concentration of electrons in the conduction band, the concentration of ionized donors, and the concentration of ionized acceptors, the

zero energy reference is arbitrary and will be taken as the zero-stress energy of the conduction band edge. That is, the zero energy reference is

$$E_{c_o} = 0 \ .$$

In light of the above assumptions, equations 3.2 may be rewritten as

$$\Delta E_1 = \Xi_u e_1 \tag{3.3a}$$

$$\Delta E_2 = \Xi_u e_2 \tag{3.3b}$$

$$\Delta E_3 = \Xi_u e_3 \ . \tag{3.3c}$$

Thus the term $\Xi_d e$ is eliminated. It is fortunate that this term is eliminated because Ξ_d is difficult to determine from experimental measurements and subsequently its value is not accurately known. On the other hand, the value of Ξ_u is fairly well established. In Table 3.1 are listed some of the values for Ξ_u and Ξ_d which have been reported in the literature. The value of Ξ_u measured by Balslev (1966) will be used in this thesis. As can be seen in Table 3.1, Balslev found that Ξ_u seemed to increase with temperature. Because of this, Ξ_u will be assumed to have a small temperature dependence. The following function,

$$\Xi_u = 8.6\text{eV} + (0.00286\text{eV}/^{o}\text{K})\,(T - 80^{o}\text{K}) \tag{3.4}$$

Table 3.1 Deformation potential coefficients for the conduction band of silicon in eV/unit dilation

Ξ_u (eV)	Ξ_d (eV)	Temperature (of Measurement)	Method of Determination
8.6±0.2[a]	-	80°K	Optical absorption edge measurements
9.2±0.3[a]	-	295°K	Optical absorption edge measurements
7.7[b]	-	< 100°K	Piezoresistance
8.3±0.3[c]	-	77°K	Piezoresistance
9.57[d]	-4.99[d]	-	Band calculations
8.5±0.1[e]	-5.2±0.3[e]	~5°K	Cyclotron resonance line width

[a] Balslev (1966).

[b] Morin et al. (1957).

[c] Aubrey et al. (1963).

[d] Kleinman (1962).

[e] Ito et al. (1964).

which is a straight line through Balslev's values for Ξ_u, will be used in all calculations of conduction band energy shifts in the work to follow.

The strain components e_i in equations 3.3 are related to the stress six vector σ_j by the tensor of the compliance coefficients of the crystal s_{ij} through the following tensor equation

$$e_i = s_{ij}\sigma_j \ . \tag{3.5}$$

Hall (1967) has shown that these constants are approximately constant over the temperature range of interest in this thesis and the s_{ij} will therefore be assumed to be independent of temperature.

In Appendix 10.1 the ΔE_i for < 100 >, < 110 >, and < 111 > type compressive stresses are calculated using equations 3.3 and 3.5. The results are tabulated in Table 3.2.

Table 3.2 Energy shifts of the conduction band edges in eV for < 100 >, < 110 >, and < 111 > compressive uniaxial stresses χ[a]

Energy Shift	< 100 >	< 110 >	< 111 >
ΔE_1	$-0.768\times10^{-12}\ \Xi_u\ \chi$	$-0.277\times10^{-12}\ \Xi_u\ \chi$	0
ΔE_2	$+0.214\times10^{-12}\ \Xi_u\ \chi$	$-0.277\times10^{-12}\ \Xi_u\ \chi$	0
ΔE_3	$+0.214\times10^{-12}\ \Xi_u\ \chi$	$+0.214\times10^{-12}\ \Xi_u\ \chi$	0

[a] In this table χ is expressed in dyne/cm^2 and is negative for compression.

3.3 The Phosphorus Donor in Silicon

All the samples studied in the experimental phase of the research comprising this thesis were phosphorus-doped, n-type silicon samples. Phosphorus has a donor level in silicon approximately 0.044 eV below the conduction band edge. This donor level is actually a multiplet, as Long and Myers (1959) have verified. The multiplet consists of two states (per phosphorus atom, including spin) at an energy approximately 0.0435 eV below the conduction band edge, and ten states at an energy 0.0335 eV below the conduction band edge. This multiplet is further split by an applied stress. The analysis of the stress-induced splitting of the phosphorus donor energy level may be performed with the method Price (1956) used to calculate the effect of stress on the donor energy levels in germanium.

However, it is found that no significant deionization of the phosphorus donors occurs in any of the samples studied for any experimental temperature or stress. This lack of donor deionization is due to

(a) relatively low donor densities and high sample temperatures ($250^{\circ}K$ - $360^{\circ}K$),

and

(b) the effect of electron-irradiation produced defects on the Fermi energy.

Since virtually all the donors are ionized for all the experimental temperatures and stresses obtained, the following equation

$$N_D^+ = N_D \tag{3.6}$$

will be used for the concentration of ionized donors throughout this thesis, where N_D^+ is the concentration of ionized donors, and N_D is the total donor concentration.

3.4 Effect of Stress on Electron-Irradiation Produced Defects

3.4.1 Introduction

Electron-irradiation produces a variety of defects in silicon. Fortunately some of these defects may be removed by annealing. Only two types of electron-irradiation produced defects, the Si-A center and the Si-E center, will be assumed to have an influence on the concentration of conduction band electrons for the samples studied in this thesis.

3.4.2 The Si-E Center

The Si-E center (also known as the Si-G8 center) is a defect composed of a silicon vacancy associated with a substitutional phosphorus atom (see Figure 3.1). Watkins and Corbett (1964) verified this composition for the defect by observing the spin resonance spectrum of the electron in the bond of the unpaired silicon atom. This defect presents an acceptor-like energy state at the energy $E_E = -0.40$ eV, where the zero stress conduction band energy is used as the zero energy reference. This acceptor-like behavior apparently is due to the trapping of an additional electron in the bond of the unpaired silicon atom.

Now the Si-A center is the defect responsible for the effect that is investigated in this thesis. Therefore all irradiated

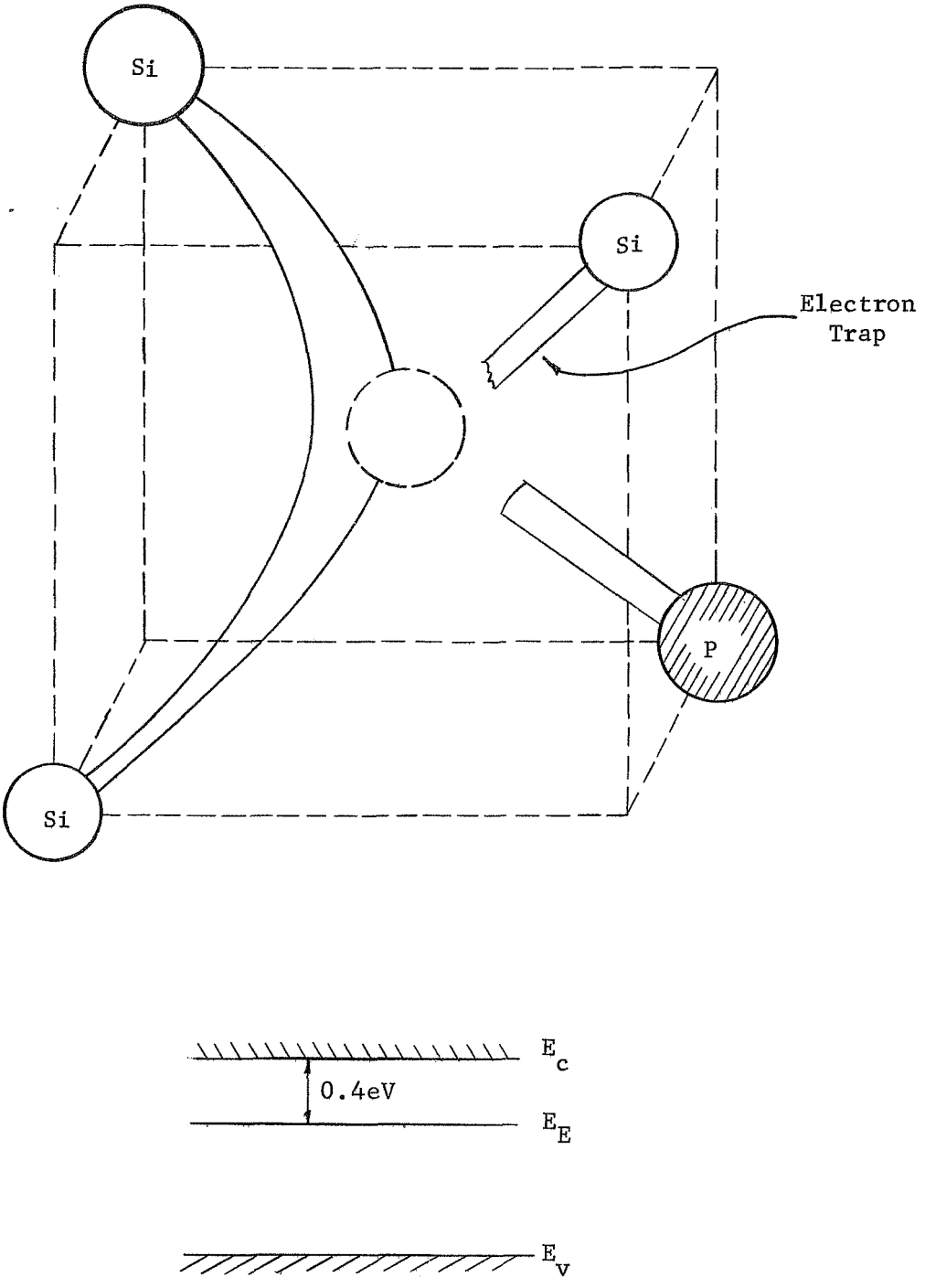

Figure 3.1 The silicon-E center

samples studied were subjected to an annealing process in an attempt to remove all irradiation-produced defects except the Si-A center. This can be conveniently done due to the fact the A-center has a higher annealing temperature than most of the other defects. For example the annealing temperature for the A-center is greater than 350°C while the E-center anneals out for temperatures greater than 125°C. Even after annealing however, the resistivity and Hall coefficient data obtained for some of these samples indicated the presence and influence of an additional defect. Due to its proximity in energy to the Si-A center, the Si-E center is the defect most likely to have an influence on the electrical properties of the samples studied here. For this reason, the additional influence indicated in the experimental data will be attributed to the presence of Si-E centers that were not removed by the annealing procedure.

It will be shown later that the concentration of Si-E centers in the samples studied here is small compared to the concentration of A-centers. It is also found that the Fermi energy in the samples studied is well removed from the acceptor-level of the Si-E center over the major part of the experimental temperature range. For these reasons the detailed splitting with stress of the Si-E center acceptor level will be assumed to have only a small and neglectable effect on the conduction band electron concentration. Thus stress-induced splitting of the Si-E center acceptor-level will be neglected in this thesis, and the following equation for the concentration of electrons on Si-E center acceptor levels

$$N_E^- = \frac{N_E}{1 + \exp((E_E - E_f)/kT)} \tag{3.7}$$

will be used in both the stressed and unstressed situations. In this equation E_f is the Fermi energy, and N_E is the concentration of Si-E center defects.

3.4.3 The Si-A Center

The Si-A center (which has been renamed the Si-B1 center) is a defect produced in pulled silicon when it is subjected to irradiation with high-energy (a few Mev) electrons. This particular defect has been extensively studied since its paramagnetic or electron spin resonance spectrum was first observed by Bemski *et al.* (1958). Around the same time, Wertheim (1957) and Hill (1959) discovered a defect with a net acceptor level 0.17 ev below the conduction band edge by means of electrical measurements made on electron-irradiated silicon. Watkins *et al.* (1959) later showed that this defect was the same one that Bemski *et al.* observed in spin resonance. This research, culminating in a thorough study of the spin resonance spectrum of the A-center by Watkins and Corbett (1961), has resulted in the positive identification of the composition of the defect as well as a model for the defect describing what happens to it in a sample subjected to an applied stress. This model, which Watkins and Corbett developed and verified by observing the effect of uniaxial stress on the spin resonance spectrum of the A-center, is essential to a theoretical description of the piezoresistivity of electron-irradiated silicon.

The composition of the A-center is that of a lattice vacancy associated with an impurity oxygen atom (see Figure 3.2). According to Watkins and Corbett, it is probably formed by the trapping of a mobile lattice vacancy by an interstitial oxygen atom. The lattice vacancies are produced by the electron-irradiation. The oxygen atom in this defect bridges two of the four broken bonds associated with the silicon vacancy. The remaining two bonds are shared by two silicon atoms as indicated in Figure 3.2. It turns out that an additional electron can be trapped in this bond shared by the two silicon atoms. This makes the A-center an acceptor-like defect.

An understanding of why the A-center acts as an acceptor may perhaps be achieved by a consideration of the energy levels presented by a diatomic molecule. Consider Figure 3.3. This figure shows the bonding and antibonding levels of a diatomic molecule as a function of the separation of the atoms (e.g. see Ballhausen and Gray (1964)). According to Watkins and Corbett the acceptor level due to the A-center is the antibonding level of the diatomic Si-Si molecule (Si_a-Si_b in Figure 3.2). The bond length between these two atoms is much longer than the normal Si-Si bond length. The overlap integral is thus smaller and the energy split between the bonding and antibonding states is thereby reduced. Effectively then, the increased length of the Si-Si bond in the A-center defect causes the antibonding state to move down in energy from the conduction band into the forbidden energy band gap. It is a stable level because it is lower in energy than the antibonding states of the normal Si-Si bond in the conduction band.

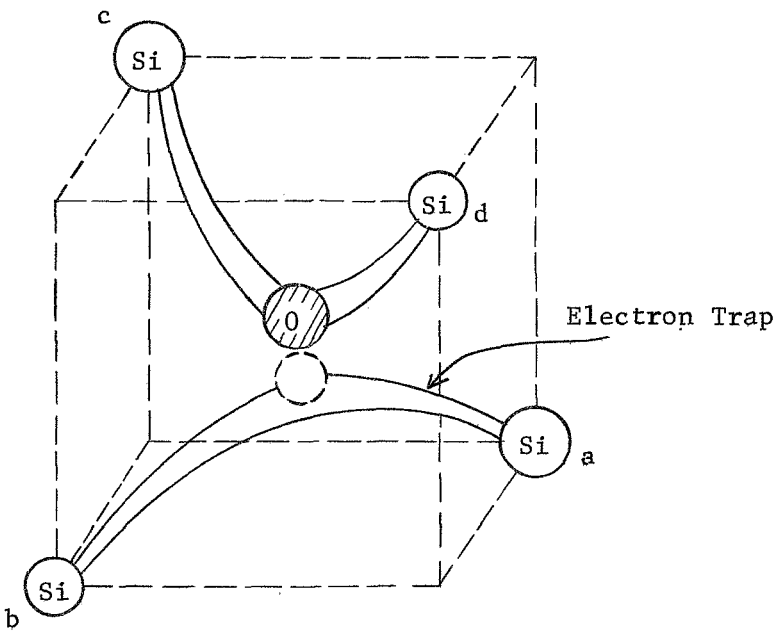

Figure 3.2 The silicon-A center

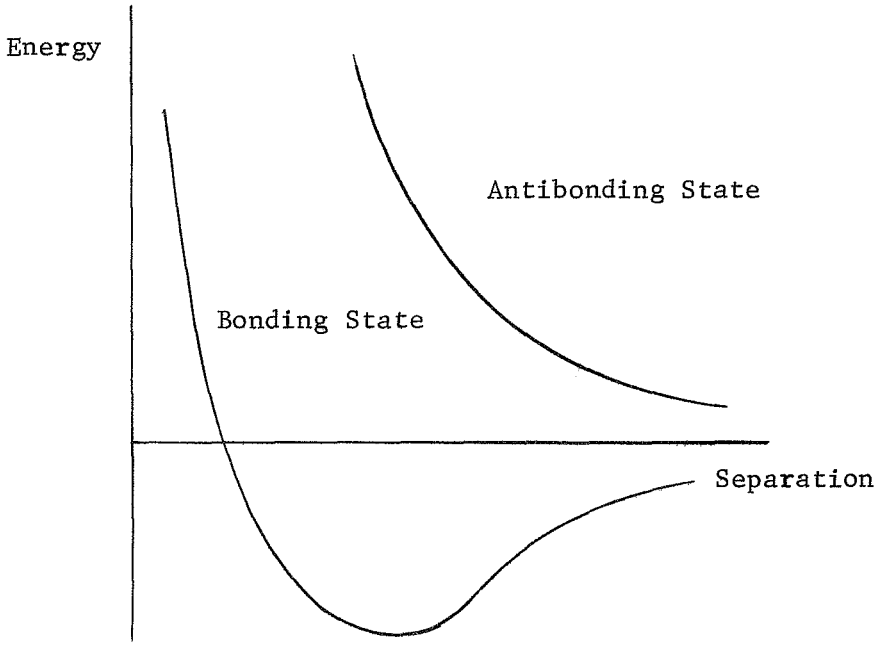

Figure 3.3 Energy of the bonding and antibonding states of a diatomic molecule versus interatomic separation

Again consider Figure 3.2. Labeling the four nearest neighbors of the oxygen-vacancy complex as a, b, c, and d, there are six possible bonding configurations which can be identified as:

ab, ac, ad, bc, bd, cd.

These pairs of letters refer to the configuration for which the electron trap is shared between the two silicon atoms designated by the given letters. For example, the configuration in Figure 3.2 is ab.

Now as might be expected, for a sample free of applied stress each of these six bonding configurations are equally probable and present the same electron trap energy. For a sample with N_A A-centers, in the absence of applied stress there are $N_A/6$ A-centers of each of the six geometrically distinguishable configurations. However when a stress is applied to the sample, certain orientations become preferred and the equi-probability of all six orientations no longer holds. The energy level of the electron trap also is split by the applied stress, into as many as three distinct levels.

Watkins and Corbett attribute this preferential reorientation of the defects with stress to the fact that there is a competition between the Si-O-Si bond and the Si-Si bonds as to which will align along the direction of the stress. Configurations having large components of strain along either the Si-Si or Si-O-Si bonds are more numerous in a stressed sample. The length of the Si-Si bond in the A-center, that is, the distance between the two silicon atoms sharing the electron trap, determines the energy of the electron trap of that

A-center. The trap energy is split by stress due to the fact that the Si-Si distance is different for the different configurations in a stressed sample. Bonding configurations for which the Si-Si bond is compressed by the stress have a higher electron trap energy (the acceptor energy level for this defect is nearer to the conduction band) than for the case of zero stress. Conversely, the electron trap energy of defects for which the Si-Si bond is lengthened by the stress is lowered (moves away from the conduction band).

Being unpaired, electrons trapped by A-centers may participate in paramagnetism and exhibit a spin resonance spectrum (see Watkins and Corbett (1961)). Because of an inherent anisotropy in the spectroscopic splitting factor for electrons belonging to the six different defect orientations, the spin resonance spectrum for the A-center contains lines at six different resonant frequencies, even for the case of zero applied stress. These lines have the same intensity or amplitude for the zero stress case because the intensity of a line is proportional to the number of electrons trapped by the particular orientation corresponding to that line, and in the absence of stress the orientations are equally populated. Evidently two pairs of these lines in the A-center spectrum have very nearly the same frequency since the zero stress spectrum given by Watkins and Corbett has only four lines (see Figure 3.4). The effect of stress on a particular orientation can be assessed by observing the effect of the stress on the intensity of the spectral line corresponding to that orientation.

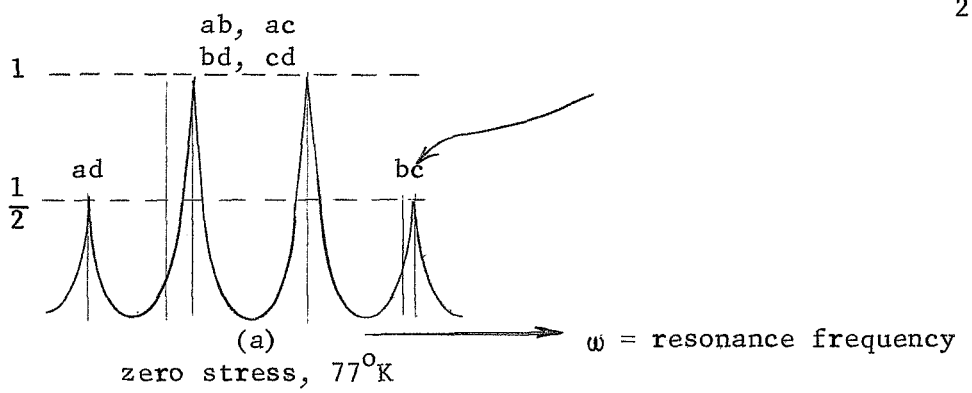

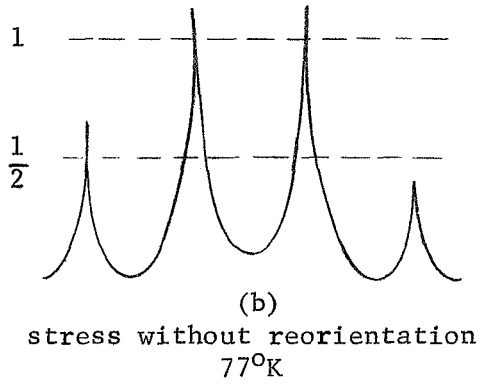

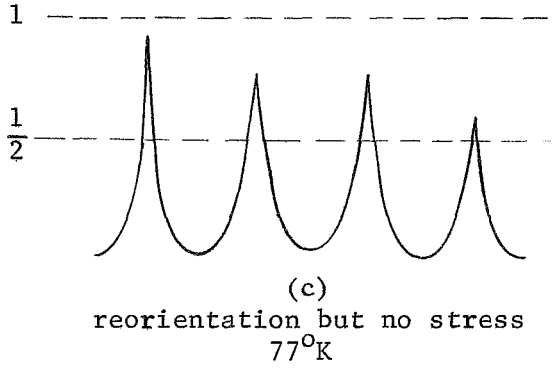

Figure 3.4 The effect of a <110> compressive stress on the A-center spin resonance spectrum

To obtain numerical values for the parameters associated with their model, Watkins and Corbett studied the change in the spin resonance spectrum of the A-center electrons with stress. Their samples were n-type silicon (phosphorus doped) with the A-center concentration at least ten times as great as the donor concentration. They then assumed that under stress the relative electron populations of the different configurations were given by a Boltzmann distribution. A-center reorientation and the splitting of the A-center energy level in a sample subjected to a < 110 > compressive stress is analyzed below using Watkins' and Corbett's model and results.

The parameters involved in Watkins' and Corbett's model are:

M^* = the change in the energy of the electron trap per unit strain along the Si-Si bond

M = the change in the energy of the Si-Si molecular bond per unit strain along this bond

N = the change in the energy of the Si-O-Si molecular bond per unit strain along this bond.

M^* determines the shift with stress of the electron trap energy. The competition between the Si-O-Si and Si-Si molecular bonds to align along the direction of the compressive stress determines the reorientation of the defects. Thus M and N determine the orientation stability of the defects.

Watkins and Corbett performed two types of experiments to obtain values for these three parameters. In one experiment the zero stress spin resonance spectrum of electrons trapped by A-centers was compared to the spectrum which resulted when stress was applied before stress-induced reorientation of the defects could occur (reorientation

takes an appreciable amount of time at low temperatures). In another experiment the zero stress spectrum was compared to the spectrum that resulted when only stress-induced reorientation was present. Watkins and Corbett performed this particular experiment in the following manner. They applied stress to a sample at 125°K and after allowing a sufficient time for the completion of stress-induced defect reorientation they quenched the sample to 77°K. They then removed the stress and observed the spin resonance spectrum before the defects had time to reorient (toward the zero-stress case). Thus the spectrum obtained reflected only the influence of stress-induced defect reorientation as all defects had the same electron trap energy (since the stress was zero there was no stress-induced splitting of the electron trap energy). The spectra that resulted from these experiments for the case of a < 110 > stress are shown in Figure 3.4.

The statistics for the A-center can be derived using the information provided by Watkins and Corbett. Consider the effect of a < 110 > stress on the reorientation of A-centers (Figure 3.5). In this figure n_{ad}, n_{bc}, etc. are the concentrations of electrons trapped on defects with ad, bc, etc. orientations without stress but with stress-induced reorientation. From Figure 3.5, it is seen that there are three groups of nonequivalent orientations and three distinct energy levels for a < 110 > stress. Divide the six orientations into groups:

group 1-----ad

group 2-----ab, ac, cd, and bd

group 3-----bc .

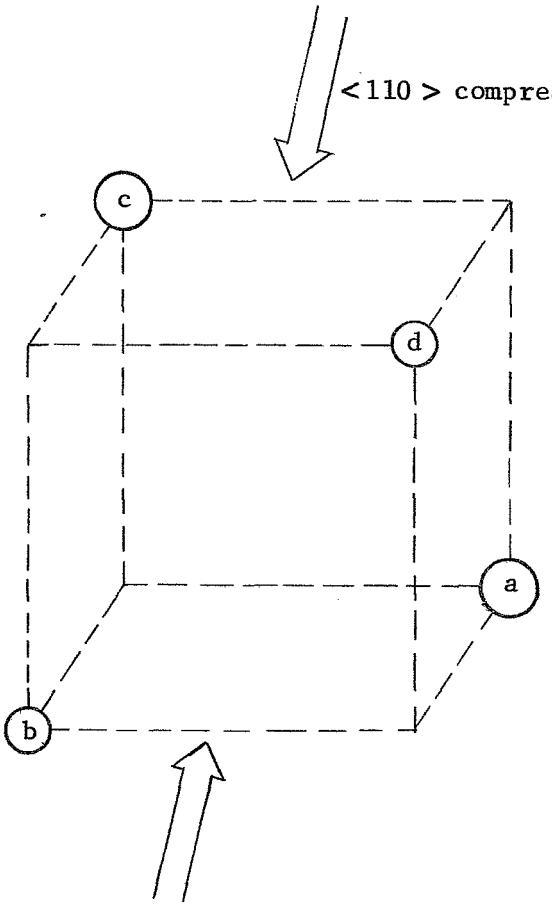

$$\frac{n_{ad}}{n_{bc}} = \exp(-T_\alpha/T)$$

$$\frac{n_{ad}}{n_{ab}} = \exp(-T_\beta/T)$$

$$n_{ab} = n_{ac} = n_{bd} = n_{cd}$$

$$KT_\alpha = (\epsilon_{ad} - \epsilon_{bc})(M - N)$$

$$KT_\beta = (\epsilon_{ad} - \epsilon_{ab})\, M + (\epsilon_{bc} - \epsilon_{ab})N$$

where ϵ_{ij} = strain along molecular bond between silicon atoms i and j

M = 16 eV/unit strain

N = 17.2 eV/unit strain

Figure 3.5 The reorientation of A-centers due to a <110> compressive stress

Call the energy level corresponding to the group 1 orientation E_1; the level correspondong to group 2 orientations E_2; and the level corresponding to the group 3 orientations E_3. For a compressive stress χ, these energy levels may be computed to be (see the paper by Watkins and Corbett):

$$E_1 = E_A + \Delta E_1 = E_A + (2.96\times10^{-13}\ \frac{eV(cm)^2}{dyne})\ \chi \qquad (3.8a)$$

$$E_2 = E_A + \Delta E_2 = E_A - (2.52\times10^{-13}\ \frac{eV(cm)^2}{dyne})\ \chi \qquad (3.8b)$$

$$E_3 = E_A + \Delta E_3 = E_A - (47.28\times10^{-13}\ \frac{eV(cm)^2}{dyne})\ \chi\ . \qquad (3.8c)$$

In these formulas χ is the stress expressed in dynes/cm^2 and is a negative quantity for compression. The quantity E_A is the zero stress energy of the A-center acceptor level and has the value $E_A = -0.17$ eV, where the zero stress conduction band energy is used as the zero energy reference.

Designate the concentration of electrons on group i type orientations without stress but with stress-induced reorientation as n_{io} (the o signifying zero stress). Then from Figure 3.5 and the discussion of Watkins' and Corbett's experiment to obtain the spin resonance spectrum without stress but with stress-induced defect reorientation, it follows that

$$\frac{n_{1o}}{n_{3o}} = \frac{N_1}{N_3} = \exp(-T_\alpha/T) = \begin{array}{l}\text{ratio of electrons trapped on}\\ \text{group 1 A-centers to electrons}\\ \text{trapped on group 3 centers}\\ \text{without stress but with stress-}\\ \text{induced reorientation}\end{array} \qquad (3.9)$$

and that

$$\frac{n_{1o}}{n_{2o}} = \frac{N_1}{N_2} = \frac{\exp(-T_\beta/T)}{4} \quad . \tag{3.10}$$

In equations 3.9 and 3.10 N_1, N_2, and N_3 are the concentrations of defects in groups 1, 2, and 3 respectively.

Now consider

$$\frac{n_i}{n_{io}} = \begin{array}{l}\text{ratio of the concentration of electrons on type i A-centers with stress and reorientation to the concentration on type i centers with reorientation only.}\end{array}$$

Assuming Fermi statistics this may be written as

$$\frac{n_i}{n_{io}} = \frac{\dfrac{N_i}{1 + 2\exp((E_i - E_f)/kT)}}{\dfrac{N_i}{1 + 2\exp((E_A - E_f)/kT)}} = \frac{1 + 2\exp((E_A - E_f)/kT)}{1 + 2\exp((E_i - E_f)/kT)} \tag{3.11}$$

where N_i is the concentration of group i orientations and E_f is the Fermi energy. The exponential term in this equation appears with a factor of two because an electron with either type of spin (spin up or spin down) may be trapped in the Si-Si bond of the A-center.

In equation 3.11 and the following equations the exponential term is greater than one. This is because these equations are formulated using Watkins' and Corbett's results, and their results were obtained on samples for which only approximately 10 percent of the A-centers had trapped an electron. Fermi statistics, rather than Boltzmann statistics, are used since although the quantity 1 is smaller than the

exponential term for this situation (i.e. only 10 percent ionization of the A-center) the quantity 1 is not completely negligible in comparison with the exponential term. Now

$$\frac{n_1}{n_3} = \left\{\frac{n_{1o}}{n_{3o}}\right\}\left\{\frac{n_1}{n_{1o}}\right\}\left\{\frac{n_{3o}}{n_3}\right\} \quad . \tag{3.12}$$

Using equations 3.9 and 3.11 this can be written

$$\frac{n_1}{n_3} = \exp(-T_\alpha/T)\left\{\frac{1+2\exp((E_A-E_f)/kT)}{1+2\exp((E_1-E_f)/kT)}\right\}\left\{\frac{1+2\exp((E_3-E_f)/kT)}{1+2\exp((E_A-E_f)/kT)}\right\} , \tag{3.13}$$

or finally

$$\frac{n_1}{n_3} = \exp(-T_\alpha/T)\left\{\frac{1+2\exp((E_3-E_f)/kT)}{1+2\exp((E_1-E_f)/kT)}\right\} . \tag{3.14}$$

Similarly

$$\frac{n_1}{n_2} = \frac{\exp(-T_\beta/T)}{4}\left\{\frac{1+2\exp((E_2-E_f)/kT)}{1+2\exp((E_1-E_f)/kT)}\right\} . \tag{3.15}$$

Let N_{iu} signify the concentration of unoccupied type i defects, and n_i the concentration of occupied type i defects. It follows from Fermi statistics that

$$\frac{n_i}{N_{iu}} = 2\exp((E_f - E_i)/kT) \quad . \tag{3.16}$$

Using this equation, equations 3.14, and 3.15, and the fact that

$$n_1 + N_{1u} + n_2 + N_{2u} + n_3 + N_{3u} = N_A \ , \tag{3.17}$$

where N_A is the total concentration of A-centers, it can be shown that

$$n_1 = \frac{N_1}{1 + 2\exp((E_1 - E_f)/kT)} \tag{3.18}$$

and that

$$n_2 = \frac{N_2}{1 + 2\exp((E_2 - E_f)/kT)} \tag{3.19}$$

$$n_3 = \frac{N_3}{1 + 2\exp((E_3 - E_f)/kT)} \quad , \tag{3.20}$$

where

$$N_1 = \frac{N_A}{1 + \eta + \zeta} \tag{3.21}$$

$$N_2 = \frac{\eta N_A}{1 + \eta + \zeta} \tag{3.22}$$

$$N_3 = \frac{\zeta N_A}{1 + \eta + \zeta} \tag{3.23}$$

and

$$\zeta = \exp(T_\alpha/T) \ , \tag{3.24}$$

$$\eta = 4\exp(T_\beta/T) \ . \tag{3.25}$$

The form of the equations for n_1, n_2, and n_3 indicates that the acceptor energy level of the Si-A center is split by an applied $< 110 >$ stress into three independent energy levels. These levels are independent in the sense that the number of trapped electrons at any one of these three energy levels, E_i, is dependent only on N_i and E_i and is independent of the occupation of the other two levels. This situation is different from the stress-induced splitting of the ground states of conventional substitutional type impurities, such as phosphorus. For the usual substitutional impurities, the donor (or acceptor) energy level splits with stress into two or more dependent levels (e.g. see Fritzsche (1959)).

In view of the above discussion, it is seen that equations 3.18, 3.19, and 3.20 would also apply in the situation in which an unstressed sample had three different acceptor energy levels due to three different types of acceptors. However, the acceptor concentrations N_1, N_2, and N_3 would be independent of stress and temperature for substitutional type impurities, whereas in a stressed sample containing A-center defects these concentrations are stress and temperature dependent as indicated in Figure 3.6.

In Figure 3.7 the effect of a $< 110 >$ compressive stress on the acceptor level of the A-center is illustrated. From part b of this figure it is seen that before preferential orientation the number of states at energy E_1 is $N_1^o = N_A/6$, the number at E_2 is $N_2^o = 4N_A/6$, and the number at E_3 is $N_3^o = N_A/6$, where N_A is the total A-center concentration. Reorientations increase the number of states at E_1 to N_1, decrease the number at E_2 to N_2, and increase the number at E_3 to N_3.

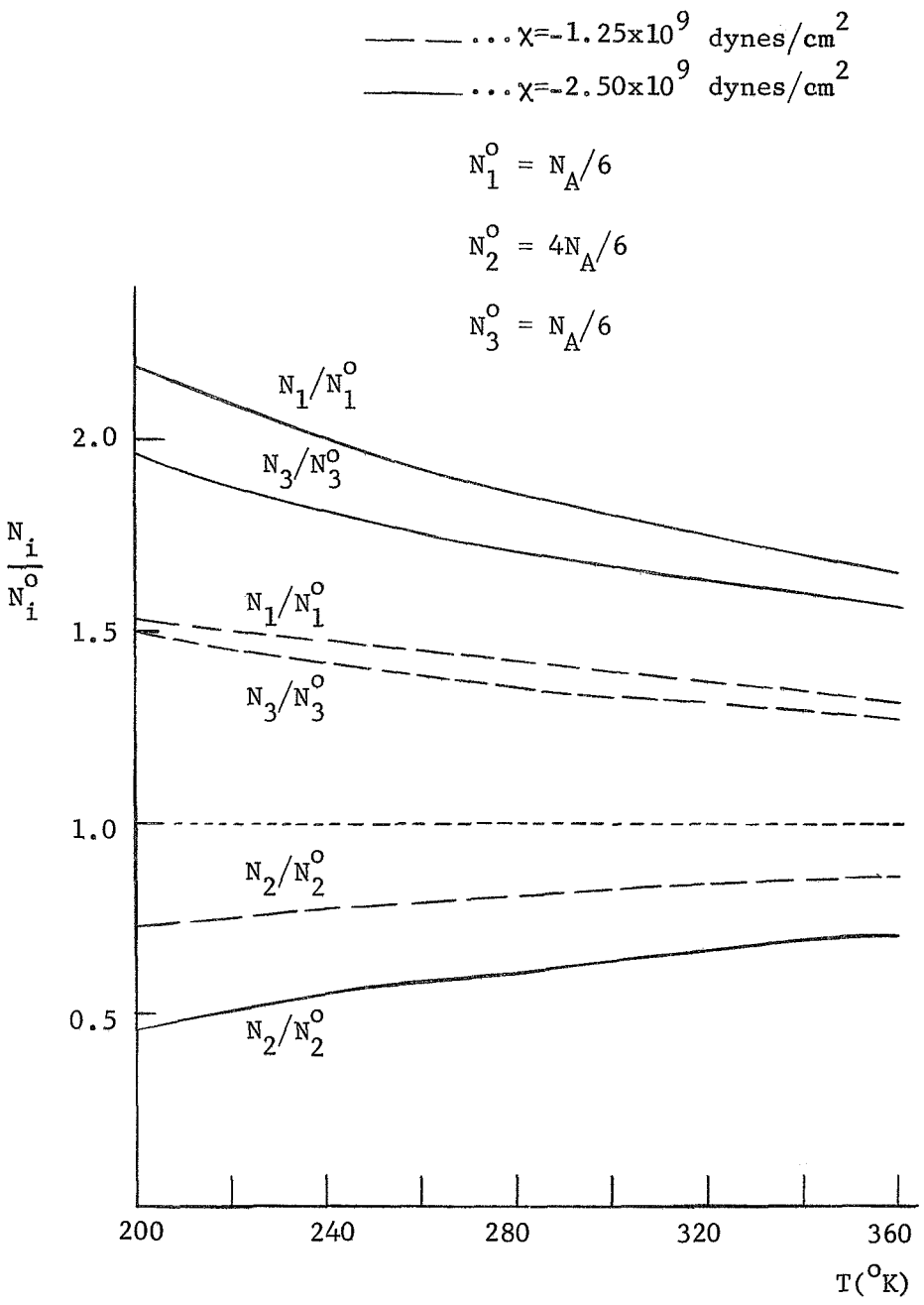

Figure 3.6 N_1, N_2, and N_3 versus temperature and stress

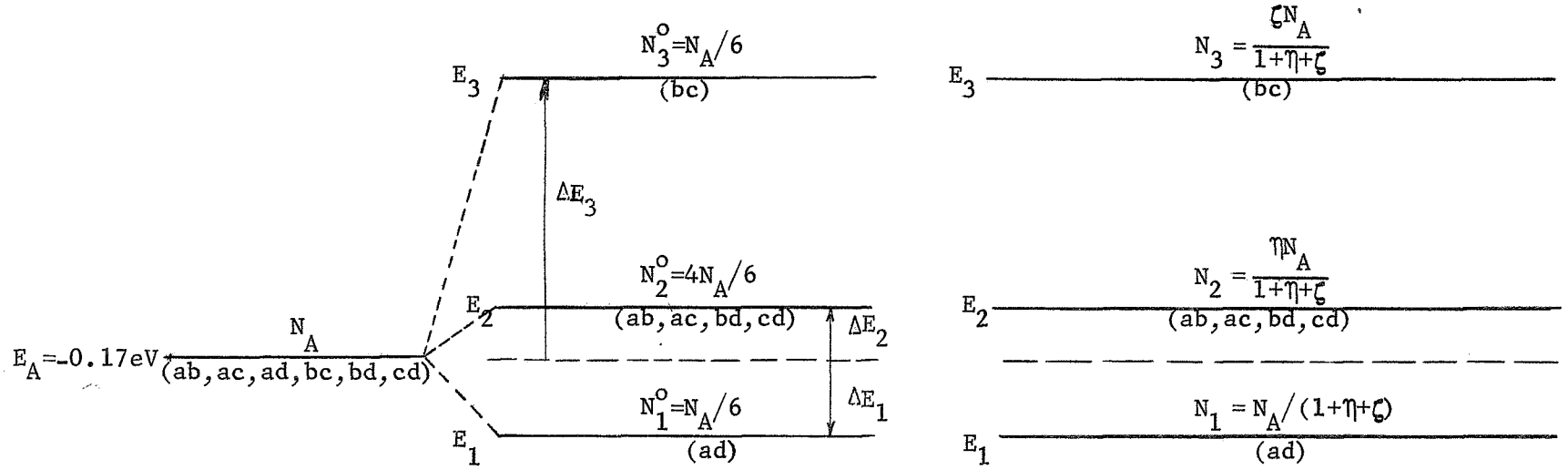

(a) zero stress

(b) with stress before preferential reorientation

(c) after preferential reorientation

Figure 3.7 The effect of a <110> compressive stress on the acceptor energy level of the A-center defect

Illustrated in Figure 3.8 is a typical A-center reorientation for the case of an applied < 110 > compressive stress.

The analyses of the effect of < 100 > and < 111 > compressive stresses on the A-center are similar to the < 110 > case. These analyses were performed and the results are tabulated in Table 3.3 along with the results of the < 110 > analysis.

The above analysis, based on the work of Watkins and Corbett (1961), is completely valid only for the case in which the A-center concentration greatly exceeds the donor concentration, i.e. for the case when the majority of A-centers do not have a trapped electron. This restriction is due to the fact that the energy involved in a stress-induced defect reorientation depends upon whether or not the electron trap is filled. For a more complete discussion of this restriction, as well as the physics of the A-center, the reader is referred to the above mentioned paper by Watkins and Corbett.

3.5 Conduction Band Electron Concentration

3.5.1 Introduction

This section presents equations which may be used to calculate the concentration of conduction band electrons in the n-type material studied in this thesis for an arbitrary stress or temperature.

3.5.2 Concentration of Conduction Band Electrons in the Absence of an Applied Stress

The following equation, a statement of the conservation of charge,

$$n_{c_o} = N_D^+ - N_A^- - N_E^- \tag{3.26}$$

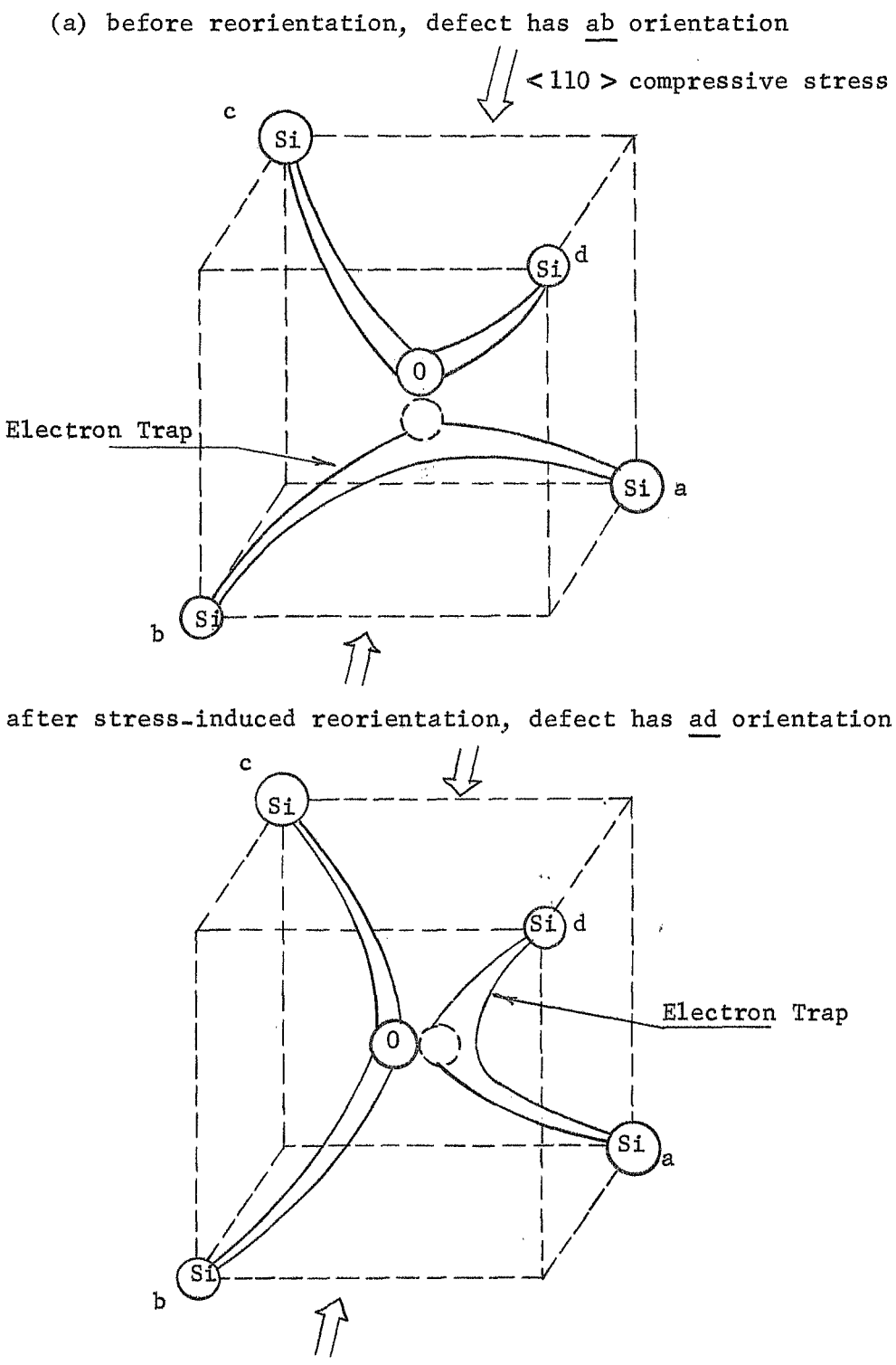

Figure 3.8 A typical stress-induced A-center reorientation for the case of a < 110 > compressive stress

Table 3.3 Effect of < 100 > , < 110 > , and < 111 > uniaxial stresses on the Si-A center acceptor level

	< 100 >	< 110 >	< 111 >
$\frac{N_1}{N_A}$	$\frac{1}{1+\gamma}$ [a]	$\frac{1}{1+\eta+\zeta}$ [b]	$\frac{1}{1+\xi}$ [c]
E_1	$E_A+(1.7\times10^{-12}\ \mathrm{eVcm^2/dyne})\chi$ [d]	$E_A+(2.96\times10^{-13}\ \mathrm{eVcm^2/dyne})\chi$	$E_A+(7.7\times10^{-13}\ \mathrm{eVcm^2/dyne})\chi$
$\frac{N_2}{N_A}$	$\frac{\gamma}{1+\gamma}$	$\frac{\eta}{1+\eta+\zeta}$	$\frac{\xi}{1+\xi}$
E_2	$E_A-(2.2\times10^{-12}\ \mathrm{eVcm^2/dyne})\chi$	$E_A-(2.52\times10^{-13}\ \mathrm{eVcm^2/dyne})\chi$	$E_A-(2.6\times10^{-12}\ \mathrm{eVcm^2/dyne})\chi$
$\frac{N_3}{N_A}$	-	$\frac{\zeta}{1+\eta+\zeta}$	-
E_3	-	$E_A-(4.73\times10^{-12}\ \mathrm{eVcm^2/dyne})\chi$	-

[a] $\gamma = 2\exp(-1.63\times10^{-11}\ \mathrm{eVcm^2/dyne})\chi/kT)$.

[b] $\eta = 4\exp((1.07\times10^{-11}\ \mathrm{eVcm^2/dyne})\chi/kT)$.

$\zeta = \exp((7.53\times10^{-13}\ \mathrm{eVcm^2/dyne})\chi/kT)$.

[c] $\xi = \exp((5.02\times10^{-13}\ \mathrm{eVcm^2/dyne})\chi/kT)$.

[d] χ is expressed in dynes/cm^2, and is negative for compressional stresses.

will be used to calculate the conduction band electron concentration n_{c_o}. The quantity N_D^+ in this equation is the unoccupied or ionized donor concentration. According to section 3.3 N_D^+ may be written as

$$N_D^+ = N_D \tag{3.27}$$

where N_D is the concentration of donors. N_A^- is the concentration of occupied or ionized A-centers, and it follows from section 3.4.2 that

$$N_A^- = \frac{N_A}{1 + 2\exp((E_A - E_{fo})/kT)} \quad , \tag{3.28}$$

where E_{fo} is the zero stress value of the Fermi energy. Similarly N_E^- is the concentration of occupied E-centers and may be written as

$$N_E^- = \frac{N_E}{1 + \exp((E_E - E_{fo})/kT)} \quad . \tag{3.29}$$

Since, for all samples studied in this thesis, the Fermi energy is well removed from the conduction band edge, the total conduction band electron concentration n_{c_o} may be expressed as

$$n_{c_o} = N_c \exp(E_{f_o}/kT) \quad , \tag{3.30}$$

where E_{f_o} is the zero stress value of the Fermi energy and the zero stress conduction band energy is used for the zero energy reference. In equation 3.30 N_c is the effective density of states for the conduction band of silicon, and has the value

$$N_c = 5.27 \times 10^{15} T^{3/2} \text{cm}^{-3} \tag{3.31}$$

if the new cyclotron resonance values $m_\ell = 0.90\ m_o$ and $m_t = 0.192\ m_o$ are used for the effective masses of the conduction band.

Now equations 3.27 through 3.30 may be substituted into equation 3.26. The resulting equation may then be solved for $\exp(E_{f_o}/kT)$ and hence n_{c_o} if the values of N_D, N_A, and N_E are known. If the following substitutions are made to condense the algebra

$$\beta_o = \exp(E_{f_o}/kT) \tag{3.32}$$

$$\alpha = 2\exp(E_A/kT) \tag{3.33}$$

$$\lambda = \exp(E_E/kT) \tag{3.34}$$

$$a_A = N_A/N_D \tag{3.35}$$

$$a_E = N_E/N_D \tag{3.36}$$

$$N_c' = N_c/N_D \tag{3.37}$$

equation 3.26 becomes

$$N_c'\beta_o = 1 - \frac{\beta_o a_A}{\beta_o+\alpha} - \frac{\beta_o a_E}{\beta_o+\lambda} . \tag{3.38}$$

Equation 3.13 may be algebraically reduced to the following polynomial in β_o

$$N_c'\beta_o^3 + \left\{ (\alpha+\lambda)N_c' + a_A + a_E - 1 \right\} \beta_o^2$$

$$+ \left\{ \alpha\lambda N_c' + a_A\lambda + a_E\alpha - \alpha - \lambda \right\} \beta_o - \alpha\lambda = 0 . \tag{3.39}$$

The roots of this equation may be found using a computer. Due to the signs of the coefficients of the various powers of β_o, it is found that there will always be one and only one positive real root and this root is retained as the value of

$$\beta_o = \exp(E_{f_o}/kT) \quad . \tag{3.40}$$

The conduction band electron concentration n_{c_o} is then found by substituting the value found for β_o into equation 3.30.

Equation 3.39 is assumed to be perfectly general for all samples studied in this thesis. However, if the concentration of Si-E centers is zero ($N_E = N_E^- = 0$), this equation is reduced to

$$N_c'\beta_o^2 + \left\{ \alpha N_c' + a_A - 1 \right\} \beta_o - \alpha = 0 \quad , \tag{3.41}$$

by setting $a_E = 0$ and $\lambda = 0$ in equation 3.39. Then for this case

$$\beta_o = \exp(E_{f_o}/kT) = \frac{1-a_A-\alpha N_c' + \sqrt{\{(1-a_A-\alpha N_c')^2 + 4\alpha N_c'\}}}{2N_c'} \quad , \tag{3.42}$$

since this is the positive real root of equation 3.41. For an unirradiated sample in which $N_A^- = N_A = 0$ and $N_E^- = N_E = 0$, equation 3.39 becomes

$$N_c'\beta_o = 1 \quad , \tag{3.43}$$

so that for this case

$$\beta_o = \exp(E_{f_o}/kT) = 1/N_c' \quad . \tag{3.44}$$

3.5.3 The Effect of Stress on the Conduction Band Electron Concentration

Consider now the calculation of the conduction band electron concentration of a sample subjected to an applied stress. The conservation of charge equation may still be written

$$n_c = N_D^+ - N_A^- - N_E^- \tag{3.45}$$

where from section 3.3 $N_D^+ = N_D$. In the presence of an applied stress, then it follows from section 3.2 that

$$n_c^{(i)} = \frac{N_c}{6} \exp[(E_f - \Delta E_i)/kT] \tag{3.46}$$

and therefore

$$n_c = \sum_{i=1}^{6} n_c^{(i)} = \left\{ \frac{N_c}{6} \sum_{i=1}^{6} \exp(-\Delta E_i/kT) \right\} \exp(E_f/kT) \tag{3.47}$$

and finally

$$n_c = N_c'' \exp(E_f/kT) \ . \tag{3.48}$$

In equation 3.46 $n_c^{(i)}$ is the concentration of electrons in the i^{th} conduction band minimum. The quantity ΔE_i is the stress-induced shift in energy (excluding the hydrostatic component Ξ_d e) of the i^{th} minimum, and N_c is the effective density of states of the conduction band (see section 3.5.1). Equations 3.47 and 3.48 serve to define N_c''. The term N_A^- in equation 3.45 is given by

$$N_A^- = n_1 + n_2 + n_3 \ , \tag{3.49}$$

where n_1, n_2 and n_3 are given by Table 3.3. The N_E^- term is given by equation 3.29 in section 3.5.2.

Consider now the case of a < 110 > applied stress. Substitution of equations 3.48, 3.49 and 3.50 into equation 3.45 yields

$$N_c'' \exp(E_f/kT) = N_D - \frac{N_1}{1 + 2\exp((E_1-E_f)/kT)} - \frac{N_2}{1 + 2\exp((E_2-E_f)/kT)}$$

$$- \frac{N_3}{1 + 2\exp((E_3-E_f)/kT)} - \frac{N_E}{1 + \exp((E_E-E_f)/kT)} \cdot \tag{3.50}$$

This equation reduces to the polynomial

$$A_5\beta^5 + A_4\beta^4 + A_3\beta^3 + A_2\beta^2 + A_1\beta + A_o = 0 \ , \tag{3.51}$$

where

$$A_5 = N_c'' \tag{3.52}$$

$$A_4 = N_c''(\alpha_1+\alpha_2+\alpha_3+\lambda) + a_1+a_2+a_3+a_E-1 \tag{3.53}$$

$$A_3 = N_c'''\{\alpha_1\alpha_2+\alpha_3\lambda+(\alpha_1+\alpha_2)(\alpha_3+\lambda)\} - (\alpha_1+\alpha_2+\alpha_3+\lambda)$$

$$+ a_1(\alpha_2+\alpha_3+\lambda) + a_2(\alpha_1+\alpha_3+\lambda) + a_3(\alpha_1+\alpha_2+\lambda) + a_E(\alpha_1+\alpha_2+\alpha_3) \tag{3.54}$$

$$A_2 = N_c''' \{\alpha_3\lambda(\alpha_1+\alpha_2)+\alpha_1\alpha_2(\alpha_3+\lambda)\} - \{\alpha_1\alpha_2+\alpha_3\lambda+(\alpha_1+\alpha_2)(\alpha_3+\lambda)\}$$

$$+ a_1\{\alpha_2\alpha_3+\alpha_2\lambda+\alpha_3\lambda\} + a_2\{\alpha_1\alpha_3+\alpha_1\lambda+\alpha_3\lambda\}$$

$$+ a_3\{\alpha_1\alpha_2+\alpha_1\lambda+\alpha_2\} + a_E\{\alpha_1\alpha_2+\alpha_1\alpha_3+\alpha_2\alpha_3\} \qquad (3.55)$$

$$A_1 = N_c''' \alpha_1\alpha_2\alpha_3\lambda - \{\alpha_3\lambda(\alpha_1+\alpha_2) + \alpha_1\alpha_2(\alpha_3+\lambda)\}$$

$$+ a_1\alpha_2\alpha_3\lambda + a_2\alpha_1\alpha_3\lambda + a_3\alpha_1\alpha_2\lambda + a_E\alpha_1\alpha_2\alpha_3 \qquad (3.56)$$

$$A_o = -\alpha_1\alpha_2\alpha_3\lambda \qquad (3.57)$$

with

$$\beta = \exp(E_f/kT) \qquad (3.58)$$

$$\alpha_1 = 2\exp(E_1/kT) \qquad (3.59)$$

$$\alpha_2 = 2\exp(E_2/kT) \qquad (3.60)$$

$$\alpha_3 = 2\exp(E_3/kT) \qquad (3.61)$$

$$\lambda = \exp(E_E/kT) \qquad (3.62)$$

$$N_c''' = N_c''/N_D \qquad (3.63)$$

$$a_1 = N_1/N_D \qquad (3.64)$$

$$a_2 = N_2/N_D \qquad (3.65)$$

$$a_3 = N_3/N_D \qquad (3.66)$$

$$a_E = N_E/N_D \ . \qquad (3.67)$$

The one and only one positive real root of equation 3.51 may be found and used as the value of $\exp(E_f/kT)$. The individual $n_c^{(i)}$ as well as the total conduction band electron concentration n_c may be calculated using this value of $\exp(E_f/kT)$ in equations 3.46 and 3.48.

For the cases of both < 100 > and < 111 > applied stresses, equation 3.45 may be reduced to the following polynomial

$$N_c''' \beta^4 + \{N_c''' (\alpha_1+\alpha_2+\lambda)+a_1+a_2+a_E-1\}\beta^3$$

$$+ [N_c''' \{\alpha_1\alpha_2+\lambda(\alpha_1+\alpha_2)\} - (\alpha_1+\alpha_2+\lambda)+a_1\alpha_2+a_1\lambda$$

$$+ a_2\alpha_1+a_2\lambda+a_E\alpha_1+a_E\alpha_2]\beta^2$$

$$+ [N_c''' \alpha_1\alpha_2\lambda-\{\alpha_1\alpha_2+\lambda(\alpha_1+\alpha_2)\}+a_1\alpha_2\lambda+a_2\alpha_1\lambda+a_E\alpha_1\alpha_2]\beta$$

$$- \alpha_1\alpha_2\lambda = 0 \ . \qquad (3.68)$$

However E_1, E_2, N_1, and N_2 have different values for a given stress for these two orientations as is seen in Table 3.3. This equation may be solved for the value of $\exp(E_f/kT)$ as before.

3.5.4 Population Transfer with Stress

Electron population transfer between the individual conduction band minima is illustrated by the following example. Consider an unirradiated n-type silicon sample doped with $N_D = 10^{15}$ cm^{-3} phosphorus donors. Using equations 3.68 and 3.46 the effect of a uniaxial < 100 > compressive stress $\chi = -2\times10^9$ $dyne/cm^2$ on the populations of the individual conduction minima for this sample was

determined using a digital computer. The results are illustrated in Figure 3.9. Also shown in this figure is the stress-induced shift in the Fermi energy as a function of temperature. Shown in Figure 3.10 are the results of a similar analysis carried out for an electron-irradiated sample with $N_D = 10^{15}$ cm^{-3}, $N_A = 10^{16}$ cm^{-3}, and $N_E = 0$. This figure shows the effect that compensation due to the presence of Si-A centers has on the total conduction band electron concentration.

3.6 Summary

In this chapter the effect of an applied stress on the concentration of conduction band electrons due to stress-induced splitting of both the conduction band energy and the acceptor energy level of the Si-A center was determined. In section 3.5.2 the equations whose solution yields the Fermi energy for the case of zero applied stress were developed. The corresponding equations for the case of nonzero applied stress were presented in section 3.5.3. Examples illustrating stress-induced population transfer and the effect of A-center compensation were presented in section 3.5.4.

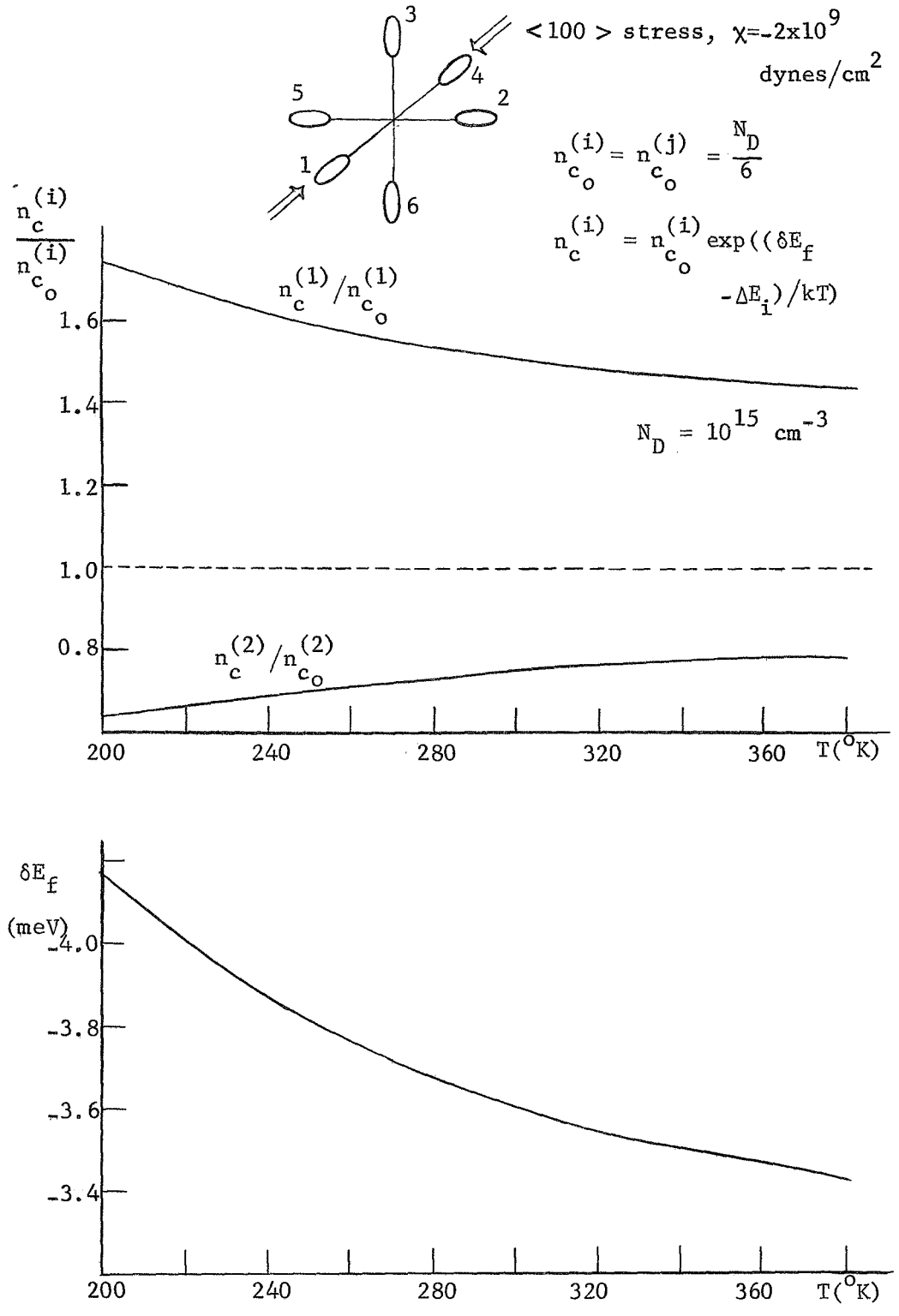

Figure 3.9 Population transfer and stress-induced Fermi energy shift versus temperature for an unirradiated <100> sample

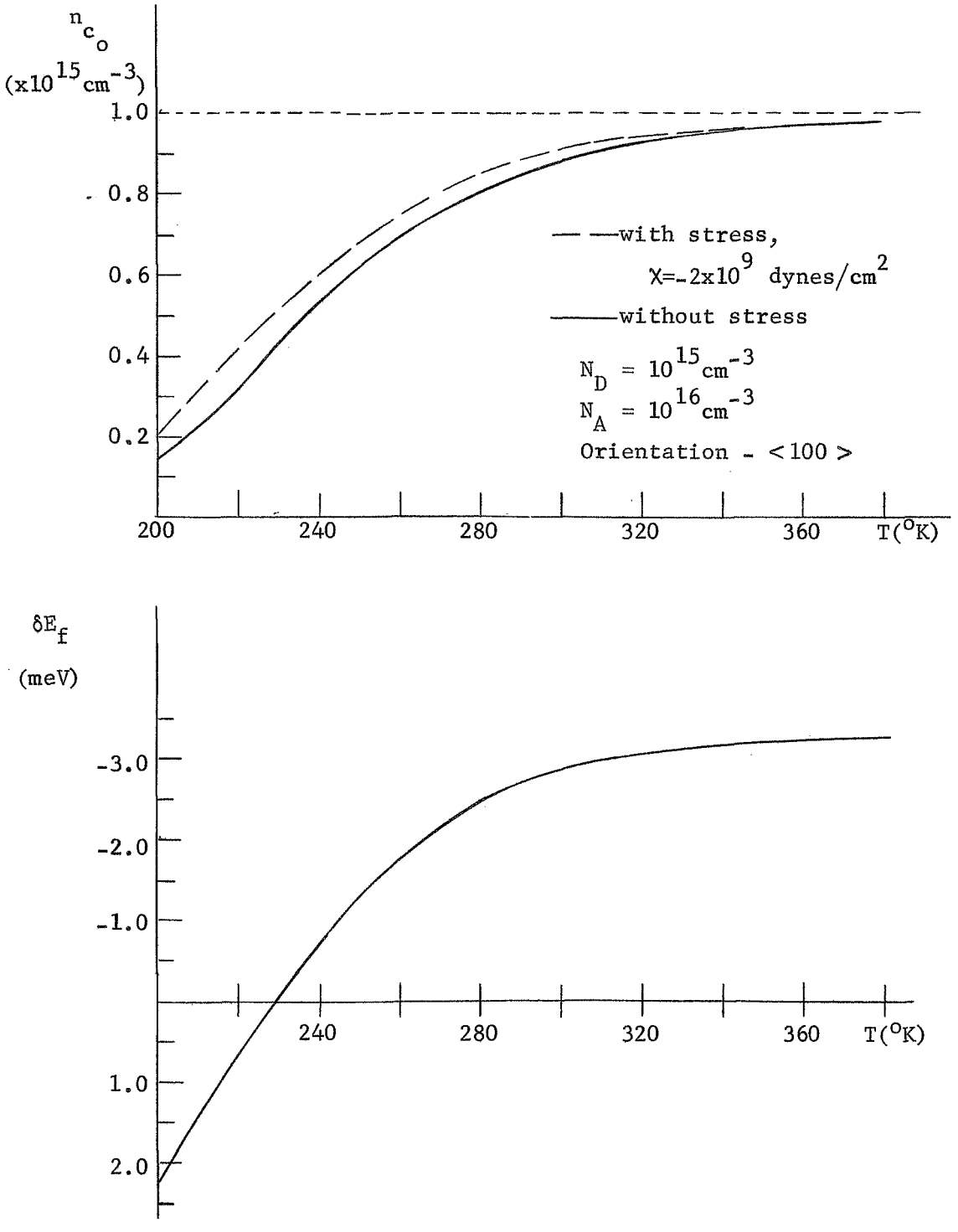

Figure 3.10 Total conduction band electron concentration and stress-induced Fermi energy shift versus temperature for an irradiated <100> sample

4. ELECTRON MOBILITY IN SILICON

4.1 Introduction

The ease with which a conduction electron moves through a semiconductor under the influence of an electric field is related to its mobility. This mobility is determined by the scattering processes in which the electron is involved. The product of electron mobility and the number of conduction electrons determines the resistivity of an n-type semiconductor. The preceding chapter provided the equations necessary to calculate the number of conduction electrons for a given temperature and stress. In the present chapter, electron mobility in silicon and the qualitative effect of stress on this mobility is discussed. The results of these two chapters are used in the computation of piezoresistivity in chapter 5.

4.2 Principal Electron Scattering Processes in Silicon

Assuming the existence of a relaxation time τ, and assuming that this relaxation time may be expressed as a function of electron energy E, i.e. $\tau = \tau(E)$, then the mobility μ is

$$\mu = \frac{q<\tau>}{m^*} \tag{4.1}$$

where

$$<\tau> = \frac{\int_0^\infty \tau(E)\, E^{3/2} \exp(-E/kT)\, dE}{\int_0^\infty E^{3/2} \exp(-E/kT)\, dE} \quad . \tag{4.2}$$

The quantity m^* is an effective electron mass determined by the curvature of the conduction band minima in $\vec{k}$-space, k is Boltzmann's constant, and q is the charge of an electron. Now consider the various scattering mechanisms that determine τ.

4.2.1 Lattice Scattering

Shown in Figure 4.1 is the lattice vibrational spectrum for [100]-directed phonons in silicon. A conduction electron can be scattered by any of the following phonons:

1. Intravalley acoustic phonons.
2. Intervalley acoustic phonons.
3. Intravalley optical phonons.
4. Intervalley optical phonons.

Intervalley scattering is the scattering of an electron from one conduction band minimum to another. For intravalley scattering the electron is scattered within a particular conduction band minimum.

Scattering by intervalley phonons is of two geometrically distinguishable types as illustrated in Figure 4.2. Shown in this figure are scattering events due to f- and g-phonons. The g-phonons are involved in scattering in a < 100 > direction from one conduction band minimum to its mirror image as is indicated. The f-phonon is involved in scattering from one conduction band minimum to any one of the four minima lying in the plane perpendicular to its ellipsoid axis. The reduced wave numbers of the g- and f-type phonons are 0.3 and 1.0 respectively, as indicated in Figure 4.1. It is seen from Figure 4.2 that the phonon involved in the f-type scattering does not lie in a < 100 > direction. However, Long (1960) has shown that

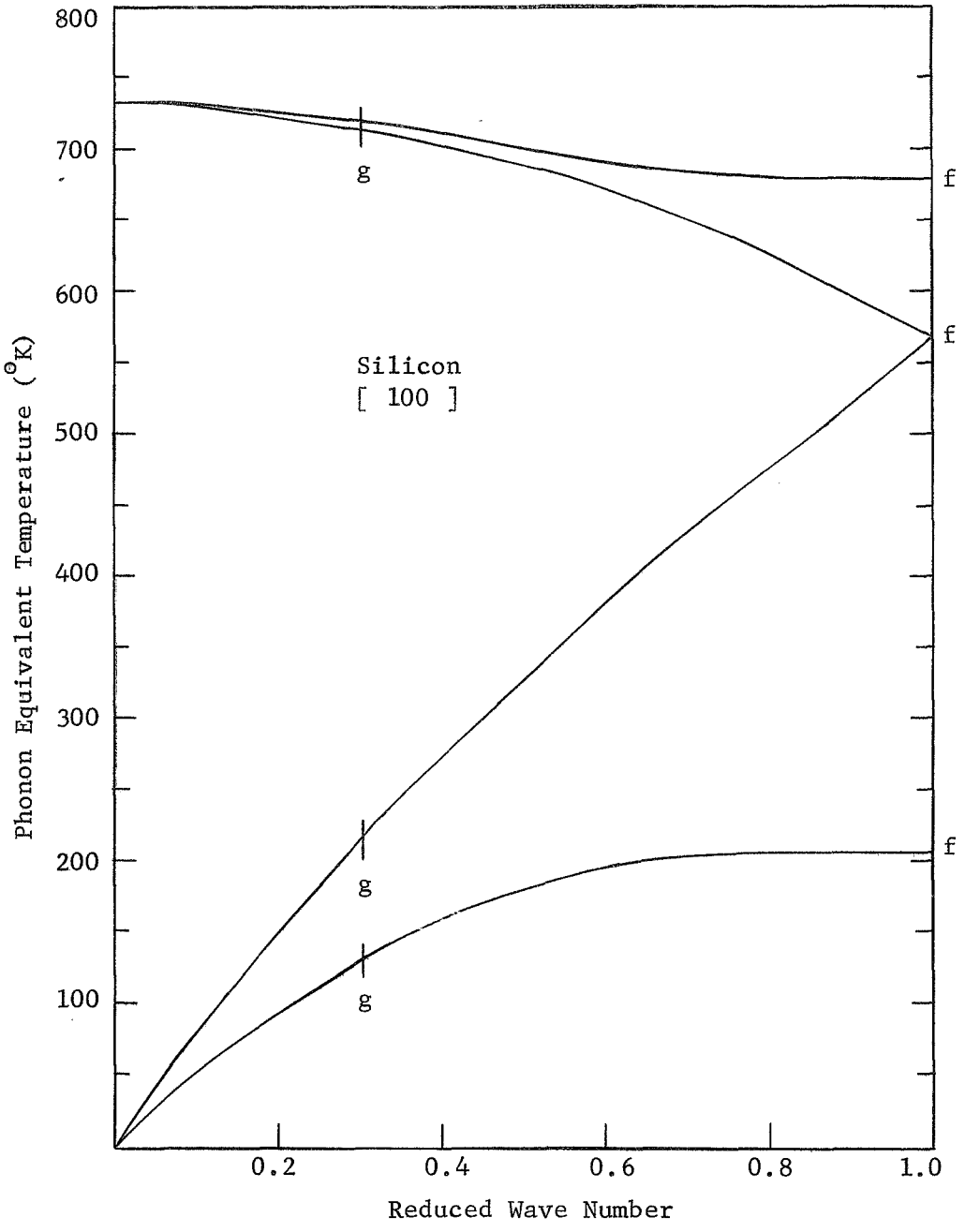

Figure 4.1 Lattice-vibrational spectrum of silicon for [100] - directed phonons (after Brockhouse (1959))

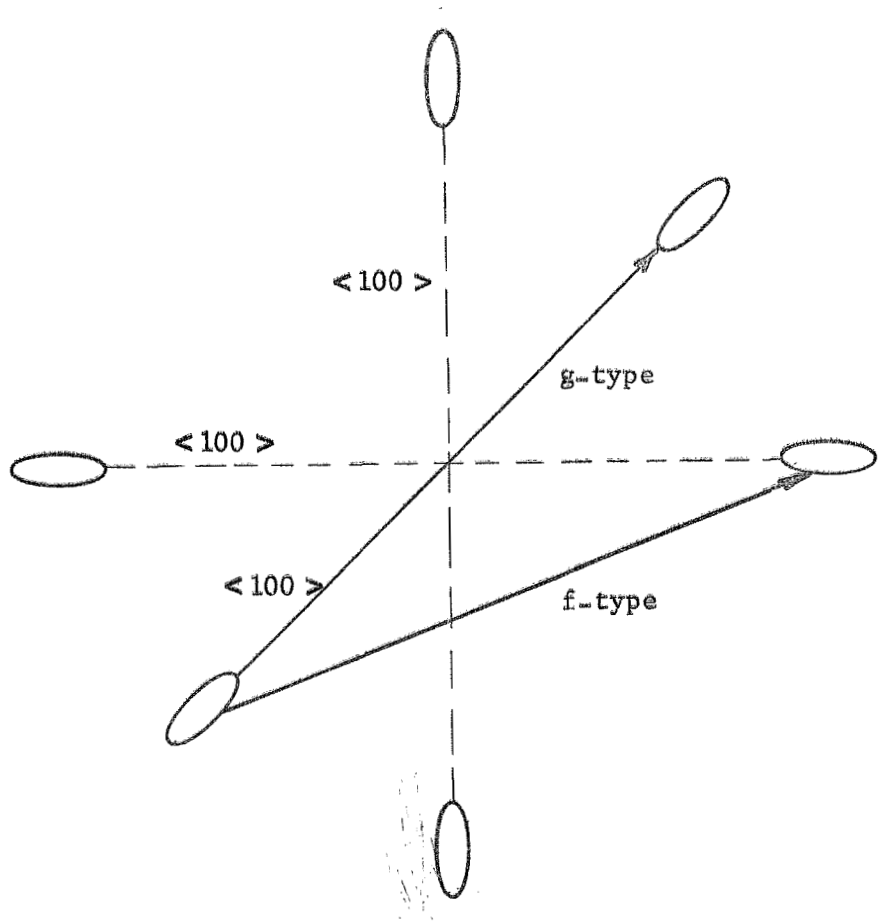

Figure 4.2 Illustration of f-type and g-type intervalley scattering

the f-phonon lies in a direction only about 11^{o} off the < 100 > direction. Due to this, Long suggests that the lattice vibrational spectrum for [100]-directed phonons should provide a good estimate of the energy of the f-phonon.

Consider now a single conduction band minimum and the scattering of the electrons in this minimum by lattice vibrations. As is shown in Figure 4.2, the constant energy surfaces of a conduction band minimum are anisotropic in that they have an ellipsoidal rather than a spherical shape. This anisotropic shape affects the mobility first of all through an anisotropic effective mass. In a direction parallel to the ellipsoid axis the effective mass is

$$m_{11}^{*} = m_{\ell} = 0.90\ m_{o} \quad \text{(Rauch } \underline{\text{et}}\ \underline{\text{al.}}\ \text{(1960))} ,$$

while for a direction perpendicular to the ellipsoid axis the effective mass is

$$m_{t}^{*} = m_{t} = 0.192\ m_{o} \quad \text{(Rauch } \underline{\text{et}}\ \underline{\text{al.}}\ \text{(1960))},$$

where $m_{o} = 9.1 \times 10^{-31}$ kg is the electron rest mass. The anisotropic shape of the conduction band minima also causes the lattice relaxation time to be direction dependent. Herring and Vogt (1956) have shown that the lattice relaxation time in silicon may be expressed as a tensor. This tensor is diagonal when referred to the crystallographic axes. Due to the rotational symmetry of the constant energy surfaces, the tensor is completely specified (for zero stress) by two components, τ_{ℓ} and τ_{t}. These quantities are, respectively, the relaxation times for scattering in a direction parallel to the

ellipsoid axis and for scattering in a direction perpendicular (transverse) to the ellipsoid axis.

According to Herring (1955) intravalley acoustic scattering is anisotropic and intervalley scattering is probably isotropic. Therefore, intravalley acoustic scattering will be assumed to be anisotropic and characterized by two relaxation times, τ_{A_ℓ} and τ_{A_t}. For the case of zero stress all types of intervalley scattering will be assumed to be isotropic. Herring and Vogt (1956) have calculated τ_{A_ℓ} and τ_{A_t} in terms of the deformation potential constants Ξ_u and Ξ_d and have plotted τ_{A_ℓ}/τ_{A_t} as a function of Ξ_d/Ξ_u, since the value of this ratio (Ξ_d/Ξ_u) is in doubt. In their calculations, Herring and Vogt assumed that $m_\ell/m_t = 5.1$, which is no longer thought to be accurate. Long (1960), using the presently accepted value $m_\ell/m_t = 4.69$, recalculated τ_{A_ℓ}/τ_{A_t} versus Ξ_d/Ξ_u. The results of his calculations are shown in Figure 4.3.

Now if Ξ_d/Ξ_u were known accurately τ_{A_ℓ}/τ_{A_t} could be determined from this curve. However, due to a difficulty in measuring Ξ_d, the value of this ratio is not known. Ito et al. (1964) have determined τ_{A_ℓ}/τ_{A_t} by measuring the cyclotron resonance line width of very pure silicon samples at extremely low temperatures ($1.5^\circ K - 5^\circ K$). Their experiment indicates that

$$\tau_{A_\ell}/\tau_{A_t} = 1.27 \pm 0.08 \ .$$

Also determined from this experiment by Ito et al. were the following values for Ξ_d and Ξ_u at $T \cong 5^\circ K$:

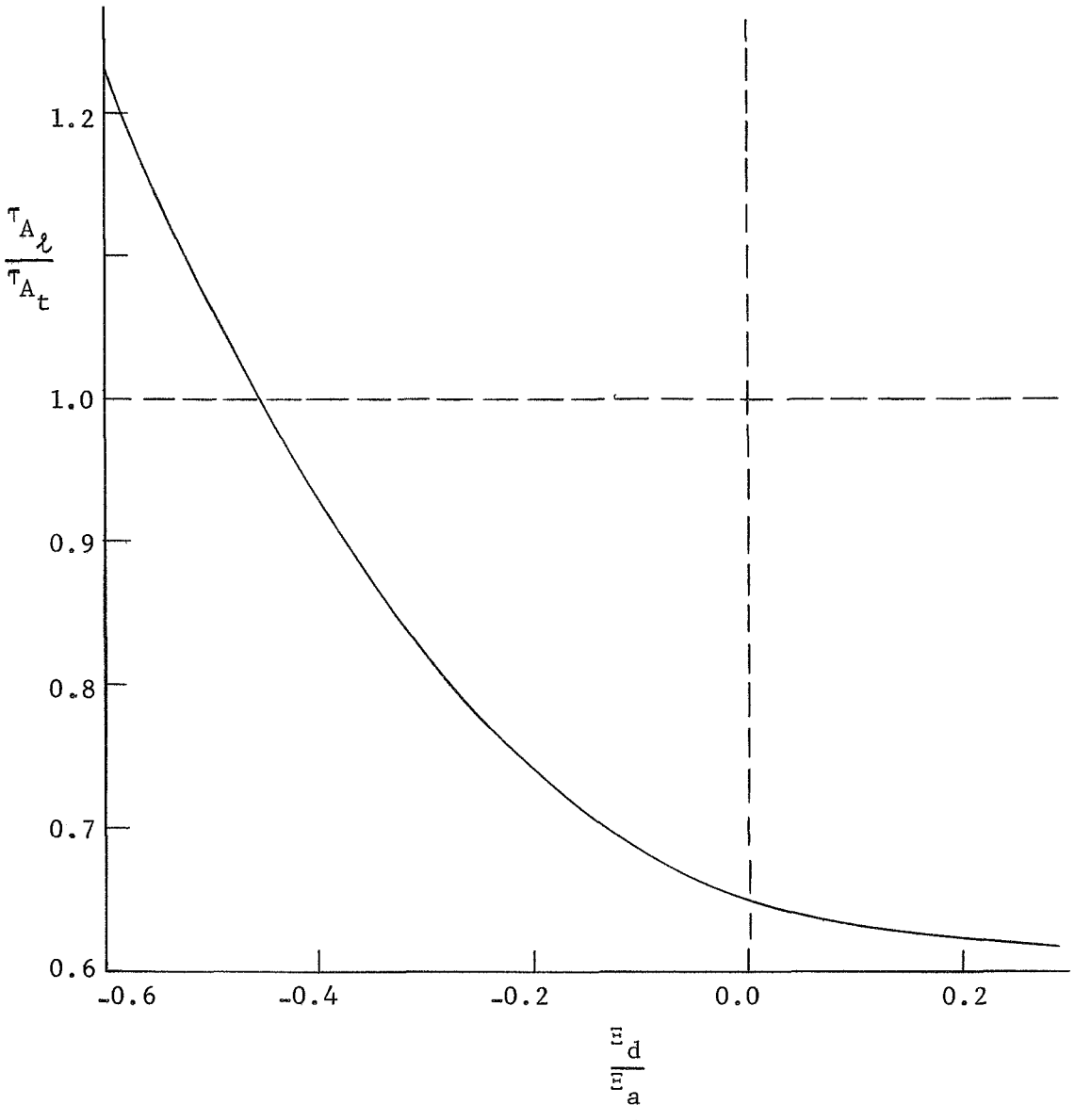

Figure 4.3 Anisotropy of acoustic intravalley scattering relaxation times as a function of Ξ_d/Ξ_u

$$\Xi_u = (8.5 \pm 0.1)\,\text{eV}$$

$$\Xi_d = (-5.2 \pm 0.3)\,\text{eV} .$$

A general expression for lattice scattering relaxation time is (see Long (1960))

$$\frac{1}{\tau_\alpha} = W_{A_\alpha} \left(\frac{E}{kT_o}\right)^{\frac{1}{2}} \left(\frac{T}{T_o}\right) + \sum_i W_i \left(\frac{T_{c_i}}{T_o}\right)^{\frac{3}{2}} \left\{ \frac{(E/kT_{c_i}+1)^{\frac{1}{2}}}{(\exp(T_{c_i}/T)-1} \right.$$

$$\left. + \frac{(E/kT_{c_i}-1)^{\frac{1}{2}} \text{ or } 0}{1 - \exp(-T_{c_i}/T)} \right\} . \qquad (4.3)$$

In this equation the W's are coupling coefficients, measuring how strongly the electron is coupled to the various types of phonon scattering. The dummy subscript α is replaced by ℓ for the longitudinal relaxation time τ_ℓ, and by t for the transverse relaxation time τ_t. E is electron energy, measured from the bottom of the conduction band. The quantities T, T_{c_i}, and T_o are temperatures. T is the temperature at which the relaxation time is to be determined, T_{c_i} is the characteristic temperature of the i^{th} intervalley phonon (such that kT_{c_i} is the energy of the i^{th} intervalley phonon), and T_o is an arbitrary reference temperature.

The first term in equation 4.3 is due to intravalley acoustic scattering, while the terms of the summation are due to scattering by high energy phonons. The first term in the brackets inside the

summation is due to the absorption of a phonon of energy kT_{c_i}, while the second term is due to the emission of a phonon of energy kT_{c_i}. The numerator of this second term is zero when $E < kT_{c_i}$. This summation includes scattering by the following phonons:

a) Intravalley optical phonon with characteristic temperature

$T_c = 735^{o}K.$

b) Type g intervalley acoustic phonons with characteristic temperatures

$T_c = 135^{o}K$ and $T_c = 224^{o}K.$

c) Type g intervalley optical phonons with approximate characteristic temperature

$T_c = 718^{o}K.$

d) Type f intervalley phonons with approximate temperatures

$T_c = 209^{o}K$ (TA phonons)

$T_c = 570^{o}K$ (LA and LO phonons)

and

$T_c = 682^{o}K$ (TO phonons).

For zero stress, the observable electron mobility as determined by

$$\mu = \frac{\sigma}{qn} \tag{4.4}$$

where σ is the conductivity and n the concentration of conduction electrons, is, in terms of the two relaxations times

$$\mu = \frac{q}{3}\left\{\frac{<\tau_\ell>}{m_\ell} + \frac{2<\tau_t>}{m_t}\right\} . \tag{4.5}$$

All that is needed to accurately calculate μ for the hypothetical case of scattering by lattice phonons only are correct values for W_{A_ℓ}, W_{A_t} and all the W_i. If these values were known, equation 4.3 could be inserted in equation 4.2 to calculate $< \tau_\ell >$ and $< \tau_t >$, and then μ could be computed using equation 4.5. However, the values of these coupling coefficients are not known and some type of curve-fitting using the W's as parameters must be used to fit theory (equation 4.3) to experiment.

Long (1960), by approximating the summation in equation 4.3 with two terms (involving phonons with characteristic temperatures 190°K and 630°K), has obtained good agreement between theory and experiment over a wide temperature range. The best fit parameter values he obtained are

$$W_1/W_{A_t} = 2.0$$

and

$$W_2/W_{A_t} = 0.15 \ ,$$

where W_1 is the coefficient of coupling to scattering by the 630°K phonon, and W_2 is the coupling coefficient to the 190°K phonon. Long used

$$\frac{\tau_{A_\ell}}{\tau_{A_t}} = \frac{W_{A_t}}{W_{A_\ell}} = \frac{2}{3}$$

in his model. This value was deduced by Long from magnetoresistance experiments (Long and Meyers (1960)) he had performed.

As noted above, Ito et al. (1964) have obtained a larger value for τ_{A_ℓ}/τ_{A_t} by a very direct method. To the author's knowledge, the discrepancy between this value and Long's value has not been explained.

4.2.2 Scattering by Ionized Impurities

Besides lattice scattering, the most important scattering mechanisms limiting the mobility of a conduction electron are

a) scattering by ionized impurities,

b) scattering by neutral impurities,

c) scattering by physical imperfections of the crystal, such as dislocations,

d) electron-electron scattering.

Of these mechanisms, only ionized impurity scattering is believed to be important in limiting electron mobility in the samples studied experimentally for this thesis. Neutral impurity scattering is important only at temperatures much lower than the temperatures obtained in the experimental work here. Scattering by dislocations and physical imperfections is assumed to be negligible due to the fact that high dislocation densities ($10^8 cm^{-2}$ - $10^9 cm^{-2}$) are required for this mechanism to be important, but the samples studied in this thesis are believed to be relatively free of physical imperfections. Inter-electron scattering can become important in degenerately-doped material but should be negligible in the non-degenerate material studied here.

Scattering by ionized impurities is known to be anisotropic. It has been suggested by Ham (1955) that the ionized impurity scattering

relaxation time can be represented by a tensor, and that this tensor is diagonal when referred to the principal axes of a conduction band energy minimum ellipsoid. Because of symmetry restrictions imposed by the ellipsoidal conduction band energy minimum, there will be only two ionized impurity scattering relaxation times, τ_{I_ℓ} and τ_{I_t}. The following equation, derived by Wang (1966), will be used in this thesis for these two relaxation times

$$\frac{1}{\tau_{I_\alpha}(E)} = W_{I_\alpha} N_i E^{-3/2} \left\{ \ln(1+2b) - \frac{2b}{1+2b} \right\} . \qquad (4.6)$$

In equation 4.6 the subscript α is to be replaced with ℓ for the longitudinal relaxation time τ_{I_ℓ}, and by t for the transverse relaxation time τ_{I_t}. The quantity N_i is the concentration of ionized impurities, E is electron energy, and W_{I_α} is a coupling coefficient. The quantity 2b has the value

$$2b = \frac{8\pi\epsilon m^* kT}{q^2 h^2 n} E , \qquad (4.7)$$

where ϵ is the dielectric constant of silicon; k is Boltzmann's constant; h is Planck's constant; T is the temperature of the crystal; q is the charge of an electron; and n is the concentration of conduction band electrons. The quantity m^* in equation 4.7 is the density of states effective mass $m^* = (m_\ell m_t^2)^{1/3}$. It should be pointed out that equation 4.6 was derived by means of perturbation theory using a screened coulomb potential as the electron-ionized impurity interaction potential.

The total relaxation times, τ_ℓ and τ_t, due to both lattice and ionized impurity scattering, are given by the familiar equations

$$\frac{1}{\tau_\ell} = \frac{1}{\tau_{\text{lattice}_\ell}} + \frac{1}{\tau_{I_\ell}} \tag{4.8a}$$

and

$$\frac{1}{\tau_t} = \frac{1}{\tau_{\text{lattice}_t}} + \frac{1}{\tau_{I_t}} \quad . \tag{4.8b}$$

The quantities $(\tau_{\text{lattice}})_\ell$ and $(\tau_{\text{lattice}})_t$ are given by equation 4.3. The correct value of the anisotropy of ionized impurity scattering τ_{I_ℓ}/τ_{I_t} is not known. The value suggested by Ham (1955), $\tau_{I_\ell}/\tau_{I_t} = 4$, will be used in this thesis. Mobility determined empirically may be fitted using equations 4.8, 4.2, and 4.5, and adjusting the values of the various coupling coefficients involved.

4.3 Effect of Uniaxial Stress on Mobility

In silicon, the effective electron mobility as defined by equation 4.4 is affected in several ways by uniaxial stress. The main effect, due to stress-induced population transfer, is discussed in chapter 5. There is an additional effect due to stress-induced changes in intervalley scattering rates. It has been estimated by Herring (1955) that this effect and population transfer are the only two first order effects contributing to silicon's piezoresistivity (in uncompensated material). The effect of stress on mobility due to stress-induced changes in intervalley scattering rates will be qualitatively assessed in this section. This assessment will be

useful in interpreting experimental results later. Only scattering by f-type (see section 4.2.1) intervalley phonons is greatly affected by stress. In Figure 4.4 the minima involved in f-type scattering are illustrated. Figure 4.4(a) illustrates the scattering of an electron from valley i to valley j due to the absorption of an f-phonon (of energy kT_{c_f}) for the zero stress case. In Figure 4.4(b) the same scattering event is illustrated for the stressed case, when an energy separation $\Delta = |\Delta E_j - \Delta E_i|$ exists between valleys i and j.

Now the probability of transition (which is the reciprocal relaxation time) from a state of energy E in valley i to a state of energy E' in valley j due to the absorption of a phonon of energy kT_{c_f} is given by (see Herring (1955)):

$$\text{transition probability} = \frac{1}{\tau} = |M_{ij}|^2 \times (\text{density of states at } E') \quad . \qquad (4.9)$$

The quantity M_{ij} is a matrix element for scattering from valley i to valley j by a phonon kT_{c_f}, and is independent of electron energy. According to Herring (1955), the effect of stress on M_{ij} is expected to be small.

Now the density of states at the scattered-to site E' is proportional to the square root of $\delta E'$, where $\delta E'$ is the energy difference between E' and the bottom of valley j. Because of this, the density of states in equation 4.9 is $(E + kT_{c_f})^{\frac{1}{2}}$ for zero stress, and $(E - \Delta + kT_{c_f})^{\frac{1}{2}}$ for the stressed case. Thus the f-type intervalley terms in the summation of equation 4.3 must be altered in the following way to account for stress. For scattering from a lower to an upper valley

for zero stress

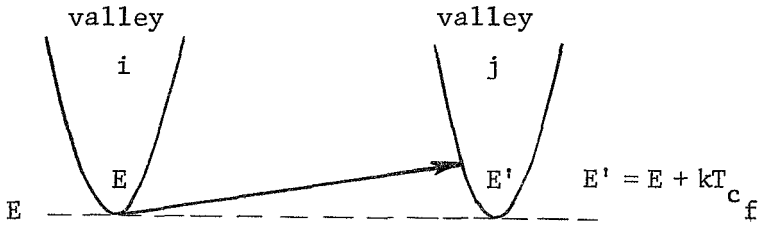

(a) f-type intervalley scattering from valley i to valley j by the f-phonon, kT_{c_f}, for zero stress

for applied stress X

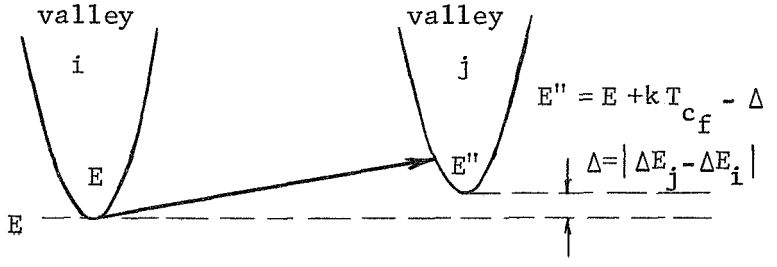

(b) f-type intervalley scattering from valley i to valley j by the f-phonon, kT_{c_f}, in the presence of a stress-induced difference, Δ, in valley energies

Figure 4.4 Effect of stress on f-type intervalley scattering

$$\frac{1}{\tau_{f\uparrow}} = \sum_i W_i \left(\frac{T_{c_i}}{T_o}\right)^{3/2} \left\{ \frac{\left((E-\Delta)/kT_{c_i} + 1\right)^{1/2}}{\exp(T_{c_i}/T) - 1} \right.$$

$$\left. - \frac{\left((E-\Delta)/kT_{c_i} - 1\right)^{1/2} \text{ or } 0}{1 - \exp(-T_{c_i}/T)} \right\} , \qquad (4.10)$$

where the sum is taken over all the different f-type phonons. Similarly for scattering from an upper to a lower valley

$$\frac{1}{\tau_{f\downarrow}} = \sum_i W_i \left(\frac{T_{c_i}}{T_o}\right)^{3/2} \left\{ \frac{\left((E+\Delta)/kT_{c_i} + 1\right)^{1/2}}{\exp(T_{c_i}/T) - 1} \right.$$

$$\left. - \frac{\left((E+\Delta)/kT_{c_i} - 1\right)^{1/2} \text{ or } 0}{1 - \exp(-T_{c_i}/T)} \right\} . \qquad (4.11)$$

The qualitative effect of stress on the relaxation times can be assessed by a consideration of equations 4.10 and 4.11. Consider the case of < 100 > stress. From Figure 4.5 it is seen that valleys 1 and 4 are shifted down by a < 100 > stress and have a relaxation time τ_ℓ in the direction of the stress and electric field (since in this thesis the applied electric field is always parallel to the stress). The zero stress value of τ_ℓ, symbolized by τ_{ℓ_o}, may be written as

$$\frac{1}{\tau_{\ell_o}} = \frac{1}{\tau_{A_\ell}} + \frac{1}{\tau_{ii}} + \frac{1}{\tau_{f_o}} + \frac{1}{\tau_{I_\ell}} \qquad (4.12)$$

where

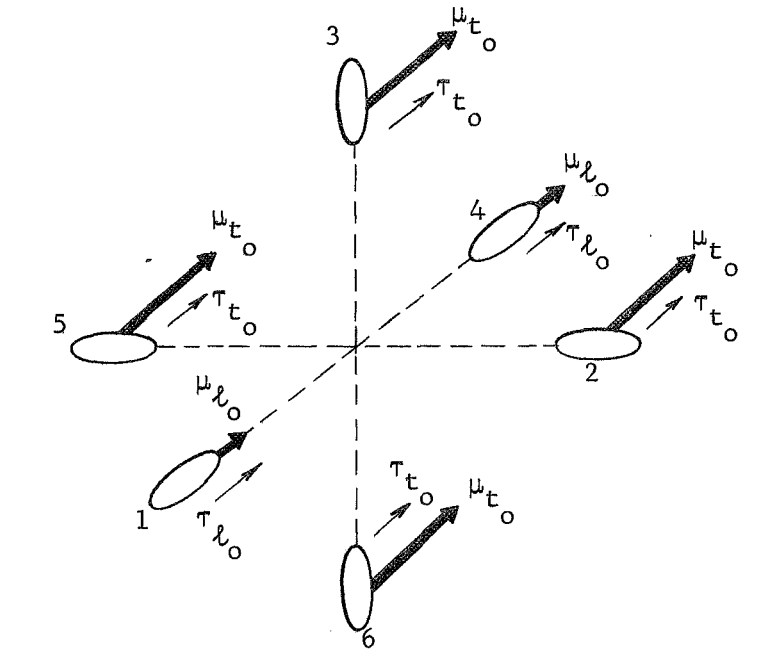

zero stress

$$\mu_{\ell_o} = \frac{q<\tau_{\ell_o}>}{m_\ell}$$

$$\mu_{t_o} = \frac{q<\tau_{t_o}>}{m_t}$$

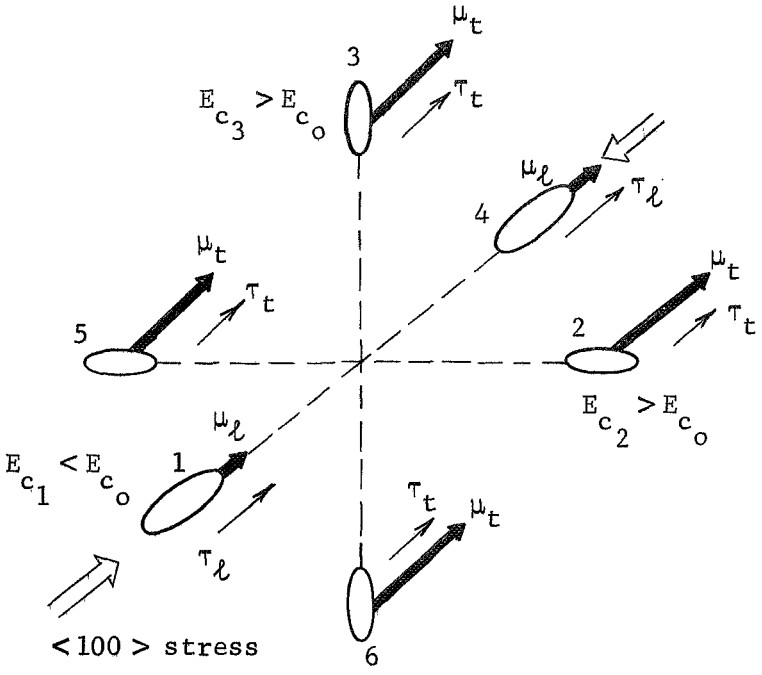

with <100> stress

$$\mu_\ell = \frac{q<\tau_\ell>}{m_\ell}$$

$$\mu_t = \frac{q<\tau_t>}{m_t}$$

Figure 4.5 Single valley relaxation times and mobilities in the <100> lattice direction

τ_{A_ℓ} = longitudinal acoustic scattering relaxation time

τ_{ii} = g-type intervalley scattering relaxation time

τ_{f_o} = f-type intervalley scattering relaxation time for zero stress

τ_{I_ℓ} = longitudinal ionized impurity scattering relaxation time.

The effect of stress on all the terms of equation 4.12 except the one due to f-type intervalley scattering will be neglected in the analysis that follows. This should be a valid approximation since Herring (1955) has estimated that the effect of stress on these terms is of second order. Now τ_ℓ has the value

$$\frac{1}{\tau_\ell} = \frac{1}{\tau_{A_\ell}} + \frac{1}{\tau_{ii}} + \frac{1}{\tau_{f'}} + \frac{1}{\tau_{I_\ell}} \tag{4.13}$$

with $\tau_{f'}$ given by equation 4.10. The comparison between τ_{f_o} and $\tau_{f'}$ is

$$\tau_{f_o} > \tau_{f'} \ . \tag{4.14}$$

Therefore, τ_ℓ is greater than τ_{ℓ_o} for every energy E and it follows that

$$\frac{<\tau_\ell>}{<\tau_{\ell_o}>} > 1 \ . \tag{4.15}$$

The four valleys 2, 3, 5, and 6 are shifted up in energy by the $<100>$ stress. Figure 4.5 indicates that these valleys have a

relaxation time τ_t in the direction of the stress and electric field. This τ_t may be written as

$$\frac{1}{\tau_t} = \frac{1}{\tau_{A_t}} + \frac{1}{\tau_{ii}} + \frac{1}{\tau_{f\downarrow}} + \frac{1}{\tau_{I_t}} \quad , \tag{4.16}$$

where τ_{A_t} is due to transverse acoustic scattering, and $\tau_{f\downarrow}$ is given by equation 4.11. The zero stress value, τ_{t_o}, of τ_t is

$$\frac{1}{\tau_{t_o}} = \frac{1}{\tau_{A_t}} + \frac{1}{\tau_{ii}} + \frac{1}{\tau_{f_o}} + \frac{1}{\tau_{I_t}} \, . \tag{4.17}$$

Now

$$\tau_{f_o} < \tau_{f\downarrow} \, . \tag{4.18}$$

It thus follows that

$$\frac{<\tau_t>}{<\tau_{t_o}>} < 1 \, . \tag{4.19}$$

If it is assumed that τ_{A_ℓ} is greater than τ_{A_t}, as the work by Ito et al. (1964) indicates, then it also follows that

$$K_\tau \equiv \frac{<\tau_\ell>}{<\tau_t>} > \frac{<\tau_{\ell_o}>}{<\tau_{t_o}>} \equiv K_{\tau_o} \, . \tag{4.20}$$

The relaxation time anisotropies K_τ and K_{τ_o} are defined by equation 4.20.

Now consider the case of < 110 > stress. In Appendix 10.2 it is shown, as is indicated in Figure 4.6, that valleys 1, 2, 4, and 5 have an effective mobility of

$$\mu = \frac{\mu_\ell + \mu_{t'}}{2} \tag{4.21}$$

in the direction of the < 110 > stress and electric field. Valleys 3 and 6 have a mobility μ_t in the < 110 > direction. Now τ_ℓ is given by equation 4.13 and τ_t by equation 4.16. Therefore equations 4.15, 4.19, and 4.20 also hold for a < 110 > stress. The relaxation time $\tau_{t'}$ may be written as

$$\frac{1}{\tau_{t'}} = \frac{1}{\tau_{A_t}} + \frac{1}{\tau_{ii}} + \frac{1}{\tau_{f'}} + \frac{1}{\tau_{I_t}} \tag{4.22}$$

The comparison between $< \tau_{t'} >$ and $< \tau_{t_o} >$ is

$$\frac{< \tau_{t'} >}{< \tau_{t_o} >} > 1 , \tag{4.23}$$

since $\tau_{f_o} > \tau_{f'}$. It also follows that

$$\frac{< \tau_{t'} >}{< \tau_t >} > 1 . \tag{4.24}$$

Under the above assumptions concerning the acoustic scattering relaxation times τ_{A_ℓ} and τ_{A_t}, it also may be seen that

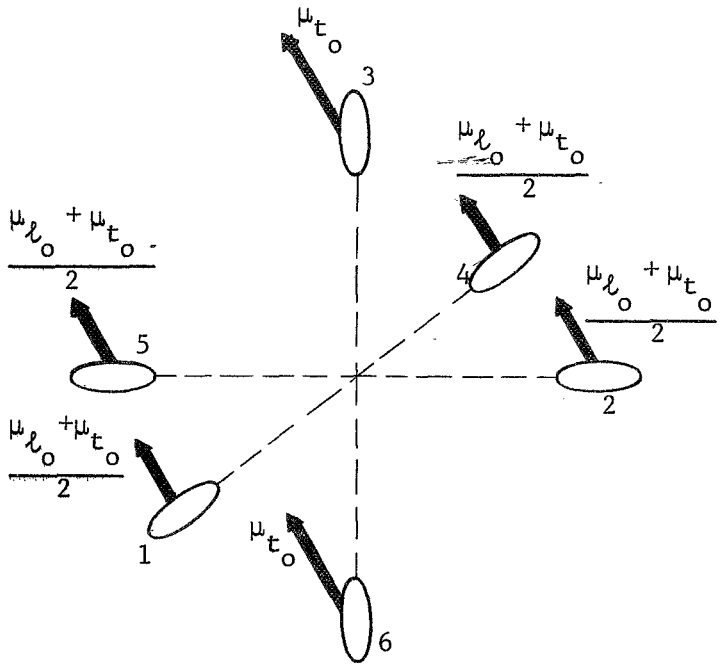

zero stress

$$\mu_{\ell_o} = \frac{q < \tau_{\ell_o} >}{m_\ell}$$

$$\mu_{t_o} = \frac{q < \tau_{t_o} >}{mt}$$

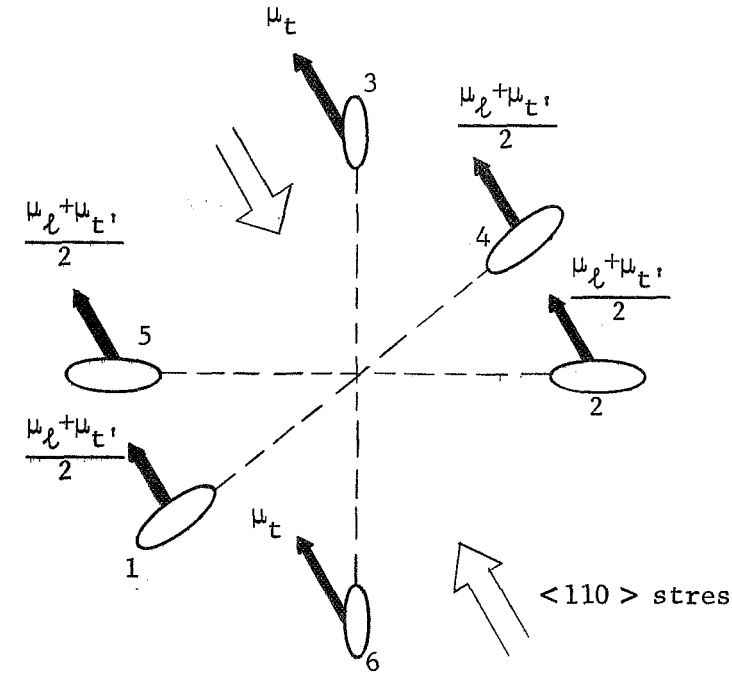

with < 100 > stress

$$\mu_\ell = \frac{q < \tau_\ell >}{m_\ell}$$

$$\mu_t = \frac{q < \tau_t >}{m_t}$$

$$\mu_{t'} = \frac{q < \tau_{t'} >}{m_t}$$

Figure 4.6 Single valley mobilities in the < 110 > lattice direction

$$\frac{<\tau_{\ell}>}{<\tau_{t'}>} > 1 , \tag{4.25}$$

and therefore that

$$<\tau_{\ell}> > <\tau_{t'}> > <\tau_{t}> . \tag{4.26}$$

Stresses in the < 111 > lattice directions should have no effect of first order importance on the various relaxation times. In the above discussion of the effect of stress on mobility, the effect of stress on the various effective masses has been neglected. Wortmann (1964) has shown that the effect of stress on effective mass is negligible unless the shear strain is several percent. This effect then should be entirely negligible in this thesis as the shear strains here do not exceed 0.2 percent.

Also neglected in the above discussion is the effect of stress on the relaxation times $\tau_{I_{\ell}}$ and $\tau_{I_{t}}$ due to ionized impurity scattering. This effect exists because of a small change of the quantities n and N_i in equations 4.7 and 4.6 with stress. However, in comparison with the effect of stress on the f-type intervalley scattering the effect should be negligible.

4.4 Summary

This chapter presented formulas for the relaxation times due to lattice and ionized impurity scattering, which are assumed to be the principal scattering mechanisms determining the relaxation times for the samples studied in this thesis. Also discussed was the use of

these formulas in fitting mobility versus temperature data obtained from experiment.

The effect of stress on mobility due to relaxation time changes with stress was qualitatively assessed in section 4.3. This assessment will be important in the comparison of experiment to theory later. The results of section 4.3 are tabulated in Table 4.1.

Table 4.1 Effect of < 100 > , < 110 > and < 111 > uniaxial compressive stresses on the relaxation times of conduction electrons

	< 100 > stress	< 110 > stress	< 111 > stress
τ_ℓ	increases with increasing stress	increases with increasing stress	no first order effect
τ_t	decreases with increasing stress	decreases with increasing stress	no first order effect
$\tau_{t'}$	-	increases with increasing stress	no first order effect
K_T	increases with increasing stress	increases with increasing stress	no first order effect

5. PIEZORESISTIVITY

5.1 Introduction

Formulas for the piezoresistivity of n-type silicon are developed in this chapter using the results of the two preceding chapters. The formulas developed take into consideration the effect of stress-induced changes in relaxation times on piezoresistivity.

5.2 < 100 > Piezoresistivity in n-Type Silicon

Piezoresistivity in silicon is a tensor property. The fractional change in resistivity tensor, written in six vector form is

$$\frac{\delta\rho_r}{\rho_o} = \frac{\rho_r - \rho_o}{\rho_o} \qquad (r = 1, 6) \ ,$$

where ρ_r is the stressed resistivity and ρ_o the unstressed resistivity. This six vector is related to the stress six vector σ_s (s = 1, 6) by

$$\frac{\delta\rho_r}{\rho_o} = \sum_s \pi_{rs}\sigma_s \qquad \begin{pmatrix} r = 1, 6 \\ s = 1, 6 \end{pmatrix} \ ,$$

where the π_{rs} are called the piezoresistance coefficients. For the present study, this tensor aspect of piezoresistivity is of no practical interest, and here the theory will not be formulated in terms of these piezoresistance coefficients. Instead the piezoresistivity will be defined by equation 5.2. The symbol Π will be retained as the symbol for piezoresistivity, but will appear without numerical subscripts, to distinguish it from the piezoresistance

coefficients. However, the piezoresistivities formulated later in this chapter are related to the π_{rs} by

$$(\rho/\rho_o)\,\Pi = \pi_{11} \qquad (< 100 > \text{stress})$$

$$(\rho/\rho_o)\,\Pi = \frac{1}{2}\,(\pi_{11} + \pi_{12} + \pi_{44}) \qquad (< 110 > \text{stress})$$

$$(\rho/\rho_o)\,\Pi = \frac{1}{3}\,(\pi_{11} + 2\pi_{12} + 2\pi_{44}) \qquad (< 111 > \text{stress}) \ .$$

Let attention now be turned to a consideration of the effect of a $< 100 >$ compressive stress on the resistivity of an n-type silicon sample.

Consider the n-type silicon sample shown in Figure 5.1. This sample is oriented with its longitudinal axis parallel to a $< 100 >$ lattice direction. The electric field $\vec{\epsilon}$ and the stress χ are applied in this $< 100 >$ direction.

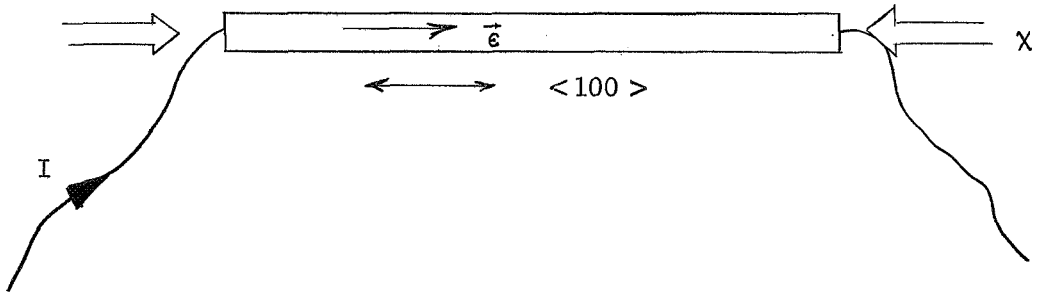

Figure 5.1 $< 100 >$ n-type silicon sample

The resistivity of this sample, in terms of the electron populations and mobilities of the individual conduction band minima, is

$$\frac{1}{\rho} = \sigma = \sum_{i=1}^{6} q n_c^{(i)} \mu^{(i)} , \tag{5.1}$$

where ρ is resistivity, σ is conductivity, and q is the magnitude of the charge of an electron. The concentration of electrons in the i^{th} conduction band minimum is denoted by $n_c^{(i)}$, and $\mu^{(i)}$ is the mobility in the $< 100 >$ direction of the electrons in this i^{th} minimum. The piezoresistivity Π is defined as

$$\Pi \equiv \frac{\Delta\rho}{\rho\chi} = \frac{\rho - \rho_o}{\rho\chi} , \tag{5.2}$$

where ρ_o is the resistivity with zero applied stress, and ρ is the resistivity with stress χ applied. Since resistivity in silicon is a function of temperature as well as stress, the measurement of both resistivities, ρ and ρ_o, must be made at the same sample temperature to insure that equation 5.2 is meaningful and consistent.

Using equation 5.1 the piezoresistivity may be written

$$\Pi = \left[1 - \frac{\sum_{i=1}^{6} n_c^{(i)} \mu^{(i)}}{\sum_{i=1}^{6} n_{c_o}^{(i)} \mu_o^{(i)}} \right] / \chi , \tag{5.3}$$

with the subscripts o denoting zero stress values. This equation is perfectly general for the piezoresistivity of n-type silicon, if $\mu^{(i)}$

is the mobility of the electrons in the i^{th} conduction band minimum in the direction of the applied electric field.

Now from section 3.5.3, the concentration of electrons in the i^{th} conduction band minimum in the presence of an applied stress is

$$n_c^{(i)} = \frac{N_c}{6} \exp((E_f - \Delta E_i)/kT) \quad . \tag{5.4}$$

From section 3.5.2, in the absence of stress the total conduction band electron concentration n_{c_o} may be expressed as

$$n_{c_o} = N_c \exp(E_{f_o}/kT) \quad , \tag{5.5}$$

then since for zero stress $n_{c_o}^{(i)} = n_{c_o}^{(j)}$ for all $i, j \leq 6$

$$n_{c_o}^{(i)} = n_{c_o}^{(j)} = \frac{n_{c_o}}{6} = \frac{N_c}{6} \exp(E_{f_o}/kT) \tag{5.6}$$

Consider Figure 5.2. Illustrated in this figure are the conductivity contributions $qn_c^{(i)}\mu^{(i)}$ of each of the six conduction band minima of silicon for the case of zero applied stress and for the case of an applied $< 100 >$ stress χ. From this figure it is found that

$$\sigma_o = \frac{1}{\rho_o} = q \sum_{i=1}^{6} n_{c_o}^{(i)} \mu_o^{(i)} = qn_{c_o}\mu_o \tag{5.7}$$

where

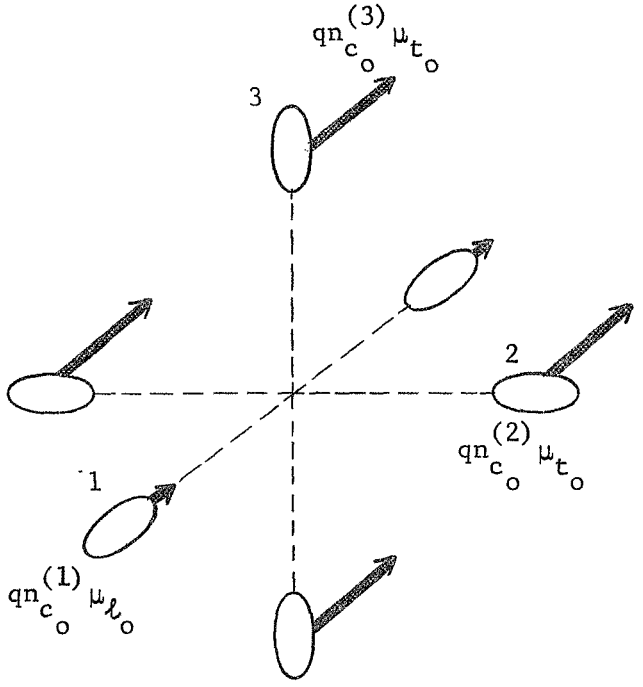

zero stress

$$n_{c_o}^{(i)} = n_{c_o}^{(j)} = n_{c_o}/6$$

$$\sigma_o = \Sigma q n_{c_o}^{(i)} \mu_o^{(i)} = q n_{c_o} \mu_o$$

$$\mu_o = \frac{\mu_{\ell_o} + 2\mu_{t_o}}{3}$$

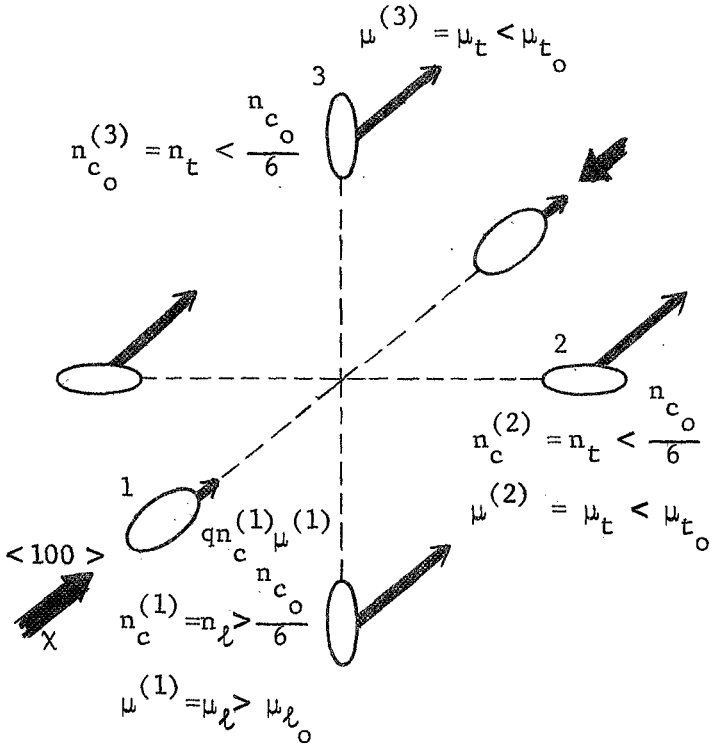

compressive <100> stress

$$\sigma = \Sigma q n_c^{(i)} \mu^{(i)}$$

$$\sigma = 2q(n_\ell \mu_\ell + 2n_t \mu_t)$$

$$n_\ell = n_{c_o} \exp((\delta E_f - \Delta E_1)/kT)$$

$$n_t = n_{c_o} \exp((\delta E_f - \Delta E_2)/kT)$$

Figure 5.2 Single valley mobility contributions in a <100> lattice direction

$$\mu_o = \frac{\mu_{\ell_o} + 2\mu_{t_o}}{3} \quad . \tag{5.8}$$

Also from Figure 5.2

$$\sigma = \frac{1}{\rho} \sum_{i=1}^{6} n_{c_o}^{(i)} \mu^{(i)} = 2q(n_\ell \mu_\ell + 2n_t \mu_t) \tag{5.9}$$

or

$$\sigma = q \frac{N_c}{3} \beta \{ \theta_\ell \mu_\ell + 2\theta_t \mu_t \} , \tag{5.10}$$

where

$$\beta = \exp(E_f/kT) \tag{5.11}$$

and

$$\theta_\ell = \exp(-\Delta E_1,/kT) \tag{5.12}$$

$$\theta_t = \exp(-\Delta E_2/kT) \quad . \tag{5.13}$$

The values of ΔE_1 and ΔE_2 in equations 5.12 and 5.13 are given in Table 3.2 in chapter 3. If equations 5.10, 5.8, and 5.7 are substituted into equations 5.2, the piezoresistivity becomes

$$\Pi = \left[1 - \exp((E_f - E_{f_o})/kT) \frac{\{\theta_\ell \mu_\ell + 2\theta_t \mu_t\}}{(\mu_{\ell_o} + 2\mu_{t_o})} \right] / \chi \, . \tag{5.14}$$

It was shown in chapter 4 that an applied stress affects the relaxation times $< \tau_\ell >$ and $< \tau_t >$. Now since

$$\mu_{\ell} = \frac{q < \tau_{\ell} >}{m_{\ell}} \tag{5.15}$$

and

$$\mu_{t} = \frac{q < \tau_{t} >}{m_{t}} \quad , \tag{5.16}$$

both μ_{ℓ} and μ_{t} are therefore expected to be stress and temperature dependent quantities. Equation 5.14 will now be rewritten in the following form

$$\Pi = (1 - \exp(\delta E_f/kT)\{r_{\ell}\theta_{\ell} + 2r_{t}\theta_{t}\})/\chi \ , \tag{5.17}$$

where the stress-induced shift in the Fermi energy, δE_f, has the value

$$\delta E_f = E_f - E_{f_o} \ , \tag{5.18}$$

and

$$r_{\ell} = \frac{\mu_{\ell}}{\mu_{\ell_o} + 2\mu_{t_o}} = \frac{< \tau_{\ell} >}{< \tau_{\ell_o} > + \frac{2m_{\ell}}{m_t} < \tau_{t_o} >} \tag{5.19}$$

$$r_{t} = \frac{\mu_{t}}{\mu_{\ell_o} + 2\mu_{t_o}} = \frac{(m_{\ell}/m_{t}) < \tau_{t} >}{< \tau_{\ell_o} > + \frac{2m_{\ell}}{m_t} < \tau_{t_o} >} \ . \tag{5.20}$$

In chapter 7 equation 5.17 will be curvefitted to the experimental

piezoresistivity data using r_ℓ and r_t as the unknown parameters. The quantities θ_ℓ and θ_t are presumably accurately given by equations 5.12 and 5.13 as the applied stress χ is measured experimentally. The stress-induced shift in the Fermi energy, δE_f, may also be determined from the equations given in sections 3.5.2 and 3.5.3 as long as N_A, N_D, and N_E are known. These doping concentrations may be determined from experimental Hall coefficient data.

5.3 Piezoresistivity in Uncompensated n-Type Silicon

Let attention now be restricted to the special case of uncompensated (for this work, unirradiated) n-type silicon. Under the assumptions discussed in section 3.3, the concentration of conduction band electrons will be constant and independent of both temperature and stress for these samples. Then from section 5.2

$$\sigma_o = q\, n_{c_o} \left\{ \frac{\mu_{\ell_o} + 2\mu_{t_o}}{3} \right\} \tag{5.21}$$

and

$$\sigma = q\, N_c \exp(E_f/kT) \{\theta_\ell \mu_\ell + 2\theta_t \mu_t\} / 3 \tag{5.22}$$

so that

$$\sigma = q\, N_c \exp(E_{f_o}/kT) \exp(\delta E_f/kT) \{\theta_\ell \mu_\ell + 2\theta_t \mu_t\} / 3 \tag{5.23}$$

$$\sigma = q\, n_{c_o} \exp(\delta E_f/kT) \{\theta_\ell \mu_\ell + 2\theta_t \mu_t\} / 3 \tag{5.24}$$

and

$$\sigma = q\, n_{c_o} \mu_{eff} \,, \tag{5.25}$$

where

$$\mu_{eff} = \exp(\delta E_f / kT)\, \frac{\{\theta_\ell \mu_\ell + 2\theta_t \mu_t\}}{3} \tag{5.26}$$

Equations 5.25 and 5.26 make it clear that piezoresistivity in uncompensated n-type silicon is due to a stress induced change in the effective macroscopic mobility of conduction electrons (so long as no donor deionization occurs). In fact, the piezoresistivity in this case may also be written

$$\Pi = \left(1 - \frac{\mu_{eff}}{\mu_o} \right) / \chi \quad . \tag{5.27}$$

Piezoresistivity in the limit of zero applied stress will now be examined to demonstrate the importance of stress-induced changes in intervalley scattering rates in determining piezoresistivity. Equation 5.2, in terms of conductivity, is

$$\Pi = \frac{\sigma_o - \sigma}{\sigma_o \chi} = - \frac{\Delta \sigma}{\sigma_o \chi} \tag{5.28}$$

and in the limit as $\chi \to o$ becomes

$$\lim_{\chi \to o} \Pi = \Pi_o = - \frac{1}{\sigma} \frac{d\sigma}{d\chi} \,, \tag{5.29}$$

where the subscript o indicates zero stress. Substitution of equation 5.25 into equation 5.29 yields

$$\Pi_o = - \frac{1}{qn_{c_o}\mu_o} \frac{d(qn_{c_o}\mu_{eff})}{d\chi} \tag{5.30}$$

$$\Pi_o = - \frac{1}{\mu_o} \frac{d\mu_{eff}}{d\chi} \quad , \tag{5.31}$$

since the total number of conduction band electrons n_{c_o} is assumed independent of χ. Now

$$\frac{d\mu_{eff}}{d\chi} = 1/3 \{ \mu_{\ell_o} \frac{d(\theta_\ell \beta_f)}{d\chi} + 2\mu_{t_o} \frac{d(\theta_t \beta_f)}{d\chi} + \frac{d\mu_{\ell_o}}{d\chi} + \frac{2d\mu_{t_o}}{d\chi} \} \tag{5.32}$$

where $\beta_f = \exp(\delta E_f/kT)$. It is found that

$$\frac{d(\theta_\ell \beta_f)}{d\chi} = \frac{(\delta E_f - \Delta E_1)}{kT} \theta_\ell \beta_f = \frac{(\delta E_f - \Delta E_1)}{kT} \tag{5.33}$$

and

$$\frac{d(\theta_t \beta_f)}{d\chi} = \frac{(\delta E_f - \Delta E_2)}{kT} \theta_t \beta_f = \frac{(\delta E_f - \Delta E_2)}{kT} \quad , \tag{5.34}$$

since θ_ℓ, θ_t, and β_f all approach unity as χ approaches o. For small χ it is found that

$$\delta E_f = \frac{\Delta E_1 + 2\Delta E_2}{3} \quad , \tag{5.35}$$

so that

$$\frac{d\mu_{eff}}{d\chi} = \frac{1}{3}\left\{ \frac{2\mu_{\ell_o}}{3kT}(\Delta E_2 - \Delta E_1) + \frac{2\mu_{t_o}}{3kT}(\Delta E_1 - \Delta E_2) + \frac{d\mu_{\ell_o}}{d\chi} + \frac{2d\mu_{t_o}}{d\chi} \right\} \quad . \tag{5.36}$$

From equation 3.3 and Appendix 10.1,

$$\Delta E_1 = \Xi_u e_1 = \Xi_u s_{11} \chi \tag{5.37}$$

$$\Delta E_2 = \Xi_u e_2 = \Xi_u s_{12} \chi \tag{5.38}$$

and equation 5.31 becomes

$$\Pi_o = \frac{2\,\Xi_u (s_{12} - s_{11})}{9kT}\left\{ \frac{\mu_{\ell_o}}{\mu_o} - \frac{\mu_{t_o}}{\mu_o} \right\} - \frac{1}{\mu_o}\frac{d\mu_o}{d\chi} \quad . \tag{5.39}$$

The first term in this equation is the piezoresistivity due to population transfer only, while the second term is due to the effect of stress on the relaxation times. In fact this second term can be written as

$$\Pi_o^{(\tau)} = -\frac{1}{\mu_o}\frac{d\mu_o}{d\chi} = -\frac{1}{\langle \tau \rangle_{eff}}\frac{d\langle \tau \rangle_{eff}}{d\chi} \tag{5.40}$$

where

$$\langle \tau \rangle_{eff} = \frac{\langle \tau_\ell \rangle + 2K_m \langle \tau_t \rangle}{3} \tag{5.41}$$

and

$$K_m = m_\ell/m_t = 4.69.$$

Now the importance of $\Pi_o^{(\tau)}$ will be estimated by comparing experimental values for Π_o with the value predicted by the population transfer term in equation 5.39 alone. At T = 298°K this population transfer term has the value

$$\Pi_o^{(pt)} = -\frac{2\Xi_u(s_{12} - s_{11})}{3kT(1 + 2K_{\mu_o})}\{1 - K_{\mu_o}\}$$

$$= -0.835 \times 10^{-10} \text{ cm}^2/\text{dyne} \qquad (5.42)$$

if Balslev's value for Ξ_u is used, and the effective mass anisotropy $K_m = 4.69$ is used for the value of $K_{\mu_o} = \mu_{t_o}/\mu_{\ell_o}$. The quantity $\Pi_o^{(pt)}$ is a function of K_{μ_o} and hence depends on the value of the relaxation time anisotropy $K_{\tau_o} = \langle \tau_{\ell_o} \rangle / \langle \tau_{t_o} \rangle$ since

$$K_{\mu_o} = K_m/K_{\tau_o} = 4.69 \langle \tau_{t_o} \rangle / \langle \tau_{\ell_o} \rangle . \qquad (5.43)$$

Therefore $\Pi_o^{(pt)}$ depends implicitly on sample doping, as doping affects the values of $\langle \tau_{\ell_o} \rangle$ and $\langle \tau_{t_o} \rangle$ through impurity scattering effects.

For most unstressed samples, it is doubtful that K_{τ_o} will be much greater than 1.25 or much less than 0.75, and for these values of K_{τ_o}, $\Pi_o^{(pt)}$ has the values

$$\Pi_o^{(pt)} = -0.76\times10^{-10} \text{ cm}^2/\text{dyne} \quad (K_{T_o} = 1.25)$$

$$\Pi_o^{(pt)} = -0.910\times10^{-10} \text{ cm}^2/\text{dyne} \quad (K_{T_o} = 0.75)$$

at $T = 298^oK$.

In Table 5.1, a theoretical value for $\Pi_o^{(pt)}$ is compared to various experimental values obtained for Π_o. Since $\Pi_o = \Pi_o^{(pt)} + \Pi_o^{(T)}$, the importance of $\Pi_o^{(T)}$ may be deduced from this table. From the values recorded in this table, it appears that $\Pi_o^{(T)}$ is equal to approximately 10 percent to 20 percent of $\Pi_o^{(pt)}$. The piezoresistivity due to $\Pi_o^{(T)}$, like that due to $\Pi_o^{(pt)}$, depends upon sample doping, and in fact should decrease with increased doping. This is because the relative importance of intervalley scattering (the only type scattering presumed to be affected by stress) decreases as scattering by ionized impurities increases. Thus it is impossible to precisely estimate the importance of $\Pi_o^{(T)}$, as this quantity will vary from sample to sample. However, the rough estimate just given should be close.

Long's model for electron mobility, discussed in chapter 4, may also be used to demonstrate the importance of $\Pi_o^{(T)}$. If Long's model is fitted to empirically derived mobility versus temperature data, and sample doping is known (and nondegenerate) then μ_{eff} versus stress may be calculated. From this curve of μ_{eff} versus χ, $\frac{d\mu_{eff}}{d\chi}$ may be calculated graphically. This procedure was carried out (see chapter 7) for one < 100 > unirradiated sample. The results are given in Figure 5.3. For this particular sample, it is found that

$$\Pi_o^{(T)}/\Pi_o^{(pt)} \sim 0.42 \quad (\text{at } T = 298^oK).$$

Table 5.1 Theoretical and experimental values for piezoresistivity ($\times 10^{-10}$ cm^2/dyne) at T = 298°K

$\Pi_o^{(pt)}$	Π_o	Reference	Resistivity (ohm-cm)	Apparent Value of $\Pi_o^{(\tau)}/\Pi_o^{(pt)}$
-0.835	-1.02	Smith (1954)	11.7	0.22
-0.835	-0.850	Morin et al. (1957)	5.0	0.018
-0.835	-1.06	Gross (1967)	1.0	0.27
-0.835	-0.99	Gross (1967)	0.1	0.18
-0.835	-0.94	Gross (1967)	0.045	0.12

The piezoresistivity predicted by equation 5.27 for large stresses will be compared to the piezoresistivity of an irradiated sample in section 5.4. In chapter 7 equation 5.17 will be curve-fitted to experimental piezoresistivity data obtained on an un-irradiated sample. This curvefitting procedure will illustrate the effect of large stresses on the relaxation time $< \tau_\ell >$ and $< \tau_t >$.

5.4 Piezoresistivity in Compensated n-Type Silicon

Donor compensation not only has a great effect on the resistivity of n-type silicon, but can also have a large effect on the piezo-resistivity of such material. The effect on the piezoresistivity due to compensation also occurs in uncompensated material if the sample temperature is low enough for donor deionization to be important.

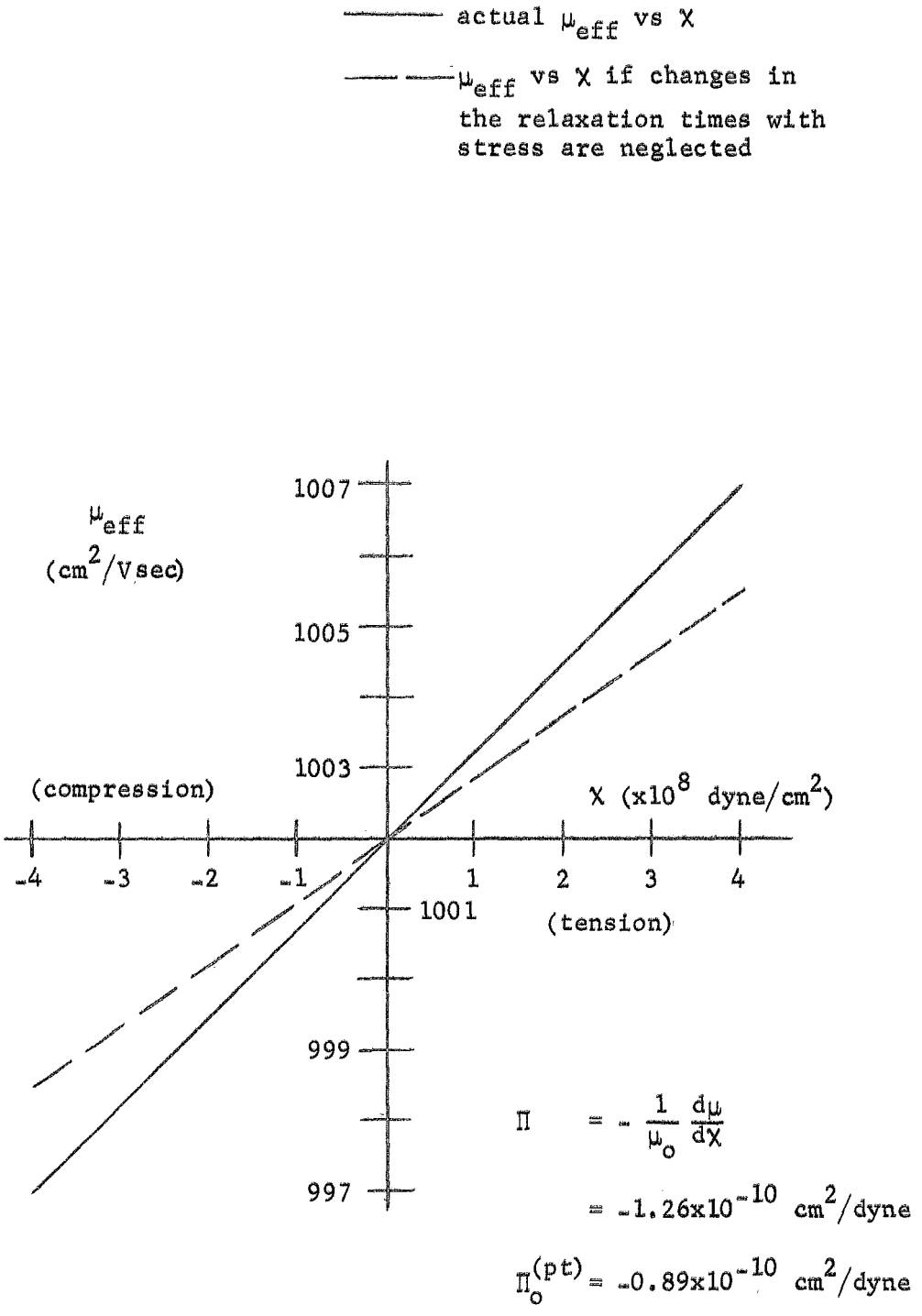

Figure 5.3 Effective mobility as a function of stress for small stresses

These temperatures, however, are quite low for uncompensated n-type silicon. Basically, piezoresistivity in compensated silicon (or in uncompensated silicon at very low temperatures) is different from the piezoresistivity of uncompensated silicon (at high temperatures) due to the fact that the total conduction band electron concentration in this material varies with stress as well as with temperature.

Consider the piezoresistivity of compensated n-type silicon in the limit as the applied stress χ approaches zero. Since the total conduction band electron concentration, n_c, as well as the effective mobility μ, varies with stress, the piezoresistivity, Π_o', may be written as

$$\Pi_o' = -\frac{1}{\sigma}\frac{d\sigma}{d\chi} = -\frac{1}{qn_c\mu}\frac{d(qn_c\mu)}{d\chi} \tag{5.44}$$

or

$$\Pi_o' = -\frac{1}{\mu}\frac{d\mu}{d\chi} - \frac{1}{n_c}\frac{dn_c}{d\chi} \quad , \tag{5.45}$$

or finally

$$\Pi_o' = \Pi_o + \Pi_o^{(n)} \tag{5.46}$$

where

$$\Pi_o^{(n)} \equiv -\frac{1}{n_c}\frac{dn_c}{d\chi} \quad . \tag{5.47}$$

The quantity Π_o is the piezoresistivity of uncompensated silicon at high temperatures as derived in section 5.3. The additional term, $\Pi_o^{(n)}$, in equation 5.47 is due to the variation of n_c with stress.

The effect on piezoresistivity due to variation of n_c with stress may also be algebraically illustrated for the case of nonzero applied stress. For an uncompensated n-type sample of arbitrary orientation, the piezoresistivity, Π, is

$$\Pi = (1 - \exp(\delta E_f/kT)F(\chi,T))/\chi \ , \tag{5.48}$$

where

$$F(\chi,T) = \frac{\sum_{i=1}^{6} \exp(-\Delta E_i/kT)\mu^{(i)}}{\mu_o} \ . \tag{5.49}$$

The quantities $\mu^{(i)}$ and μ_o are defined in section 5.2, and ΔE_i is defined in chapter 3. The stress-induced shift in the Fermi energy, δE_f, is determined by

$$\exp(\delta E_f/kT) = \frac{1}{\sum_{i=1}^{6} \exp(-\Delta E_i/kT)} \tag{5.50}$$

The factor $F(\chi,T)$ in equation 5.48 is a function of sample orientation since both the ΔE_i and the $\mu^{(i)}$ depend upon the orientation of the sample with respect to the crystal lattice axes (see Appendices 10.1 and 10.2).

The piezoresistivity, Π', of a compensated sample may be written

$$\Pi' = (1 - \exp(\delta E_f'/kT)F'(\chi,T))/\chi \ , \tag{5.51}$$

with

$$\exp(\delta E_f'/kT) = \exp(\delta E_f/kT)\ \frac{n_c}{n_{c_o}}\ , \tag{5.52}$$

where n_{c_o} is the total conduction band electron concentration with zero stress, and n_c is the concentration in the presence of applied stress χ. Compensation has only a small effect on $F(\chi,T)$, therefore it is permissible to assume that $F'(\chi,T) = F(\chi,T)$. Under this assumption, Π' may be expressed in terms of Π as

$$\Pi' = \Pi + \exp(\delta E_f/kT)\left(1 - \frac{n_c}{n_{c_o}}\right)F(\chi,T)/\chi\ . \tag{5.53}$$

The sign of the additional term, in both equation 5.46 and equation 5.53, which is due to variation of n_c with stress, depends upon whether n_c increases or decreases with stress. To accurately assess the effect of stress on n_c, the detailed splitting of all electrically important defect levels, as well as the splitting with stress of the conduction band edge, must be taken into consideration (see chapter 3). For the sign convention used here, Π in equation 5.53 is negative. The sign of the second term in equation 5.53 is positive if $n_c > n_{c_o}$, and is negative if $n_c < n_{c_o}$.

Donor compensation was produced in the samples studied in this thesis by bombarding them with high energy electrons. This irradiation produced Si-A center and Si-E center acceptor levels that greatly affected both the resistivity and piezoresistivity of these samples. To graphically illustrate the effect that compensation (such as that produced by electron irradiation) has on piezoresistivity, the following hypothetical example will be considered.

The piezoresistivity, for $\chi = -2\times10^{9}$ dynes/cm^2, of each of the following hypothetical < 100 > oriented samples was computed using equation 5.17 and the results of chapter 3:

Sample U : $N_D = 10^{15}\text{cm}^{-3}$; $N_A = 0$

Sample I1: $N_D = 10^{15}\text{cm}^{-3}$

$N_A = 5\times10^{15}\text{cm}^{-3} = 5N_D$

Sample I2: $N_D = 10^{15}\text{cm}^{-3}$

$N_A = 10^{16}\text{cm}^{-3} = 10N_D$

Sample I3: $N_D = 10^{15}\text{cm}^{-3}$

$N_A = 2\times10^{16}\text{cm}^{-3} = 20N_D$.

N_D is the donor concentration, and N_A is the Si-A center acceptor concentration. In performing the calculations it was assumed that the effect of stress on the Si-A center is correctly described by the model discussed in section 3.4.3 for all three irradiation levels. The effect of stress on the relaxation times was neglected, and the values

$$r_{\ell} = \frac{1}{1+2K_m} = \frac{1}{10.38}$$

$$r_t = \frac{K_m}{1+2K_m} = \frac{4.69}{10.38}$$

were used in equation 5.17. These values correspond to assuming

that

$$\frac{<\tau_\ell>}{<\tau_t>} = \frac{<\tau_\ell>}{<\tau_{\ell_o}>} = \frac{<\tau_t>}{<\tau_{t_o}>} = 1 \ .$$

Figure 5.4 shows that the irradiation produced A-centers reduce the piezoresistivity at the lower temperatures, while having only a small effect on the piezoresistivity at the higher temperatures. The experimental data obtained agrees qualitatively with the curves shown in this figure, as will be seen in chapter 7.

5.5 Piezoresistivity as a Function of Stress

It is well known that for small stresses (less than $\sim 10^8$ dynes/cm^2) the piezoresistivity is linear with stress. However, for large stresses nonlinearity with stress is observed. The approximate stress dependence of piezoresistivity may be calculated using equation 5.17 and the assumptions made in section 5.4 concerning the relaxation times. This calculation was carried out for an unirradiated n-type sample, doped with $N_D = 10^{15}$cm^{-3} donors, for $T = 300^oK$. The results are shown in Figure 5.5.

5.6 Piezoresistivity for < 110 > and < 111 > Orientations

The formulas for the piezoresistivity for the < 110 > and < 111 > orientations may be derived using Appendix 10.2 and chapter 3. For a < 110 > sample it is found that

$$\Pi = (1 - \exp(\delta E_f/kT)\{(r_\ell + r'_t)\theta_{\ell t} + r_t\theta_t\})/\chi \ , \qquad (5.54)$$

where r_ℓ and r_t are defined by equations 5.19 and 5.20 respectively,

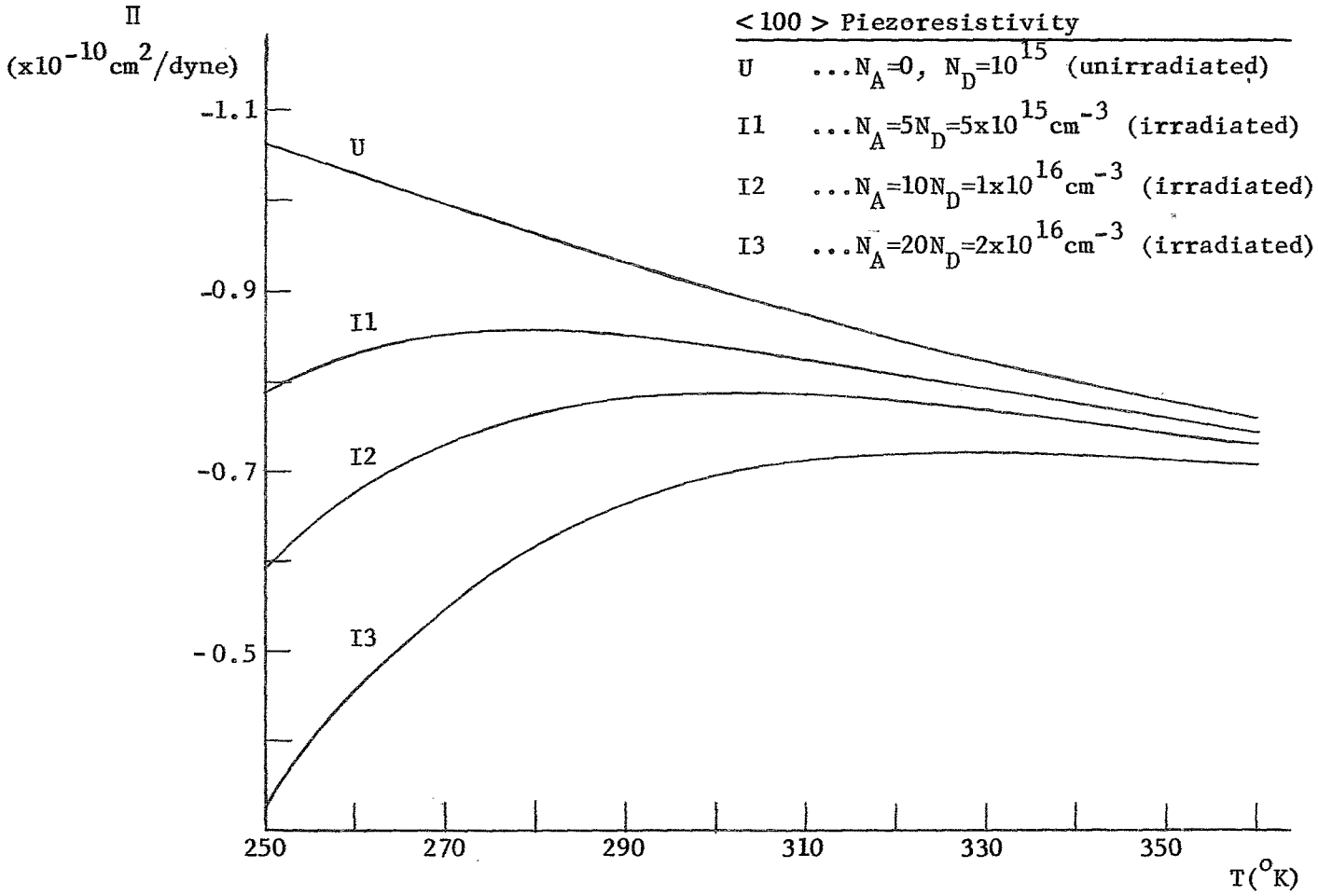

Figure 5.4 Effect of the silicon-A center on piezoresistivity

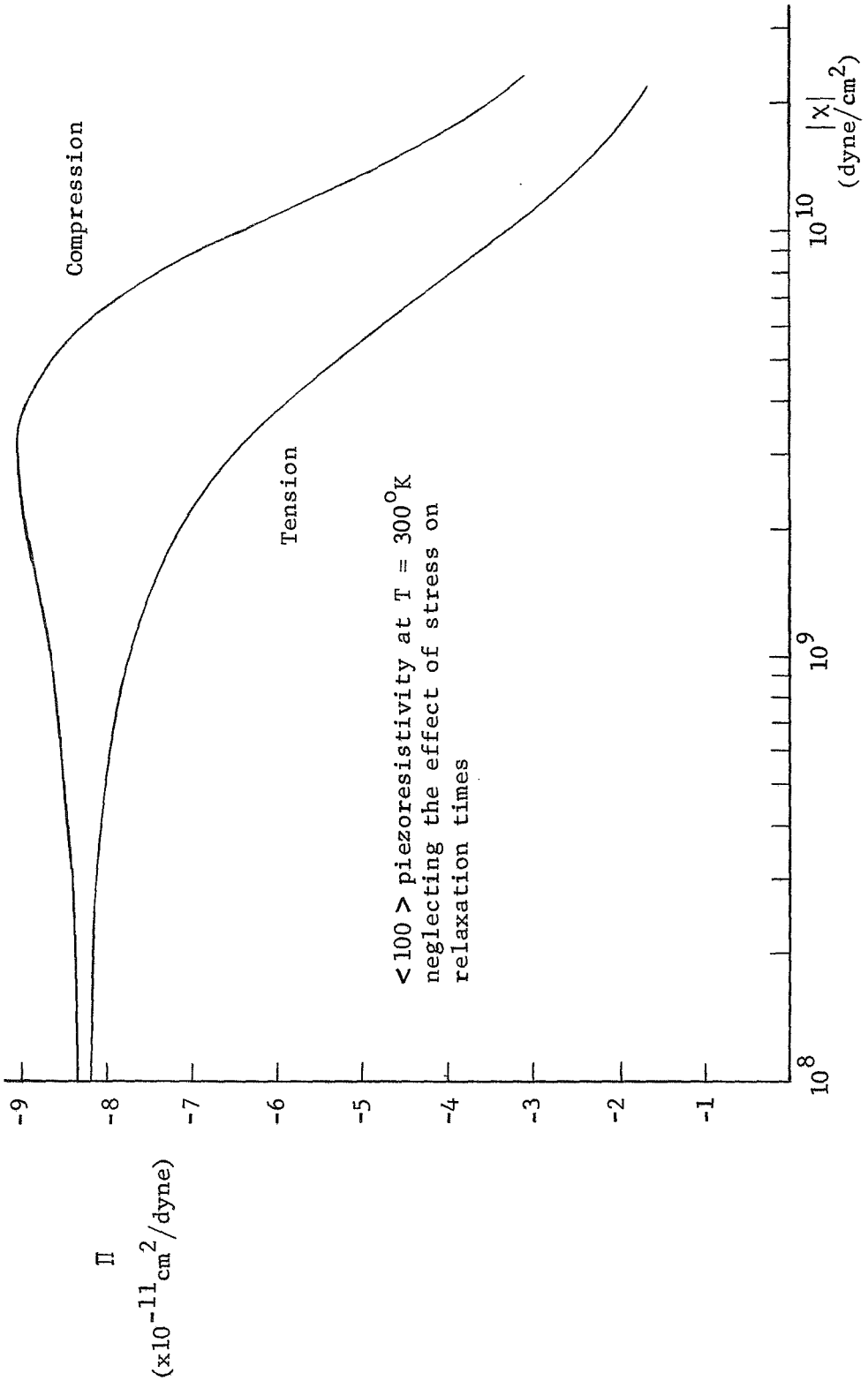

Figure 5.5 Theoretical piezoresistivity versus stress

and

$$\theta_{\ell t} = \exp(-\Delta E_1/kT) \tag{5.55}$$

$$\theta_{t} = \exp(-\Delta E_3/kT) \tag{5.56}$$

with ΔE_1, and ΔE_3 given by Table 3.2. The quantity $r_{t'}$ is defined by

$$r_{t'} = \frac{\mu_{t'}}{\mu_{\ell_o} + 2\mu_{\tau_o}} = \frac{K_m \langle \tau_{t'} \rangle}{\langle \tau_{\ell_o} \rangle + 2K_m \langle \tau_{t_o} \rangle} \tag{5.57}$$

where $\tau_{t'}$ is a relaxation time for scattering from a lower to an upper valley in a direction perpendicular to the ellipsoid axis of the lower valley (see section 4.3).

For a <111> sample it is found that

$$\Pi = (1 - \exp(\delta E_f/kT))/\chi \ . \tag{5.58}$$

Piezoresistivity for a <111> sample has this simple form since for a <111> stress there is no stress-induced energy shift between the conduction band minima (see Table 3.2). Since there is no relative shift between the conduction band minima, a <111> stress is presumed to have a negligible effect on the relaxation times, that is

$$\mu_{\ell} = \mu_{\ell_o}$$

$$\mu_{t} = \mu_{t_o}$$

for a <111> stress. Equations 5.54 and 5.58 will be fitted to experimental data in chapter 7.

5.7 Summary

In this chapter, a general formula for the piezoresistivity of a <100> n-type silicon sample was developed. Effects due to stress-induced relaxation time changes were included in this formulation. Piezoresistivity in unirradiated (uncompensated) silicon was then discussed, and an attempt was made to evaluate the importance of stress-induced changes in relaxation times in determining piezoresistivity. Next the effect of irradiation-produced defects on piezoresistivity was considered, and this effect was graphically illustrated by comparing the predicted piezoresistivity of irradiated samples with that of an unirradiated sample. The stress dependence of piezoresistivity at $T = 300^{o}K$ was computed to illustrate the nonlinearity of Π for large stresses. Finally, the formulas for <110> and <111> piezoresistivity were presented.

6. EXPERIMENTAL PROCEDURES

6.1 Introduction

The object of the experimental phase of this study is experimental data for piezoresistivity as a function of temperature. In addition Hall coefficient data must be obtained in order to accurately determine the various impurity concentrations in the samples studied. The equipment and measurement techniques required to make the measurements necessary to obtain these data are described in sections 6.4 and 6.5 respectively. First of all, however, the procedures used to prepare the silicon samples used in this work are described.

6.2 Sample Preparation

In this study piezoresistivity and Hall coefficient data were obtained on n-type silicon samples of three different crystallographic orientations ($<100>$, $<110>$, and $<111>$). Both unirradiated and electron-irradiated samples were studied. The sample configuration used was that of a standard bridge type Hall sample with six side arms (see Figure 6.3). These samples were cut from single crystal ingots of phosphorus-doped silicon, grown by the Czochralski method and purchased from General Diode Corporation. The samples were prepared according to the following procedure.

The end surfaces of the ingots were lapped using 100 grit silicon carbide powder and were then etched for two minutes at $100^{\circ}C$ in a 10 percent by weight NaOH aqueous solution. This preferential etch reveals etch pits on the end surfaces of the ingot which are necessary

for ingot orientation by optical goniometry. The ingots were oriented using a Micromech Optical Goniometer. Immediately after ingot orientation, wafers were cut from the ingot using a Micromech Precision Wafering Machine with a 220 grit diamond blade. The wafers were cut by first cutting a reference plane in the ingot, and then wafering by cuts made perpendicular to this reference plane. Each resulting wafer had a reference edge, and this edge was later used in cutting the Hall samples from the wafers. The ingots were mounted on ceramic tile using glycol phthalate wax throughout the orientation and wafering procedures.

After removing the glycol phthalate wax from the wafers with acetone, the wafers were lapped on plate glass using 400 grit silicon carbide powder. This lapping procedure removed most of the surface damage due to the diamond saw. An additional lapping using 800 grit silicon carbide powder gave the wafers a smooth finish for a later chemical polishing etch. Care was taken in these lapping steps to keep the wafer surfaces parallel to each other and to their original (unlapped) surfaces.

Bridge type Hall samples were cut from these wafers using a Sheffield Sonipak ultrasonic cutter. The cutting tool was accurately aligned using the reference edge on the wafer as a guide. The resulting samples were 600 mils in length with a cross section approximately 79 mils square. The side arms of the samples were spaced approximately 150 mils apart. The long axis (600 mil) of each of these samples was parallel to either the $<100>$, $<110>$, or $<111>$ lattice direction. The approximate angular alignment error in the orientation of these samples was about 2^{o} or 3^{o}.

Next these samples were cleaned, using the following procedure:

1. Rinse with distilled water.
2. Boil in "Micro" cleaning solution for several minutes.
3. Boil 5 minutes in acetone.
4. Boil 5 minutes in methanol.

The samples were removed from the methanol with tweezers and dried with a jet of nitrogen gas, and then were immediately placed in a 95 percent HNO_3 - 5 percent HF polishing etch. After approximately two minutes in etch, the surface of the sample became shiny. At this point the etch was diluted, and the sample was removed and rinsed with distilled water. This polish etch left the samples with smooth reflecting surface areas.

The next step in the preparation of the samples was the nickel plating of the electrical contact areas of the sample. Prior to plating, however, these contact areas were sandblasted to insure good plating. The samples then had to be thoroughly cleaned before plating. They were washed thoroughly using an artist's brush and alconox detergent, and then rinsed in both plain and distilled water. They were then boiled in acetone for five minutes. Samples were then removed from the acetone and held in the air until they were dry. Immediately upon drying, the samples were placed in an electroless nickel plating solution developed by Sullivan and Eigler (1957). The samples were plated for approximately two minutes at $90^{o}C$ and were then removed and rinsed with distilled water.

The plating step covered the entire surface of the samples with nickel plate. The following technique was used to remove the nickel

plate from the noncontact areas of the samples. The contact areas were painted with apiezon wax dissolved in trichlorethylene. After the trichlorethylene evaporated, leaving only the hard apiezon wax on the contacts, the samples were placed in a 95 percent HNO_3 - 5 percent HF etch. This etch removed the nickel plate from the noncontact areas of the sample, while the apiezon wax insulated the nickel plate on the contact areas from the etch. As soon as the nickel plate had been removed, the etch was diluted and the sample was removed and rinsed with distilled water. The samples were then soaked in trichlorethylene to remove the apiezon wax on the contacts. After this the samples were rinsed with distilled water, and sample preparation was complete.

The nickel plate contacts on the samples were tested for ohmicity using a Tektronix Type 575 Transistor Curve Tracer. All samples with nonohmic contacts were rejected and were not studied.

6.3 Sample Irradiation

Next, some of the samples were irradiated with high energy electrons. This irradiation was carried out in the Space Radiation Effects Laboratory located near the NASA facilities at Langley Research Center. A linear accelerator was the primary source, and energies in the range 1-10 MeV were used depending on the sample resistivity. It is usually necessary to irradiate the samples to an accumulated dosage such that the total number of irradiation-produced defects is approximately equal to the number of donors in the n-type silicon samples. Thus defect concentrations in the 10^{15}-10^{17} defects $/cm^3$ range were required for the samples studied here. A given

sample required from ten minutes to several hours exposure depending on its resistivity and the electron beam energy.

Electron irradiation produces several different types of defects in n-type silicon. Fortunately, for the samples studied here, only the Si-A center and the Si-E center are expected to have an influence on the sample resistivity in the experimental temperature range obtained. The Si-A center is the defect producing the effect which is to be observed in these experiments, and it would simplify the theoretical analysis if the Si-E center were not present. The annealing stage of the E-center occurs at a much lower temperature than that of the A-center, and thus the E-center should be removed by an appropriate annealing procedure without affecting the A-center concentration. All irradiated samples were annealed at $350^{o}F$ for approximately 12 hours in order to remove the E-center damage.

After annealing, the temperature coefficient of sample resistance (dR/dT) was checked on a Tektronix Type 575 Transistor Curve Tracer. This was done by observing the V-I characteristic of the sample while increasing the power level to the point where Joule heating occurs. The change in the slope of the V-I curve is an indication of the temperature coefficient of resistance. A properly irradiated sample should have a small negative temperature coefficient of resistivity at room temperature and the samples were tested using this as the criterion.

Twenty-five samples of the various orientations were irradiated. The experimental data was obtained by measurements made on certain samples out of this group.

6.4 Equipment

In addition to the equipment used to make the electrical measurements (described in section 6.5), the experimental work required only a dewar and a device for stressing the samples. A cross section of the dewar used is shown in Figure 6.1. This figure shows that stress is applied to a sample by means of a hydraulically driven vise. A sample is installed in the dewar in the following manner. Fine copper leads are soldered to four of the side arm tabs as indicated in Figure 6.1, and then the ends of the sample are fitted into epoxy filled, circular flat-bottomed holes cut in two brass discs. A thin (approximately .001 inch thick) mica disc is placed between each brass sample disc and the stainless steel pistons of the vise to provide electrical insulation. All electrical leads are connected, and the epoxy is then cured while the sample is under stress. Phenolic rings hold the brass discs in place during the measurements. By stressing the sample while the epoxy cures, accurate sample alignment is achieved, and maintained by the cured epoxy.

The system used to develop the hydraulic force is illustrated in Figure 6.2. Lead bricks calibrated in weight to an accuracy of 0.1 percent are loaded on the circular loading platform. This platform is connected to a small area (0.25 inch diameter) piston. The diameter of the large piston in the dewar is 1.25 inches giving the hydraulic system a mechanical advantage of 36. One three-pound lead brick on the loading platform develops a stress of about 1.3×10^9 dynes/cm^2 in a typical sample. As indicated in Figure 6.2 the loading platform is rotated. This is done to insure that the small

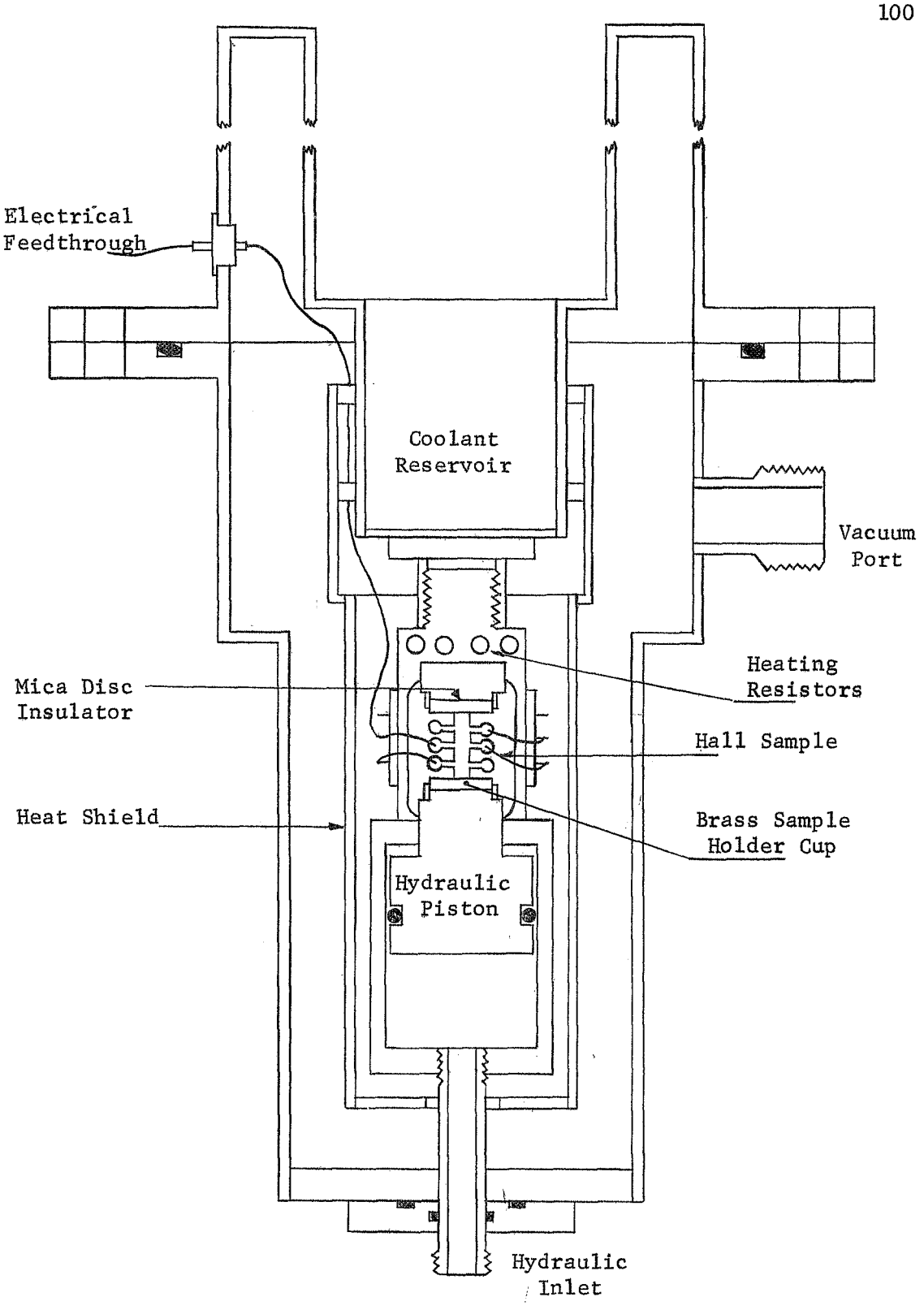

Figure 6.1 The experimental dewar

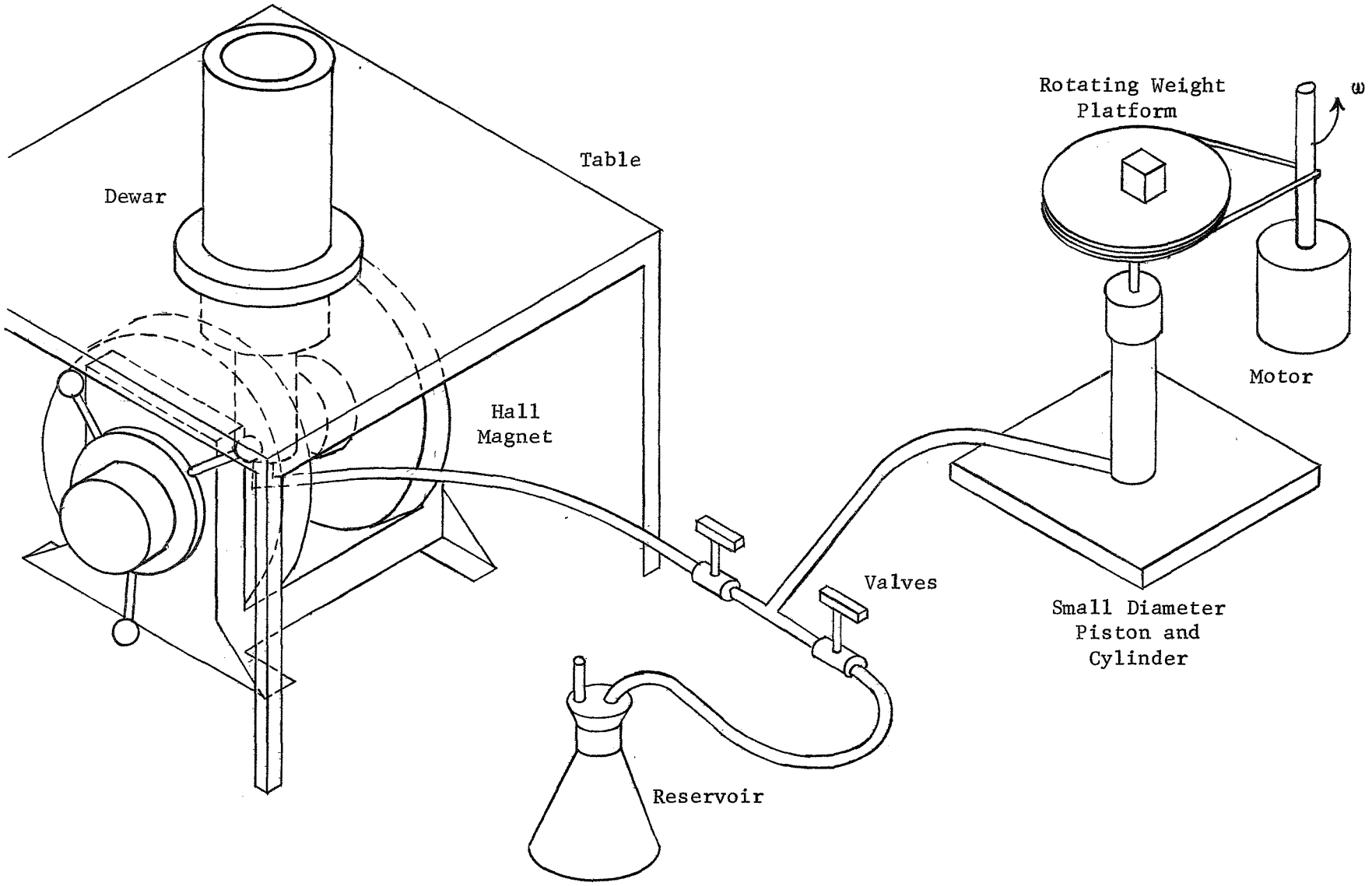

Figure 6.2 The hydraulic system and Hall magnet

piston doesn't stick so that the stress applied to the sample will be maintained constant. The hydraulic fluid used was Gulf Paramount transformer oil.

6.5 Measurement Technique

Piezoresistivity and Hall data was taken using the arrangement diagrammed in Figure 6.3. An 8.1 volt mercury battery was used to supply the sample current in order to keep down the noise in the voltages measured. Typical sample currents were maintained in the one milliampere range to avoid producing high electric fields in the samples. The magnetic flux density used was typically about 2000 gauss. This flux was produced by a Varian four-inch electromagnet and was automatically reversible. In taking the data, the dewar was placed between the poles of the electromagnet and aligned so that the sample was perpendicular to the direction of the magnetic field. Sample current was supplied and the resistivity and Hall voltage signals were amplified by a Keithley Model 140 Nanovolt D.C. Amplifier. The amplified voltages were read from a Doric Integrating Digital Microvoltmeter connected to the output of the amplifier. The sample temperature was monitored by means of a copper-constantan thermocouple mounted on one of the brass sample holder cups.

The sample resistivity was calculated from the voltage measurements using the following formulas.

$$\rho_A = \frac{1}{2}\left[\frac{V_2(+I)}{V_1(+I)} + \frac{V_2(-I)}{V_1(-I)}\right]\frac{R_{std} W_s t_s}{d_1} \text{ ohm cm} \qquad (6.1)$$

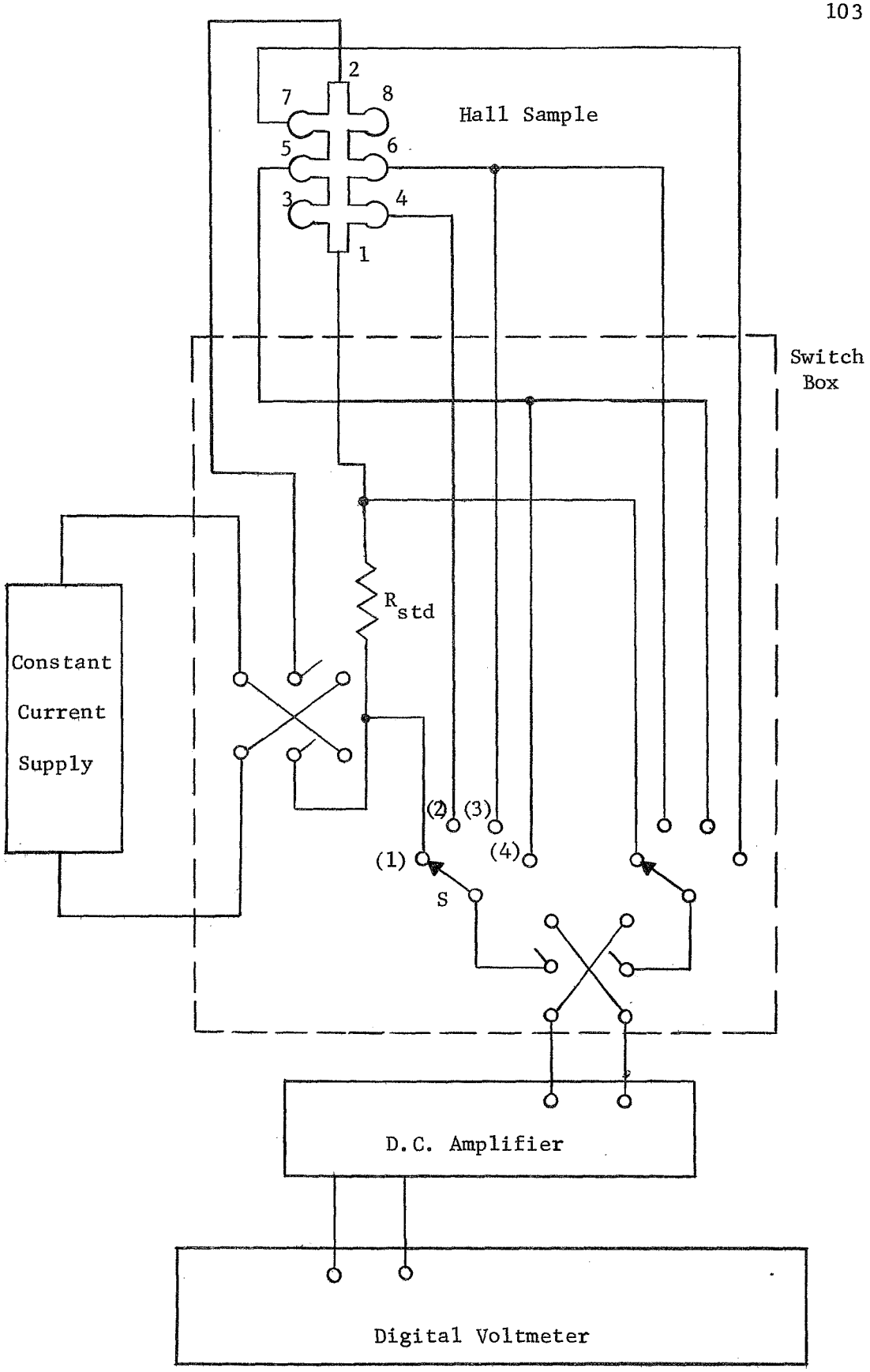

Figure 6.3 The experimental circuit

$$\rho_B = \frac{1}{2}\left[\frac{V_4(+I)}{V_1(+I)} + \frac{V_4(-I)}{V_1(-I)}\right]\frac{R_{std}W_s t_s}{d_2} \text{ ohm cm} \qquad (6.2)$$

$$\rho_{AV} = \frac{1}{2}(\rho_A + \rho_B) \qquad (6.3)$$

In these formulas $V_n(\pm I)$ is the voltage measured with the switch S in Figure 6.3 in position n, R_{std} is the resistance of the standard resistor, W_s the width and t_s the thickness of the sample. The quantity d_1 is the distance between sample tabs 4 and 6, and d_2 the distance between sample tabs 5 and 7. All of these dimensions are expressed in centimeters. $V_n(+I)$ is an algebraic voltage measured when the sample current is positive and $V_n(-I)$ is the same voltage with the sample current reversed.

The Hall coefficient was calculated from the voltage data by the following formula.

$$R_H = 2.50 \times 10^7 \left[\frac{V_3(+I,+B)}{V_1(+I,+B)} + \frac{V_3(-I,+B)}{V_1(-I,+B)} - \frac{V_3(-I,-B)}{V_1(-I,-B)} - \frac{V_3(+I,-B)}{V_1(+I,-B)}\right]\frac{R_{std}t_s}{B} \text{ cm}^3/\text{coulomb} \qquad (6.4)$$

In this equation B is the magnetic flux density in gauss, $V_n(\pm I,+B)$ is an algebraic voltage measured with the magnetic field in the positive direction and $V_n(\pm I,-B)$ is the same voltage measured with magnetic field reversed.

The following procedure was used to take the data. The sample temperature was set and stabilized at a desired value and voltage

measurements were made with no stress applied to the sample. Stress was then applied to the sample and voltage measurements were again made. The switching procedure was: measure V_1, V_2, V_3, and V_4 with positive sample current and positive magnetic field, reverse the sample current and remeasure the four voltages, then reverse the magnetic field and measure the voltages once more, then reverse the sample current and make a final measurement of the four voltages.

This technique for measuring resistivity and Hall coefficient is the one suggested in ASTM F76-68 (see ASTM (1969)). The switching procedure used eliminates errors due to the presence of unwanted voltages of thermogalvanomagnetic origin. Lindberg (1952) has shown that the errors due to all the thermogalvanomagnetic voltages except the Ettingshausen voltage are removed by this switching technique. Fortunately, the Ettingshausen voltage is negligibly small in comparison to the Hall voltages measured and introduced no significant error in these measurements.

7. ANALYSIS OF EXPERIMENTAL RESULTS

7.1 Introduction

Resistivity versus temperature, and Hall coefficient versus temperature data were obtained for several samples by the techniques described in chapter 6. This data was obtained with zero stress applied to the samples, as well as for applied uniaxial compressive stresses of approximately 1.25×10^9 dynes/cm^2 and 2.5×10^9 dynes/cm^2. Results obtained on five samples, of three different orientations, are analyzed.

The piezoresistivity and electron mobility were computed for the samples studied. Theoretical expressions, derived in chapter 5, are fitted to most of the experimental piezoresistivity results. Long's model for mobility (discussed in chapter 4) is fitted to the mobility obtained for one of the samples. The effect of electron irradiation on electron mobility and phosphorus donor concentration is also discussed.

7.2 Resistivity and Hall Coefficient Results

7.2.1 Introduction

The resistivity and Hall coefficient of several silicon samples were determined for the temperature range $250^\circ K$ - $360^\circ K$ by the techniques described in chapter 6. The results of these measurements are presented and discussed in this section.

7.2.2 Unirradiated <100> Sample CZ4B

Figure 7.1 shows the resistivity data obtained on the unirradiated sample CZ4B. For this <100> oriented sample it is found from

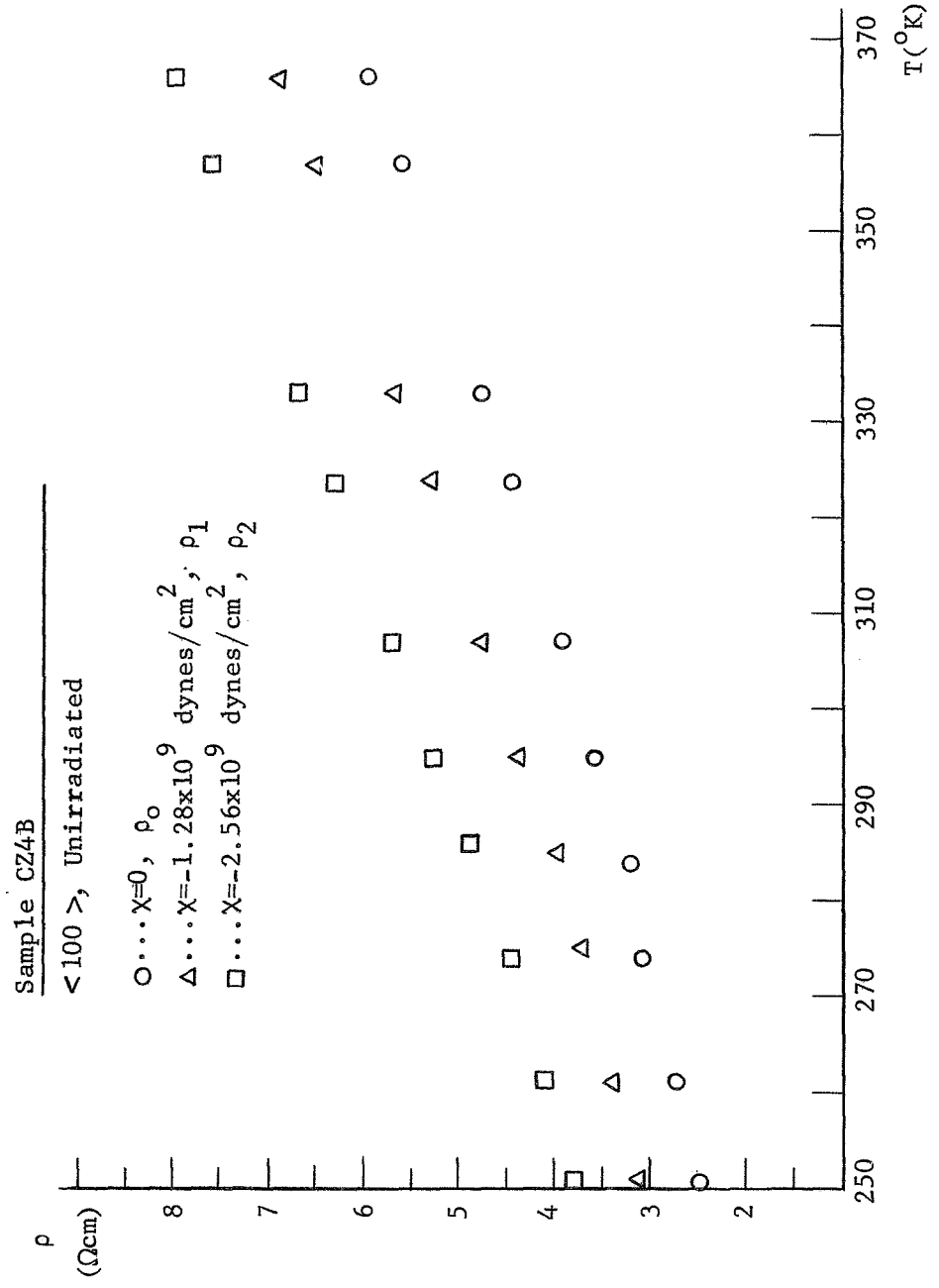

Figure 7.1 Resistivity versus temperature for sample CZ4B

Figure 7.1 that $\Delta\rho/\rho \sim .2$ over the experimental temperature range, where $\Delta\rho$ is either $\rho_2 - \rho_o$, or $\rho_1 - \rho_o$. Thus for this <100> sample, the resistivity is changed approximately 20 percent by the applied stresses used here. Over the experimental temperature range obtained for this sample, the concentration of conduction band electrons n_c is constant (see section 3.3). Therefore, the temperature dependence of the curves shown in Figure 7.1 is due to the temperature variation of the effective electron mobility, as defined by equation 5.26. It was found that for all three stress levels, a straight line was obtained if log (ρ) were plotted as a function of log (T). By least squares curvefitting to these straight lines, it is found that

$$\rho_o = 0.488 \times 10^{-5} T^{2.37} \quad \Omega cm \qquad (\chi = 0) \tag{7.1}$$

$$\rho_1 = 0.262 \times 10^{-4} T^{2.11} \quad \Omega cm \qquad (\chi = 1.28 \times 10^9 \text{ dynes/cm}^2) \tag{7.2}$$

$$\rho_2 = 0.804 \times 10^{-4} T^{1.95} \quad \Omega cm \qquad (\chi = 2.6 \times 10^9 \text{ dynes/cm}^2), \tag{7.3}$$

where T is sample temperature in ^oK. Since the concentration of conduction band electrons is constant it follows that

$$\mu_o \alpha T^{-2.37} \qquad (\chi = 0) \tag{7.4}$$

$$\mu_1 \alpha T^{-2.11} \qquad (\chi = -1.28 \times 10^9 \text{ dynes/cm}^2) \tag{7.5}$$

$$\mu_2 \alpha T^{-1.95} \qquad (\chi = -2.6 \times 10^9 \text{ dynes/cm}^2), \tag{7.6}$$

where $\mu_o = 1/(qn_{c_o}\rho_o)$, $\mu_1 = 1/(qn_c\rho_1)$, and $\mu_2 = 1/(qn_c\rho_2)$.

The temperature dependence of the zero stress mobility, μ_o, obtained compares favorably with experimental values obtained by other workers. For example Ludwig and Watters (1956) obtained

$$\mu_{Lattice} \propto T^{-2.5} \tag{7.7}$$

for the lattice mobility of electrons in silicon by drift mobility measurements made for temperatures in the range 160^oK - 400^oK. The difference in the exponents of T for equations 7.4 and 7.7 is probably due to greater ionized impurity scattering rates in the samples studied here. The presence of additional scattering by ionized impurities would certainly tend to make the exponent of T less negative since ionized impurity scattering mobility varies approximately as $T^{3/2}$.

In Figure 7.2 the Hall coefficient obtained for sample CZ4B is plotted versus temperature. It is noted that compressive stresses decrease the Hall coefficient. Even though the concentration of conduction band electrons remains constant with stress, the Hall coefficient decreases. This effect, like piezoresistivity, is primarily due to the stress-induced transfer of electrons from one conduction band minima to another. If the conductivity contributions of individual conduction band minima are taken into consideration (e.g., see Herring and Vogt (1956)), the formula for the Hall coefficient of n-type silicon in the presence of a $<100>$ stress may be shown to be

$$R_H = \frac{-K_m\{(n_c^{(1)} + n_c^{(2)}) <\tau_\ell \tau_t> + K_m n_c^{(2)} <\tau_t^2>\}}{2q\{n_c^{(2)} <\tau_\ell> + (n_c^{(1)} + n_c^{(2)}) K_m <\tau_t>\}\{n_c^{(1)} <\tau_\ell> + 2K_m n_c^{(2)} <\tau_t>\}}, \tag{7.8}$$

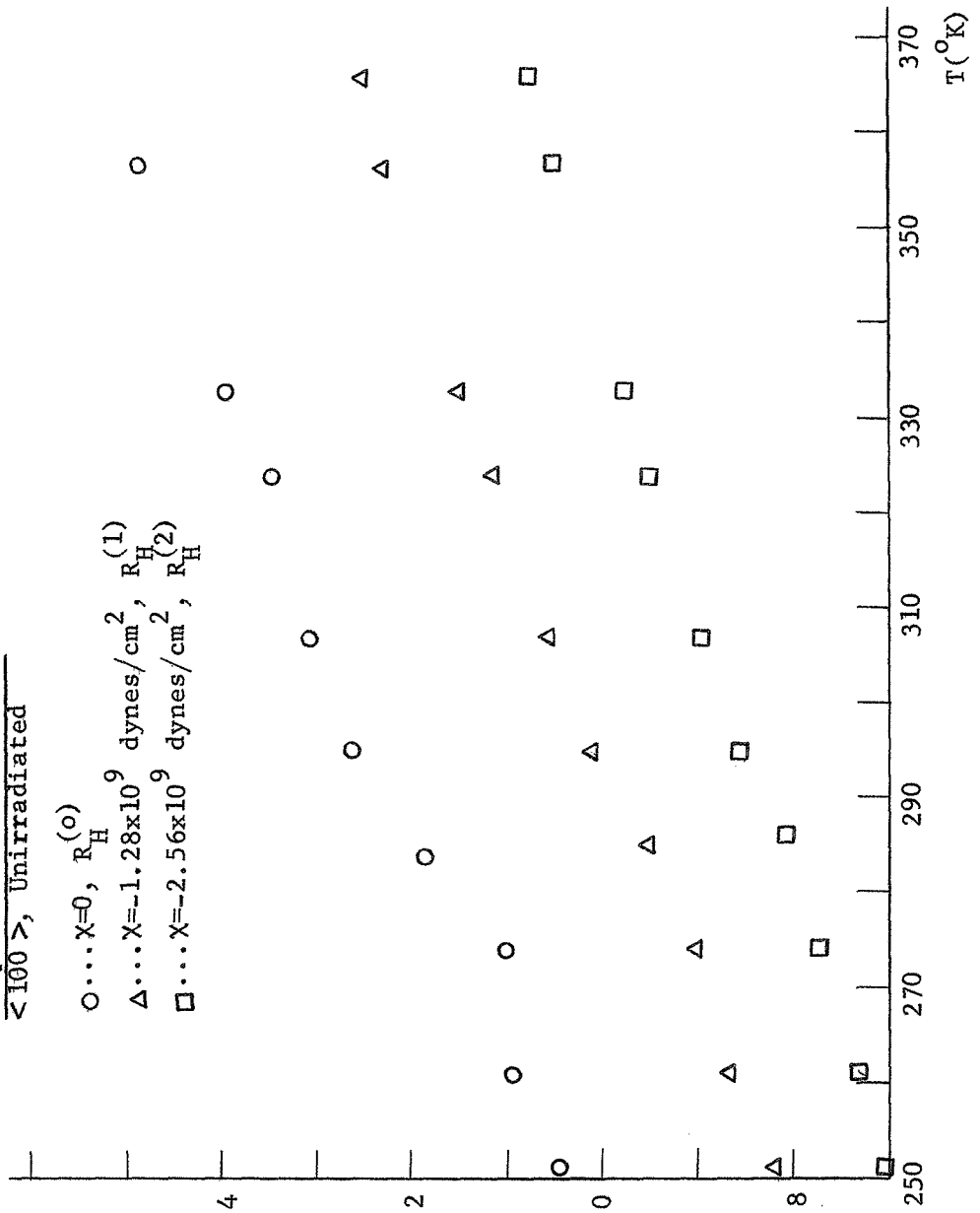

Figure 7.2 Hall coefficient versus temperature for sample CZ4B

where $K_m = m_\ell/m_t = 4.69$, and $n_c^{(1)}$, $n_c^{(2)}$ are the concentration of conduction electrons in valleys 1 and 2 respectively (in the presence of stress) in Figure 5.2. The quantity q is the magnitude of the charge of an electron. For the case of zero stress, equation 7.8 reduces to the familiar form

$$R_H^{(o)} = \frac{-r}{qn_c} \quad , \tag{7.9}$$

where the Hall factor r is given by (see Herring and Vogt (1956))

$$r = \frac{3K_m\{2<\tau_{\ell_o}\tau_{t_o}>+K_m<\tau_{t_o}^2>\}}{\{<\tau_{\ell_o}>+2K_m<\tau_{t_o}>\}^2} \tag{7.10}$$

The quantities τ_{ℓ_o} and τ_{t_o} are defined in chapter 4, and $<f>$, for any function (f) of energy (E), is the following average:

$$<f> = \frac{\int_o^\infty f\, E^{3/2} \exp(-E/kT)\, dE}{\int_o^\infty E^{3/2} \exp(-E/kT)\, dE} \quad . \tag{7.11}$$

The variation of the zero stress Hall coefficient, $R_H^{(o)}$, with temperature is due to the variation of the Hall factor r with temperature, since n_c (in equation 7.9) is temperature independent.

The value of n_c for sample CZ4B was computed from Figure 7.2 in the following way. A best fit straight line (visually estimated) was drawn through the $R_H^{(o)}$ versus T data points in Figure 7.2. This best fit straight line yields $R_H^{(o)} = -4.25 \times 10^3$ cb^{-1}cm^{-3} at T = 300°K.

A value for the Hall factor r was obtained from a figure given by Long (1960), in which r is plotted as a function of temperature. At T = 300°K Long's figure gives r = 1.185. Then for sample CZ4B

$$n_c = -\frac{r}{qR_H^{(o)}} = \frac{1.185}{1.6 \times 10^{-19} \times 4.25 \times 10^3} = 1.73 \times 10^{15} cm^{-3},$$

and since $n_c = N_D$

$$N_D = 1.73 \times 10^{15} cm^{-3} ,$$

where N_D is the net number of phosphorus donor atoms in sample CZ4B. Using this value for n_c in equation 7.9, r for CZ4B may be computed to be

$$r = 0.829 + (1.1 \times 10^{-3}/^{o}K)\ T , \qquad (7.12)$$

where T is the temperature in °K. Now that n_c is known, the conductivity mobility of sample CZ4B may be directly computed using Figure 7.1 and the formula

$$\mu = \frac{1}{qn_c\rho} \quad . \qquad (7.13)$$

This was done, and the results may be found in section 7.4.

No attempt was made to extract any information from the stressed Hall coefficient versus temperature curves. However, a successful fitting of equation 7.8 to these curves would help verify any theoretical model for τ_ℓ and τ_t developed to fit the observed temperature dependence of the conductivity mobility.

7.2.3 Irradiated <100> Sample CZ7B

Shown in Figure 7.3 is the resistivity data obtained on the electron-irradiated sample CZ7B. This sample was exposed to a total electron flux of approximately 4×10^{16} electrons/cm^2. It is noted that the resistivities (for the three different levels of stress) of this sample each have a minimum at about 280°K, and that below this temperature the resistivities increase with decreasing temperature.

This behavior is due to the compensating influence that the Si-A center acceptors have on the conduction band electron concentration. Consider the general equation for the zero stress conduction band electron concentration in electron irradiated silicon

$$n_{c_o} = N_D - \frac{N_A}{1 + 2\exp((E_A - E_{f_o})/kT} - \frac{N_E}{1 + \exp((E_E - E_{f_o})/kT} \qquad (7.14)$$

where N_A is the Si-A center concentration, and N_E the Si-E center concentration, and E_A and E_E are the energy levels in the forbidden energy band gap of these irradiation produced defects. The influence of the Si-E center on the resistivity is very small and is not apparent in Figure 7.3. However, it is presumed that the Si-E is present, if only in a relatively small concentration, due to the results of measurements made on other irradiated samples. In essence the presence of the Si-A centers (and the Si-E centers) causes n_{c_o} to monotonically decrease with decreasing temperature (see Figure 3.10). This is because as temperature decreases, E_{f_o} moves nearer to E_A causing a larger fraction of the Si-A center acceptors to be ionized, at the expense of the conduction band electron concentration.

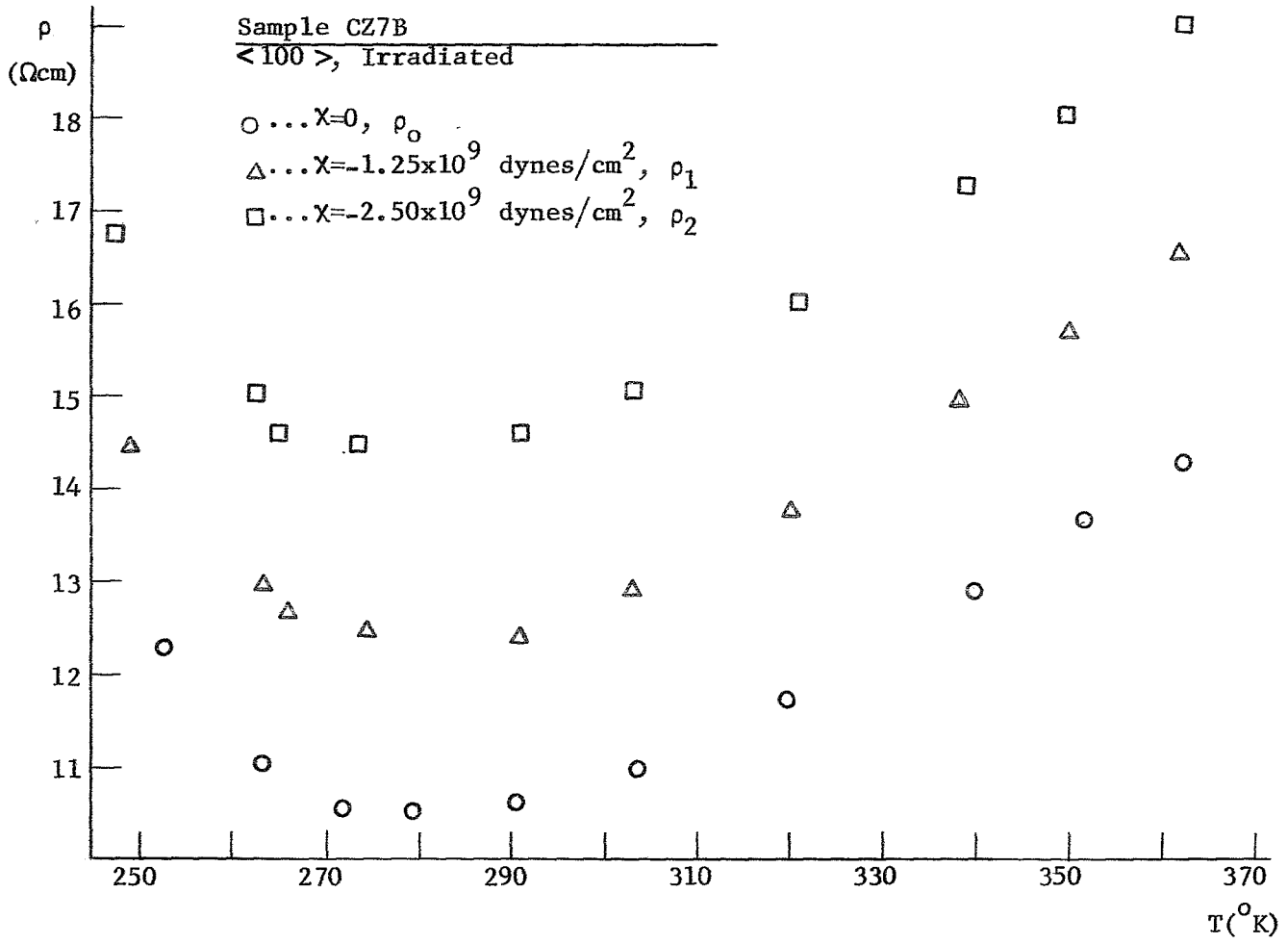

Figure 7.3 Resistivity versus temperature for sample CZ7B

For E_{f_o} very near E_A, this decrease of n_{c_o} with decreasing temperature is very rapid and more than offsets the normal decrease in resistivity due to the increase in electron mobility with decreasing temperature.

It appears that irradiation decreases the stress sensitivity of resistivity since from Figure 7.3 it is found that $\Delta\rho/\rho \sim .15$ as compared to $\Delta\rho/\rho \sim .2$ for the unirradiated sample CZ4B.

The Hall coefficient data obtained on CZ7B is shown in Figure 7.4. The curves shown in this figure have a completely different temperature behavior than the corresponding curves of the unirradiated sample CZ4B. The irradiated Hall coefficient monotonically decreases with temperature due to the monotonic increase of the conduction band electron concentration with temperature. The irradiated Hall coefficients are larger than the corresponding values for the unirradiated sample due to donor compensation by the Si-A and Si-E centers in the irradiated sample.

The doping concentrations N_D (phosphorus donors), N_A and N_E of sample CZ7B were computed by a method described in Appendix 10.3. In order to obtain accurate values for these doping concentrations, the Hall factor r must be accurately known. The value of r depends upon the relative strengths of the various scattering mechanisms that determine electron mobility. Since electron radiation damage may result in increased ionized impurity scattering, the Hall factor of CZ7B may be expected to differ from that of the unirradiated sample CZ4B, particularly at the lower temperatures where ionized impurity scattering is more important. However, at high temperatures lattice

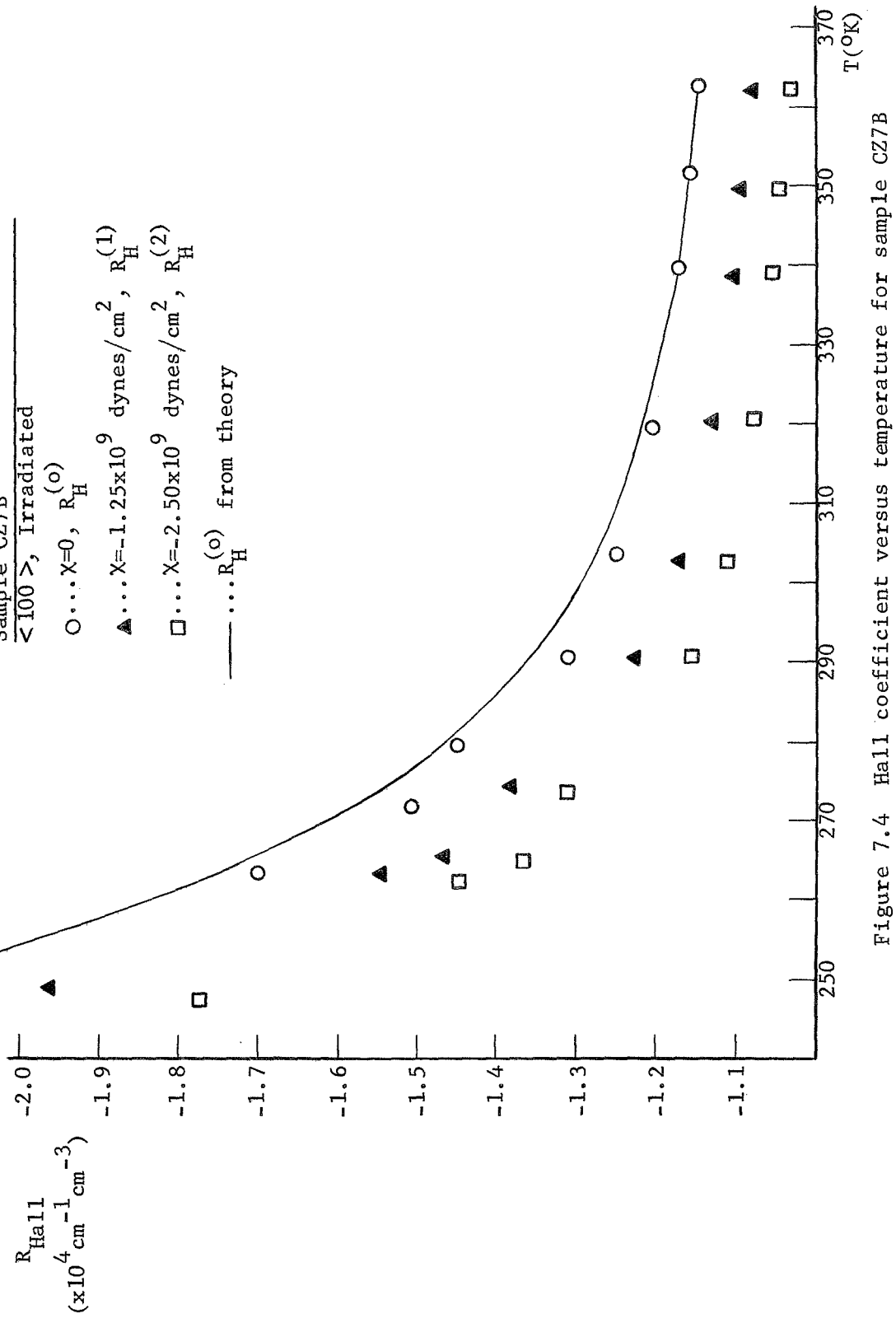

Figure 7.4 Hall coefficient versus temperature for sample CZ7B

scattering predominates regardless of the concentration of ionized impurities in a sample.

Thus it was assumed in the computation of N_D, N_A and N_E, that for $T > \sim 325^oK$ the Hall factor of CZ7B is equal to the Hall factor of CZ4B. With this assumption, the following values were obtained for the doping concentrations of CZ7B:

$$N_D = 0.803 \times 10^{15} \text{ cm}^{-3}$$

$$N_A = 0.189 \times 10^{17} \text{ cm}^{-3}$$

$$N_E = 0.105 \times 10^{15} \text{ cm}^{-3} .$$

A good fit to the zero stress Hall coefficient curve is obtained using these doping concentrations, and equation 7.12 for the value of the Hall factor r (see Figure 7.4).

Using these values for the doping concentrations, n_{c_o} may be calculated as a function of temperature and hence the conductivity mobility, μ_o, may be determined from

$$\mu_o = \frac{1}{q n_{c_o} \rho_o} . \qquad (7.15)$$

These computations were carried out and the results are given in section 7.4, where the effects of electron irradiation on mobility are illustrated by a comparison of the mobilities of the irradiated samples studied to the mobility of the unirradiated sample CZ4B.

The value obtained here for N_A, the concentration of Si-A centers, corresponds to an A-center "introduction rate" of

$$\frac{N_A}{\text{total electron flux}} = \frac{0.189 \times 10^{17}\ \text{cm}^{-3}}{4.3 \times 10^{16}\ \text{electrons cm}^{-2}} = 0.44\ \frac{\text{A-center cm}^{-3}}{\text{electrons cm}^{-2}}.$$

Thus approximately one A-center per cubic centimeter is created for every two electrons per square centimeter incident on the sample.

7.2.4 Irradiated <110> Sample CZ17A

Figure 7.5 shows the resistivity data obtained on the irradiated <110> sample CZ17A. This sample was subjected to a total electron flux of approximately 6×10^{16} electrons/cm^2.

It is noted that the resistivity curves obtained for this sample are similar to those obtained for sample CZ7B. One significant difference, however, is that for CZ17A the three resistivity curves merge at low temperature while this is not observed in the data for sample CZ7B. The temperature at which the minimum resistivity occurs for sample CZ17A is 297^{o}K compared to 280^{o}K for CZ7B.

In Figure 7.5 it is also observed that the slope of the resistivity, for all three levels of stress, decreases with increasing temperature for $T > \sim 325^{o}$K. This behavior is presumably due to the presence of a significant concentration of Si-E centers. Sample CZ17A, like all the irradiated sampled studied, was annealed for 12 hours at 350^{o}F in an attempt to remove the Si-E centers.

However, other workers have observed that an irradiation-produced defect level 0.4eV below the conduction band edge (presumably the Si-E center level) is sometimes not completely removed by annealing (e.g., see Corbett (1966)). The behavior of the resistivity of CZ17A is consistent with the hypothesis that a significant Si-E

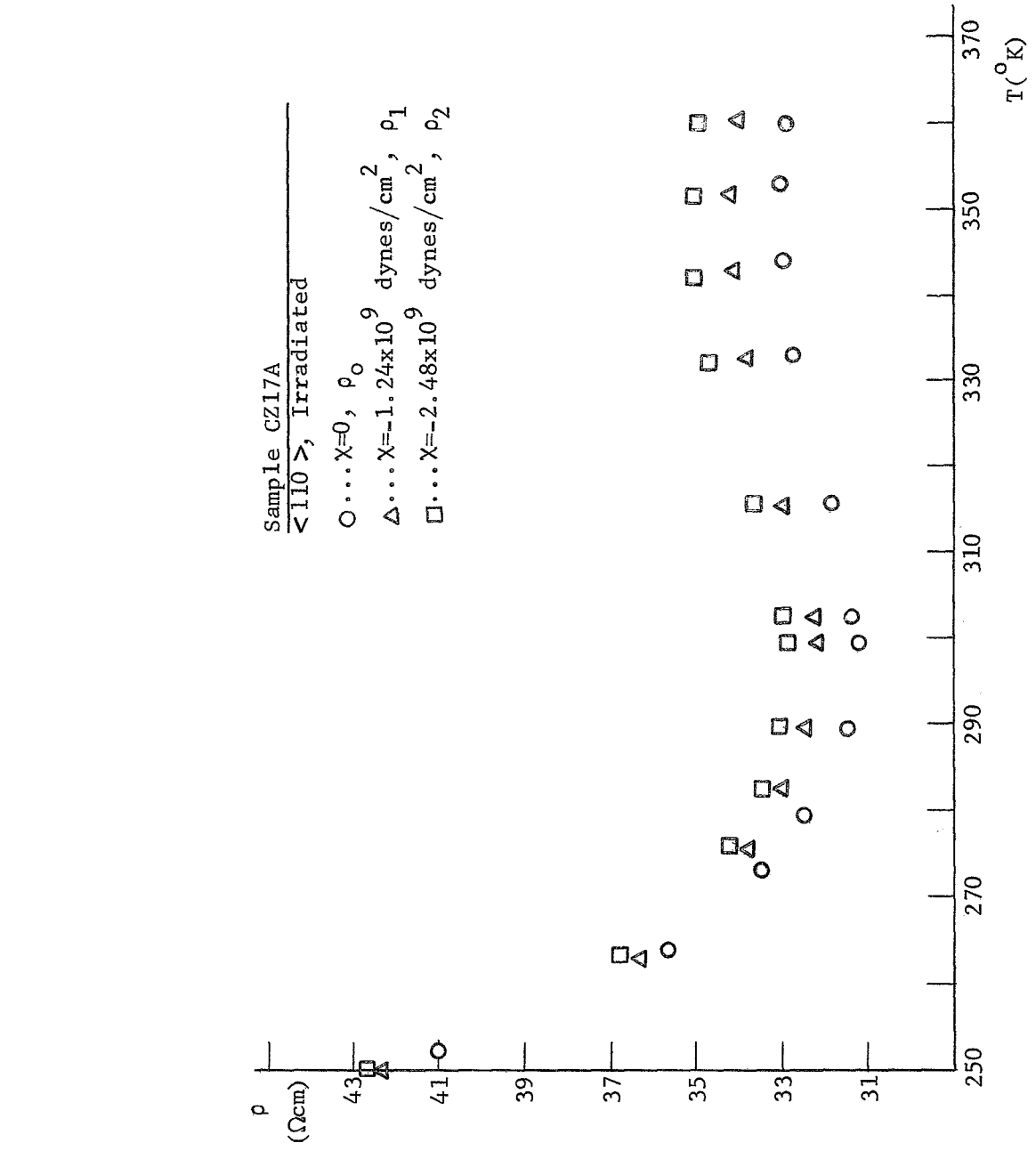

Figure 7.5 Resistivity versus temperature for sample CZ17A

center concentration is present, since as temperature increases the Fermi energy would approach the energy level of the Si-E center, freeing the electrons on these acceptor levels. This would account for the decrease in the slope of the resistivity with increasing temperature.

One final observation that can be made from the results shown in Figure 7.5 is that for CZ17A, $\Delta\rho/\rho$ has a maximum value of about 0.04 or 4 percent compared to 15 percent for CZ7B. This is to be expected, since it is well known that the $<110>$ orientation is less sensitive to stress than is the $<100>$ orientation.

The Hall coefficient data obtained on CZ17A is plotted in Figure 7.6. These curves are similar to the corresponding curves obtained for CZ7B. However, there is a slight downward bending of the R_H versus T curves obtained for CZ17A at the highest temperatures, presumably due to a greater Si-E center influence.

The doping concentrations of CZ17A were determined by the same procedure used for sample CZ7B. The following values were obtained

$$N_D = 0.441 \times 10^{15} \text{ cm}^{-3}$$

$$N_A = 0.258 \times 10^{17} \text{ cm}^{-3}$$

$$N_E = 0.191 \times 10^{15} \text{ cm}^{-3} .$$

The theoretical Hall coefficient, calculated using these values to determine n_{c_o} from equation 7.14 and using equation 7.12 for the value of the Hall factor r, is shown in Figure 7.6. The A-center concentration obtained here corresponds to an A-center "introduction rate" of 0.40 A-center cm^{-3} per electron cm^{-2}.

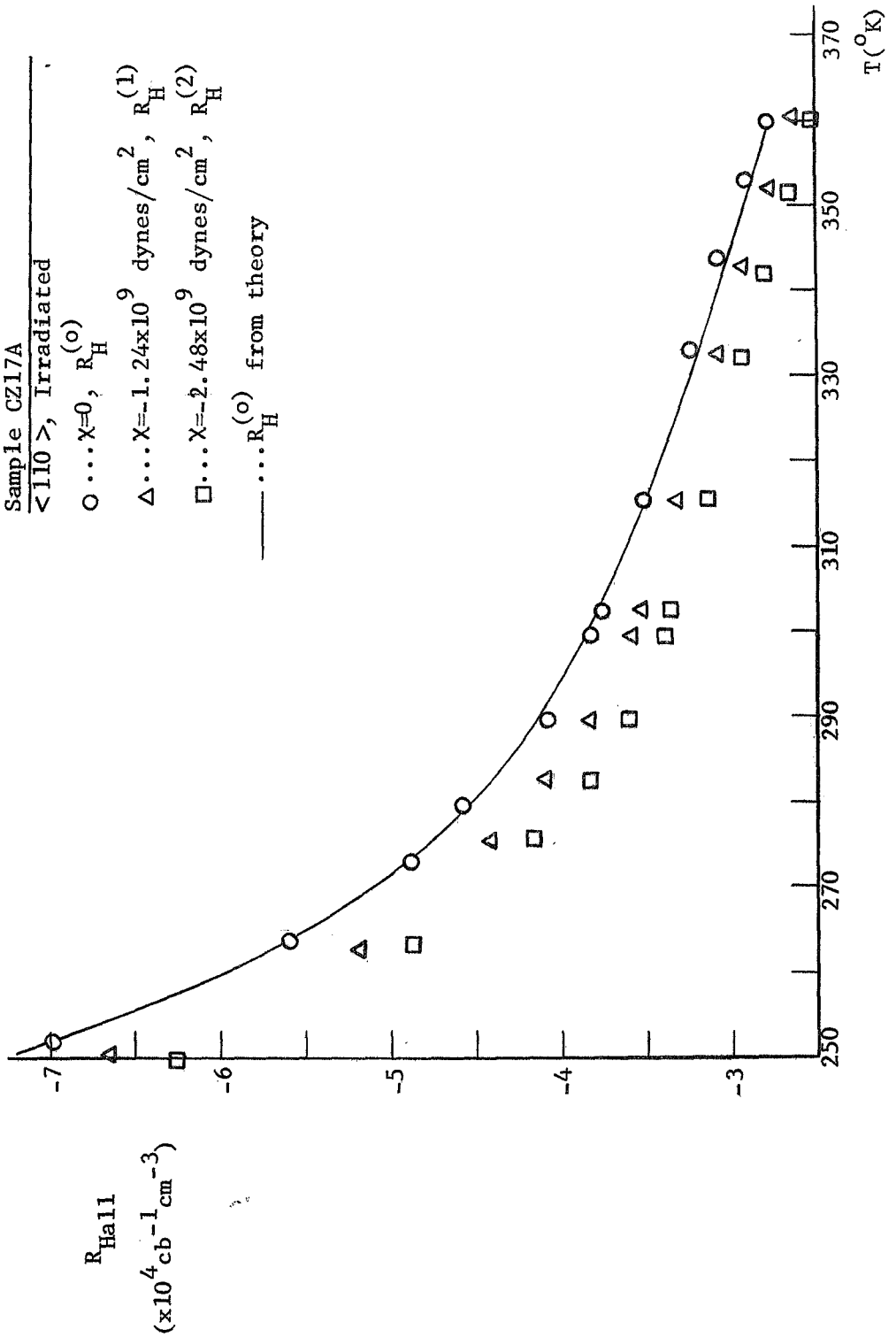

Figure 7.6 Hall coefficient versus temperature for sample CZ17A

7.2.5 Irradiated <111> Sample CZ12B

The resistivity data obtained on the <111> oriented sample, CZ12B, is shown in Figure 7.7. The curves shown in this figure each have a minimum at about T = 284°K. Sample CZ12B was subjected to a total dosage of about 4×10^{16} electrons/cm^2, which incidently is the same dosage received by CZ7B. The general shape of the resistivity versus temperature curves for CZ12B is between those of CZ17A and CZ7B. That is, for higher temperatures, the data obtained on sample CZ12B indicates a greater Si-E center influence than the data for CZ7B. However, the Si-E center influence in sample CZ17A appears to be greater than that in CZ12B.

Below about 260°K, the resistivity curves in Figure 7.7 are seen to completely merge. Lack of a sufficient number of data points below 260°K makes it impossible to be certain of the interrelationship of the three curves for low temperatures. For low temperatures, these curves may cross one another, causing a reversal in the sign of piezoresistivity. In any event, $\Delta\rho/\rho$ is extremely small (less than .003) for temperatures between 250°K and 265°K. The maximum $\Delta\rho/\rho$ for CZ12B is about 0.014 or 1.4 percent. This <111> orientation is less sensitive to stress than any other orientation for n-type silicon. This is because there is no population transfer between the conduction band minima for the case of <111> applied stresses.

As can be seen in Figure 7.8, a <111> stress has only a very small effect on the Hall coefficient. Since there is no population transfer for the case of a <111> stress, any change in the Hall coefficient with stress must be due to

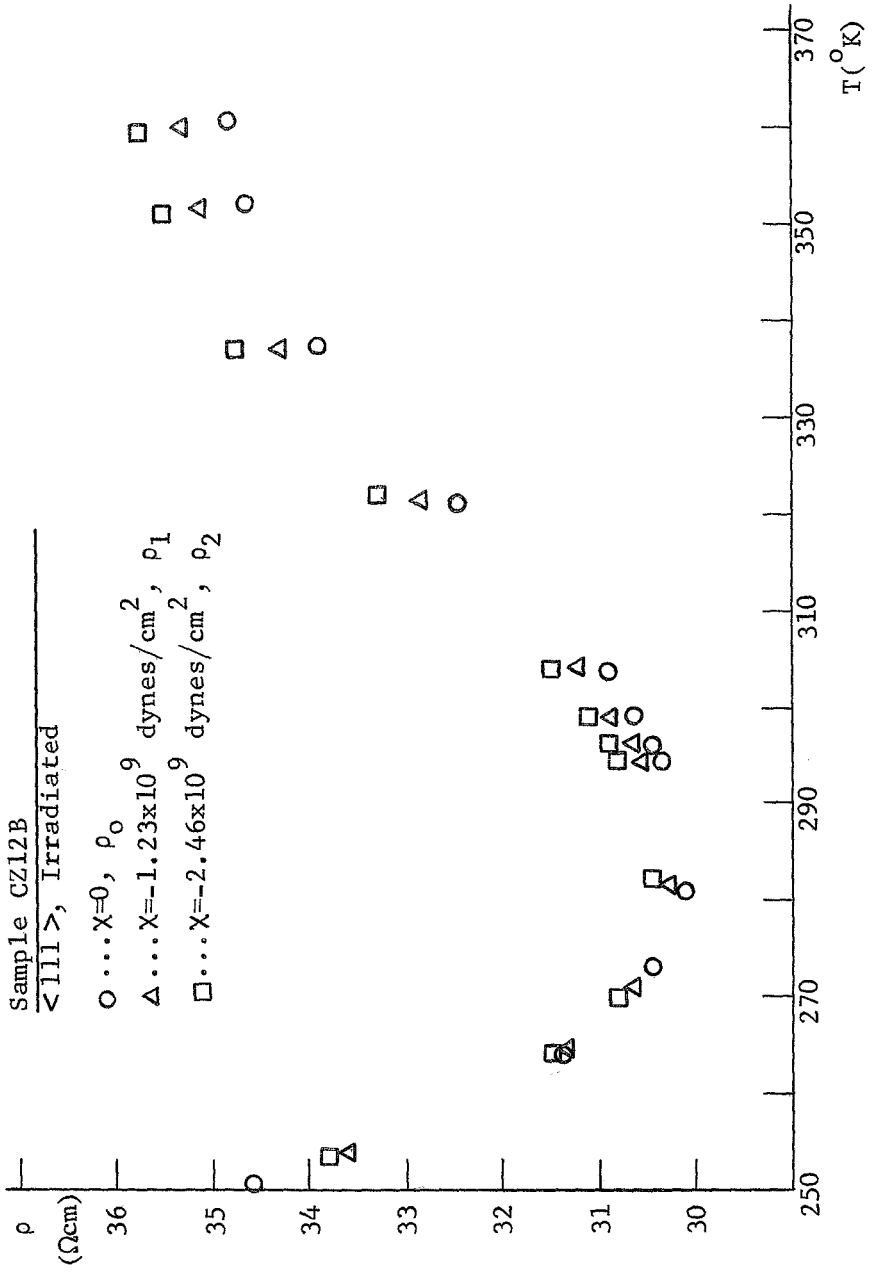

Figure 7.7 Resistivity versus temperature for sample CZ12B

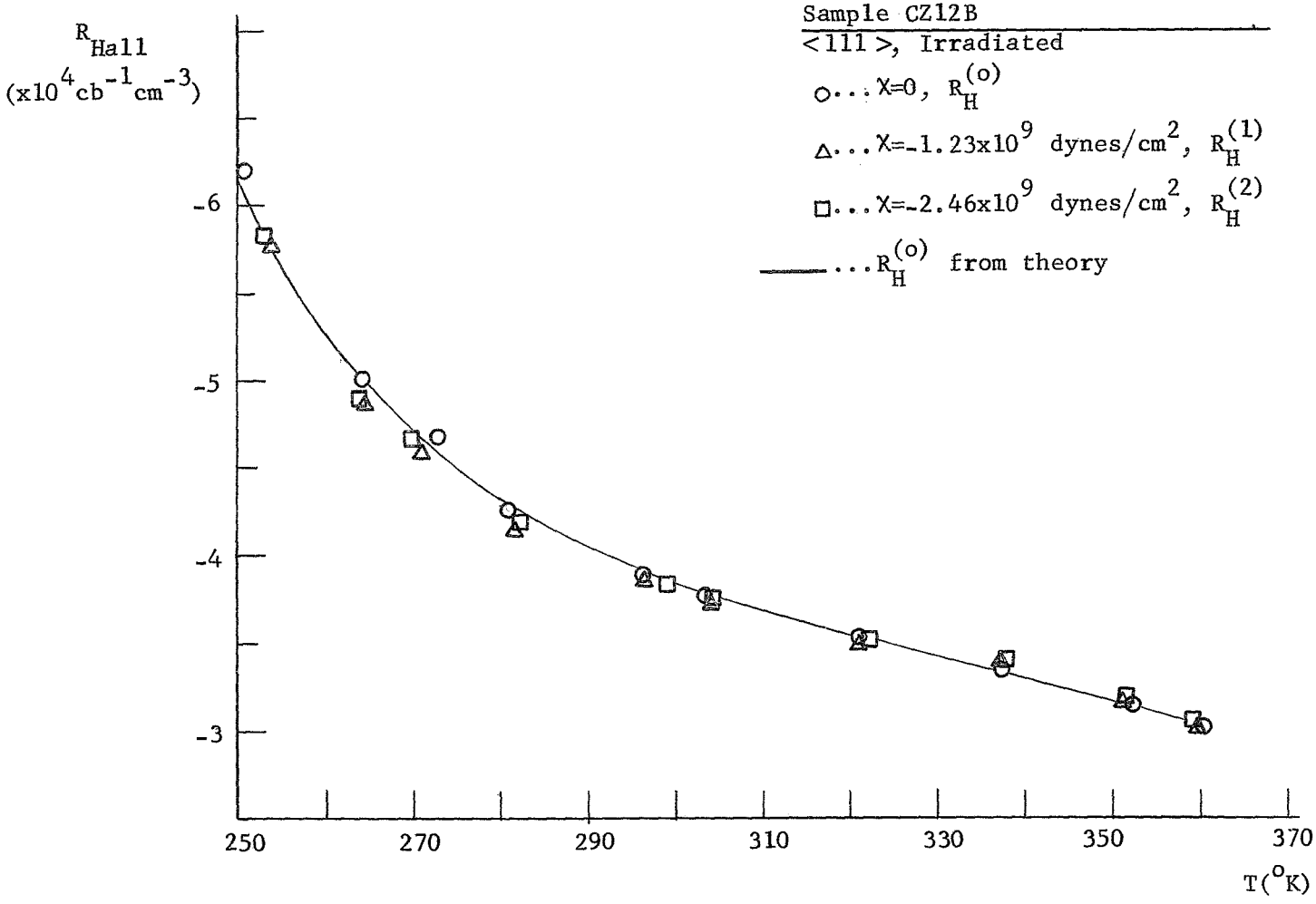

Figure 7.8 Hall coefficient versus temperature for sample CZ12B

1) slight misorientation of sample off the <111> direction,

2) second order effects of stress on relaxation times, and

3) a small change in total conduction band electron concentration with stress.

The doping concentrations for CZ12B were computed to be

$$N_D = 0.389 \times 10^{15} \text{ cm}^{-3}$$

$$N_A = 0.156 \times 10^{17} \text{ cm}^{-3}$$

$$N_E = 0.166 \times 10^{15} \text{ cm}^{-3} .$$

The value computed for N_A corresponds to an A-center "introduction rate" of approximately 0.36 Si-A center per electron cm^{-2}.

7.2.6 Irradiated <100> Sample D-1

Resistivity measurements were made on the <100> oriented sample D-1 using a commercial dewar, manufactured by Andonian Associates, Inc. This dewar was equipped with a stressing unit, designed in such a way that it was possible to make resistivity measurements at temperatures as low as 77°K. The stressing unit was hydraulically operated, but had a very long (about three feet) stainless steel piston that thermally isolated the hydraulic cylinder from the sample.

The resistivity data obtained on this sample is shown in Figure 7.9. As is seen in this figure, the resistivity increases extremely rapidly at the lower temperatures. The minimum resistivity of D-1 occurs at 325°K.

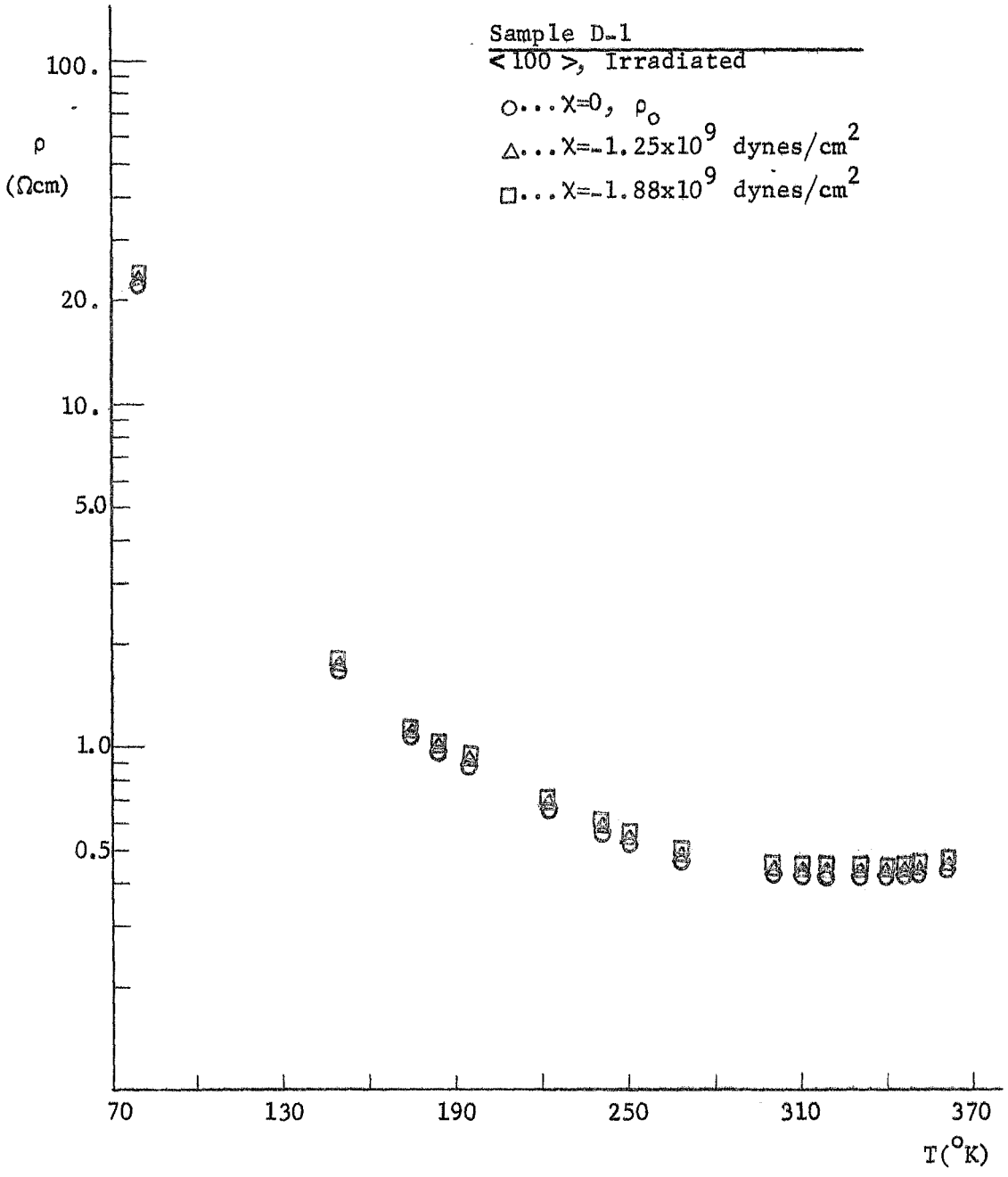

Figure 7.9 Resistivity versus temperature for sample D-1

Sample D-1 was a low resistivity sample, with a preirradiated room temperature resistivity of about 0.02 Ωcm. It was subjected to a total electron flux of approximately 2×10^{17} electrons/cm^2.

Due to the size of the Andonian dewar, it was impractical to make Hall coefficient measurements on sample D-1. Therefore the doping concentrations of this sample are not known.

7.3 Piezoresistivity Results

7.3.1 Experimental Results

The piezoresistivity of the samples studied was computed in the following way. The best smooth curves (visually estimated) were drawn through the experimental data points for resistivity. Resistivity values were then read off these curves at 10°K intervals and used in the formula

$$\Pi = \frac{\rho - \rho_o}{\rho X} = \frac{\Delta\rho}{\rho X} \quad , \tag{7.16}$$

where ρ is resistivity in the presence of applied stress X, and ρ_o is the unstressed resistivity at the same temperature.

The piezoresistivities of the $<100>$ oriented samples CZ4B (unirradiated), and CZ7B (irradiated) are compared in Figure 7.10. It is observed that electron irradiation has a great effect on piezoresistivity. The piezoresistivity of the unirradiated sample decreases monotonically with increasing temperature, while the piezoresistivity of the irradiated sample increases with temperature for the lower temperatures, goes through a maximum, and then decreases

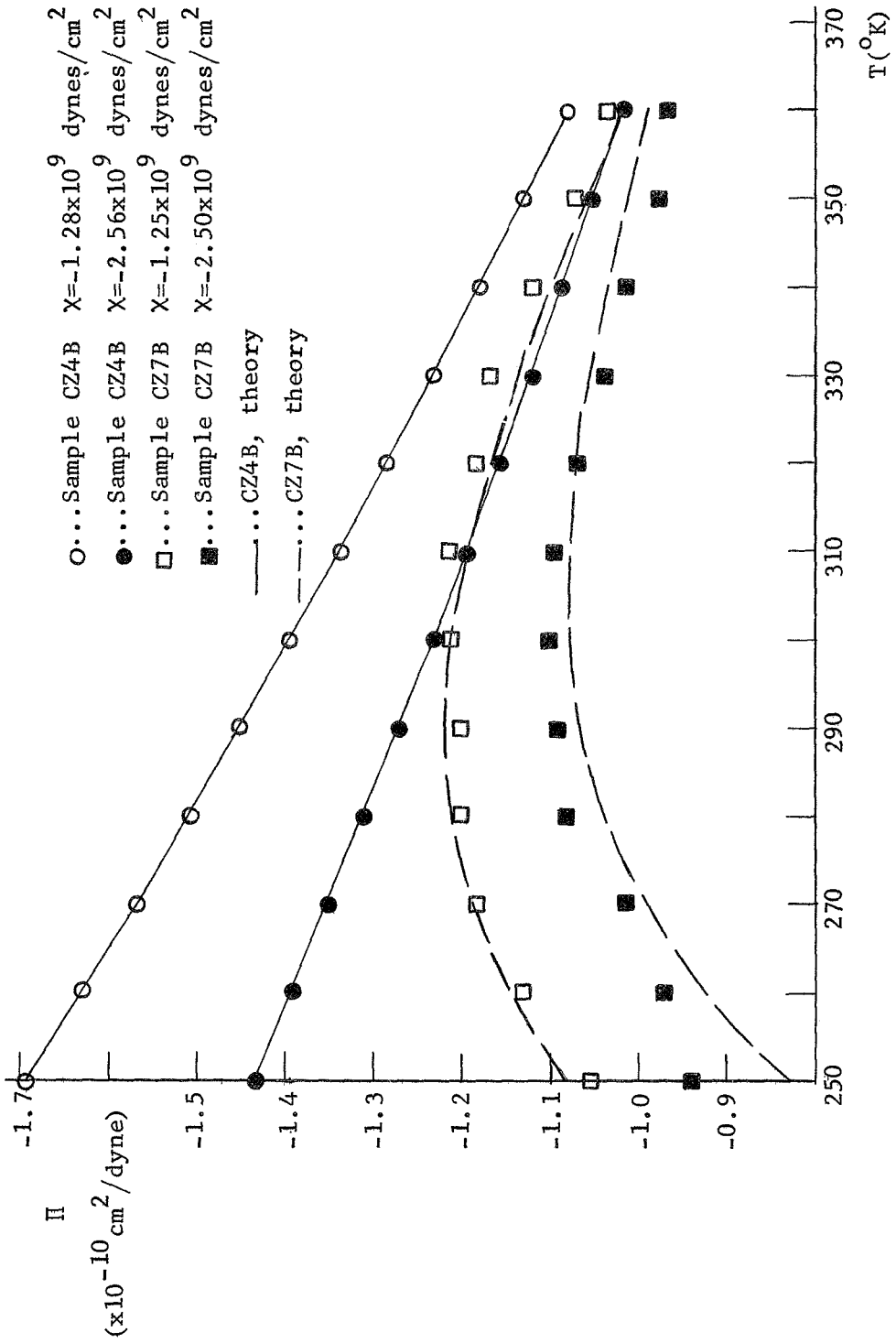

Figure 7.10 Piezoresistivity versus temperature for samples CZ4B and CZ7B

with increasing temperature. For the stresses used here, the piezoresistivity of both the irradiated and unirradiated samples decrease with increasing stress.

At 300°K the piezoresistivity, Π, of the unirradiated sample CZ4B has the values

$$\Pi = -1.4 \times 10^{-10} \text{ cm}^2/\text{dyne} \qquad (\chi = -1.28 \times 10^{9} \text{ dyne/cm}^2)$$

$$\Pi = -1.26 \times 10^{-10} \text{ cm}^2/\text{dyne} \qquad (\chi = -2.56 \times 10^{9} \text{ dyne/cm}^2) \ .$$

These values may be compared to the room temperature values obtained for $\Delta\rho/\rho_o\chi$ at low stresses by other workers (see Table 5.1).

The piezoresistivities computed for irradiated <100> sample D-1, irradiated <110> sample CZ17A, and irradiated <111> sample CZ12B, are given in Figures 7.11, 7.12, and 7.13 respectively. The piezoresistivity obtained for <100> sample D-1 is amazingly constant with temperature. As mentioned in section 7.2, no Hall data was taken on this sample so that the values of N_D, N_A, and N_E are not known. However, a study of Figure 5.4 reveals that the value of the ratio N_A/N_D essentially determines the general shape of the piezoresistivity versus temperature curve. The trend evident in the results shown in Figure 5.4 leads one to conclude that N_A/N_D for D-1 is smaller than N_A/N_D for CZ7B. Also note that the piezoresistivity of sample D-1 (for $\chi = -1.25 \times 10^{9}$ dynes/cm^2) is approximately -0.5×10^{-10} cm^2/dyne as compared to approximately -1.1×10^{-10} cm^2/dyne for CZ7B. This difference in the piezoresistivities of sample CZ7B and sample D-1 is consistent with their preirradiated resistivities. From resistance measurements made on CZ7B and D-1

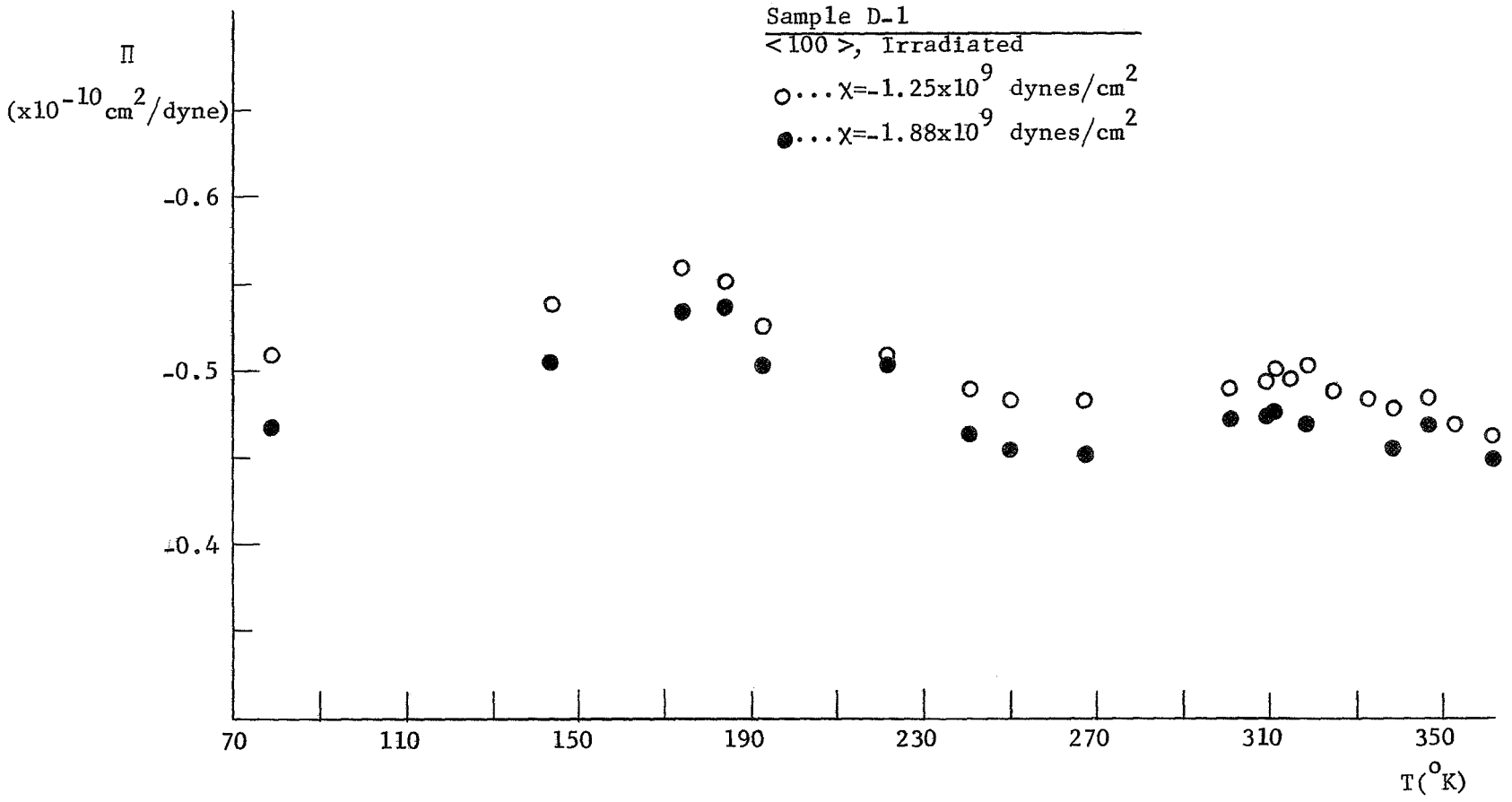

Figure 7.11 Piezoresistivity versus temperature for sample D-1

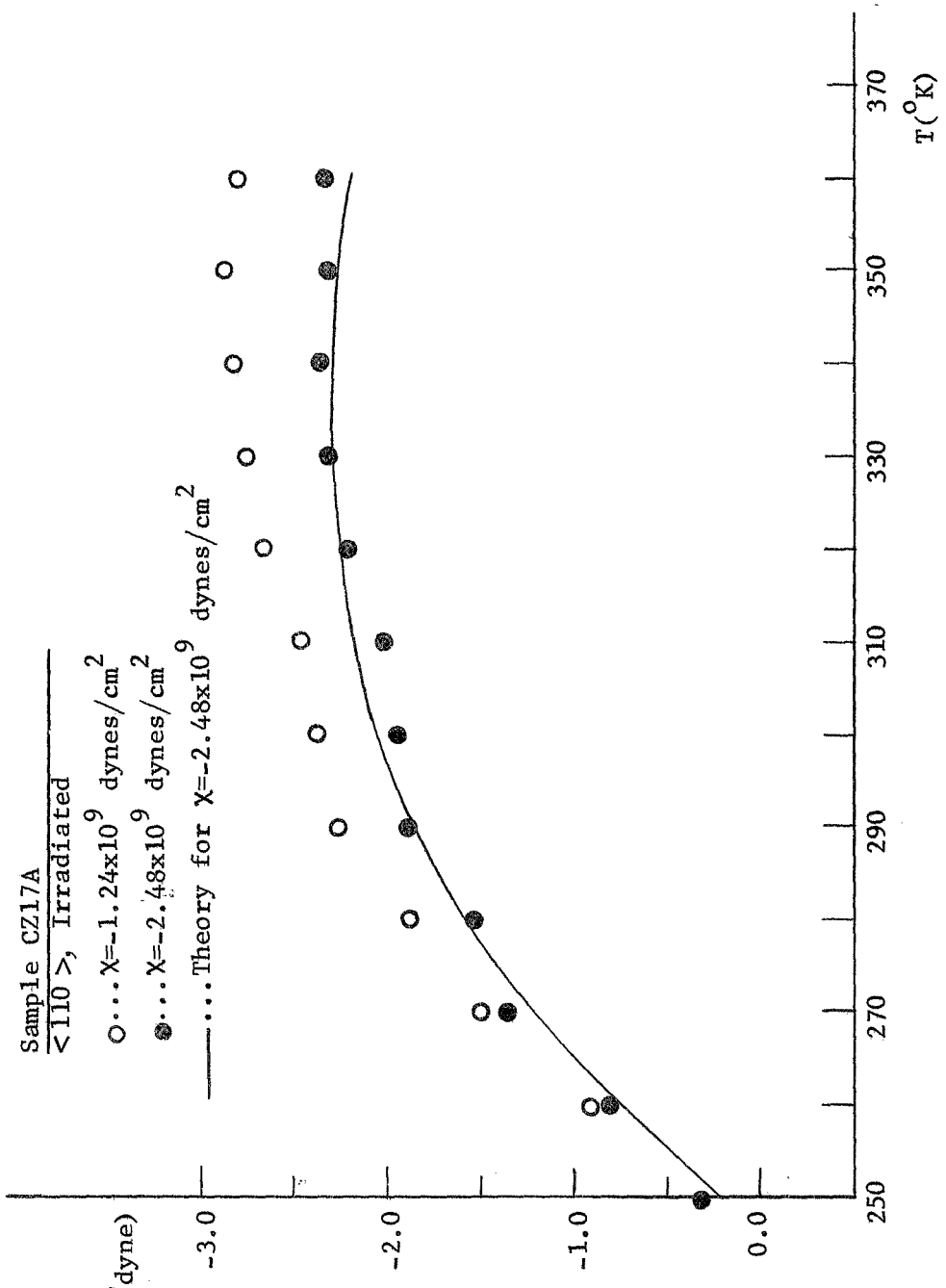

Figure 7.12 Piezoresistivity versus temperature for sample CZ17A

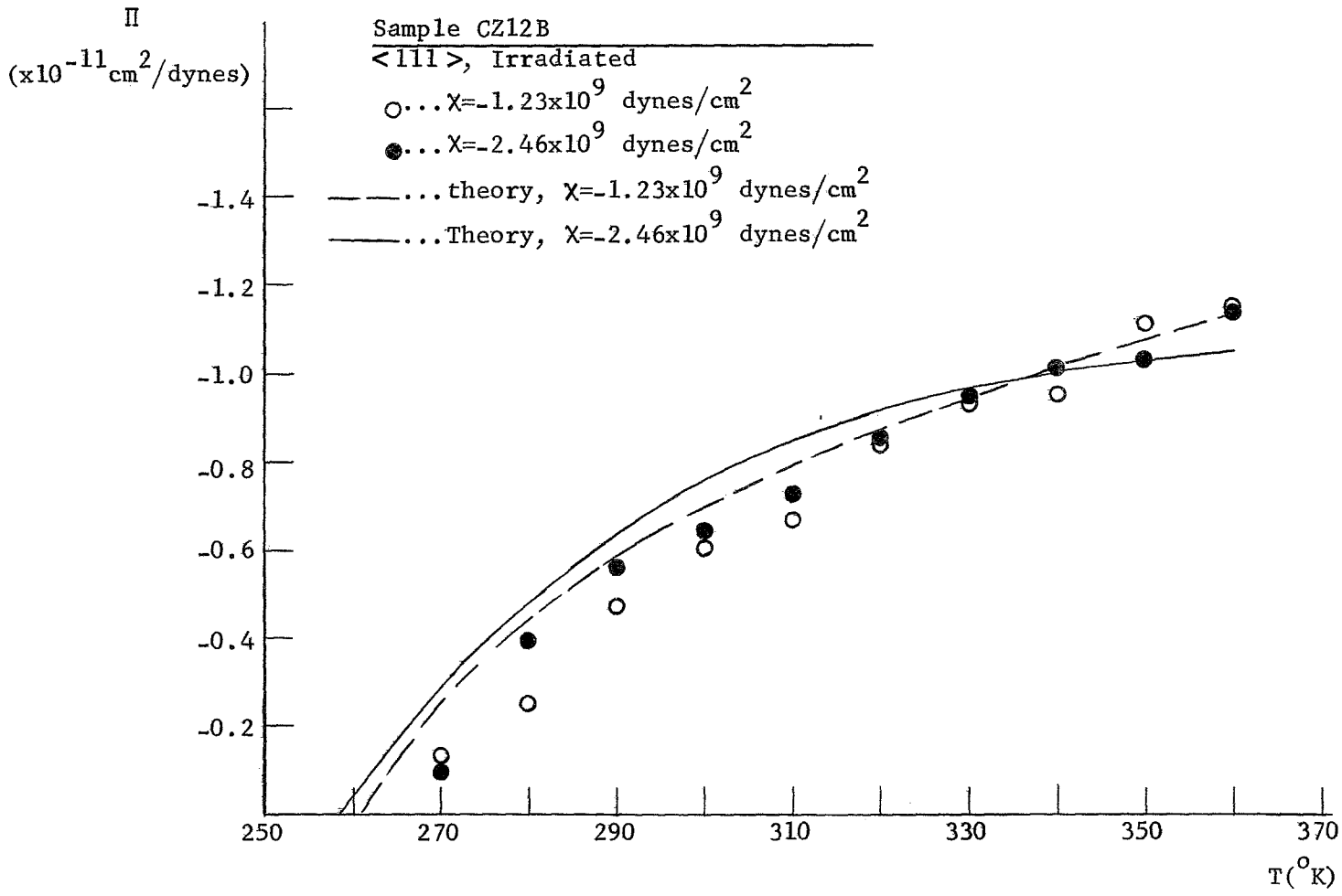

Figure 7.13 Piezoresistivity versus temperature for sample CZ12B

before electron irradiation it was found that D-1 had a donor concentration approximately 40 times as large as the donor concentration of CZ7B. It is well known that piezoresistivity decreases with increasing donor concentration.

No data was taken on unirradiated <110> or <111> samples, so that no comparison may be made with the data obtained on CZ17A and CZ12B to illustrate the effect of irradiation on the piezoresistivities of these two orientations. However, for the <110> orientation, classical theory (analysis in the limit of zero stress) predicts a $1/T$ variation for piezoresistivity. For the <111> orientation, classical theory predicts a piezoresistivity of zero.

7.3.2 Curvefitting to Piezoresistivity

The equations developed and presented in chapter 5 were fitted to the experimental data. A nonlinear least squares method, developed by Marquardt (1963) and implemented in the SHARE program "NLIN" (Nonlinear Least Squares Curvefitting), was used in the curvefitting procedure.

As discussed in chapter 5, the procedure followed in the curvefitting was to assume that δE_f, ΔE_1, ΔE_2, and ΔE_3 are accurately known, and to use r_ℓ, r_t, and $r_{t'}$ (see chapter 5) as the unknown parameters. For example, the piezoresistivity of a <100> sample is (see chapter 5)

$$\Pi = (1 - \exp(\delta E_f/kT)(r_\ell \theta_\ell + 2r_t \theta_t))/\chi \ . \qquad (7.17)$$

In this equation, all the quantities are presumed to be accurately

known except r_ℓ and r_t. These parameters, r_ℓ and r_t, are assumed to be temperature dependent.

Equation 7.17 was successfully fitted to the piezoresistivity of unirradiated sample CZ4B. The best fit values of r_ℓ and r_t were found to be

$$r_\ell = 0.09588 - (.2891 \times 10^{-4}/^{o}K)\,T \qquad (7.18)$$

$$(\chi = -1.28 \times 10^{9} \text{ dynes/cm}^2)$$

$$\left(\frac{r_t}{K_m}\right) = 0.07389 + (.5313 \times 10^{-4}/^{o}K)\,T \qquad (7.19)$$

and

$$r_\ell = 0.1160 - (.4193 \times 10^{-4}/^{o}K)\,T \qquad (7.20)$$

$$(\chi = -2.56 \times 10^{9} \text{ dynes/cm}^2)$$

$$\left(\frac{r_t}{K_m}\right) = 0.05759 + (.7741 \times 10^{-4}/^{o}K)\,T\,, \qquad (7.21)$$

where $K_m = m_\ell/m_t = 4.69$. The closeness of the fit is indicated in Figure 7.10. In Figure 7.14, r_ℓ and (r_t/K_m) are shown as a function of temperature. The trends, r_ℓ increasing and r_t decreasing with increasing stress, evident in this figure are consistent with the discussion in chapter 4 of the effect of stress on the relaxation times τ_ℓ and τ_t.

Shown in Figure 7.15 is $K_\tau \equiv \langle \tau_\ell \rangle / \langle \tau_t \rangle = K_m r_\ell / r_t$ as a function of temperature for the two different stresses. Again the observed increase of K_τ with stress is consistent with the predictions

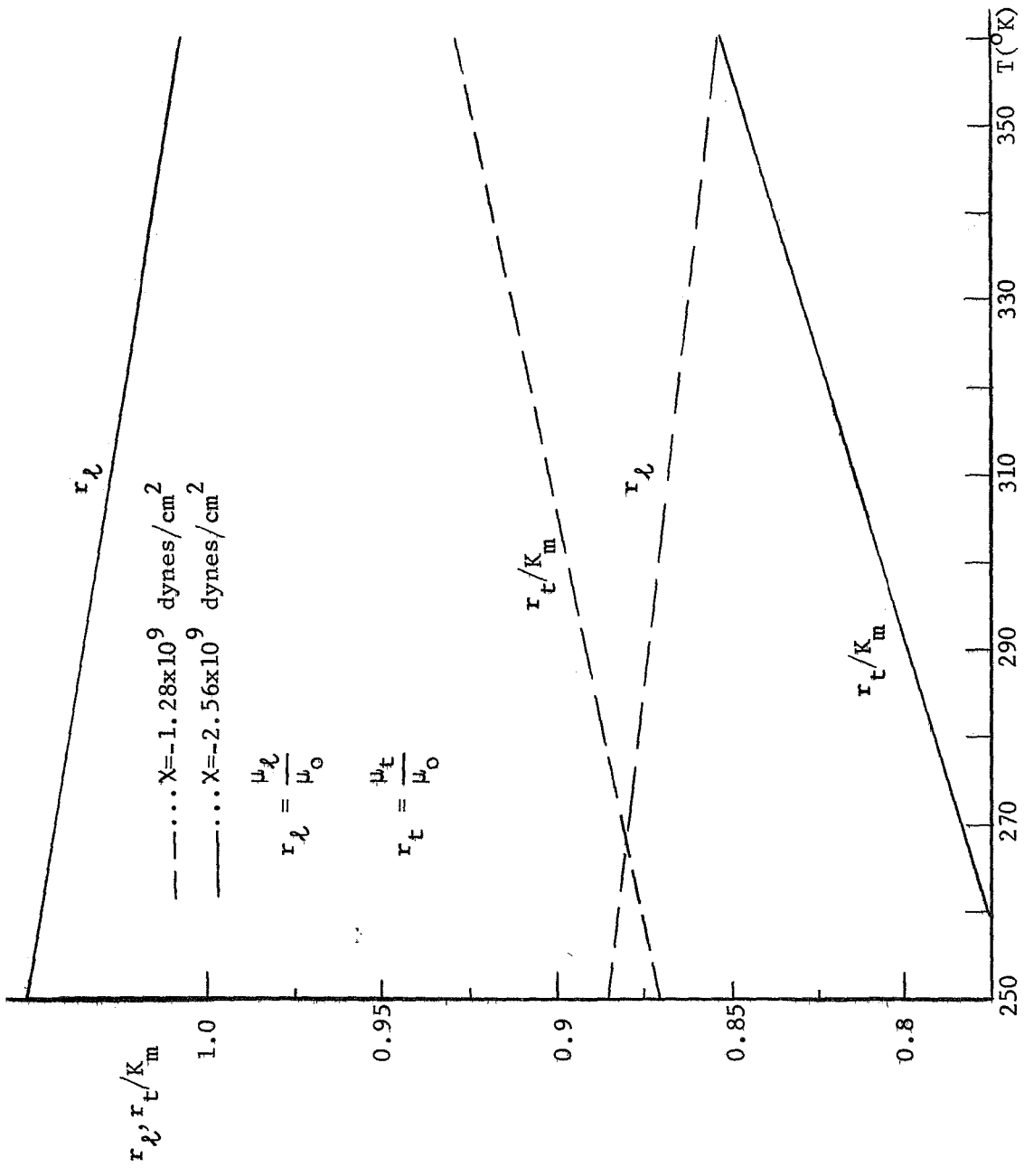

Figure 7.14 Empirical values of r_ℓ and r_t as functions of temperature

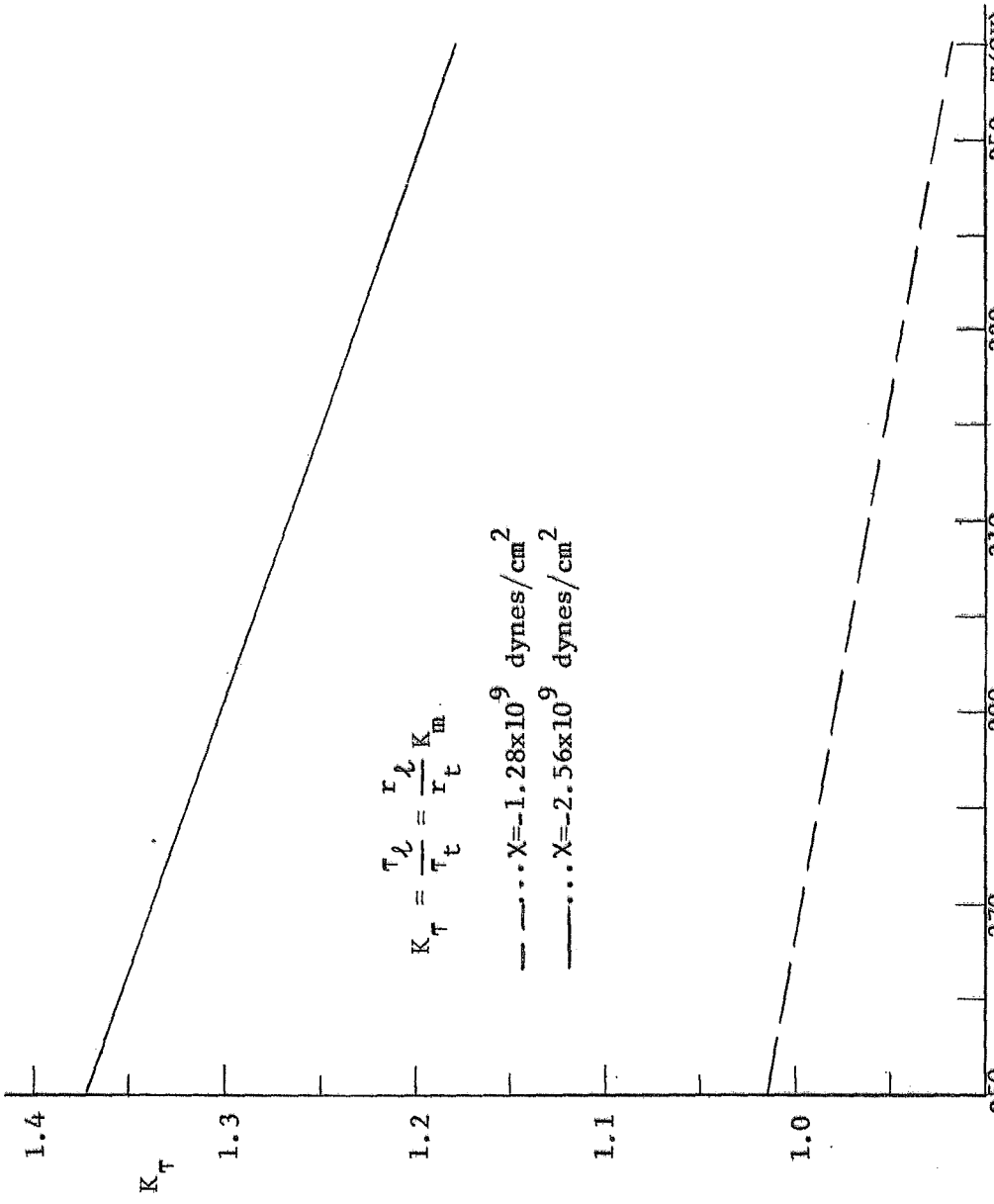

Figure 7.15 Empirical values for relaxation time anisotropy as a function of temperature

of chapter 4. If one assumes that the results shown in Figure 7.15 are accurate, and that the increase in K_τ with stress is approximately linear, extrapolation to zero stress yields a room temperature (298^oK) value of the zero stress mobility anisotropy, K_{τ_o}, of $K_{\tau_o} = .66$. This result indicates that τ_{A_ℓ}/τ_{A_t} (see chapter 4) is less than unity as deduced by Long (1960). To the author's knowledge, the only published experimental values for K_τ are those of Aubrey et al. (1963). Aubrey et al. obtained a range of values, 1.18 - .925, for K_τ at $T = 77^oK$.

These values obtained for r_ℓ and r_t for sample CZ4B also gave a good fit to the piezoresistivity of CZ7B. The piezoresistivity predicted for CZ7B by equation 7.17, with r_ℓ and r_t given by equations 7.18 - 7.21, is indicated in Figure 7.10. That such a good fit was obtained indicates that the effect of radiation damage on the relaxation times, τ_ℓ and τ_t, is small over the temperature range 250^oK - 360^oK.

The following equations were found to fit the piezoresistivity observed for the <111> sample CZ12B:

$$\Pi = (1 - 0.985 \exp(\delta E_f/kT))/\chi \qquad (7.23)$$

for $\chi = -1.23 \times 10^9$ dynes/cm^2, and by

$$\Pi = (1 - 0.97 \exp(\delta E_f/kT))/\chi \qquad (7.23)$$

for $\chi = -2.46 \times 10^9$ dynes/cm^2. The theoretical expression for <111> piezoresistivity is

$$\Pi = (1 - \exp(\delta E_f/kT))/\chi \ . \qquad (7.24)$$

Any slight misorientation of CZ12B off the <111> direction would require modification of the theoretical expression for piezoresistivity (equation 7.24), and could account for the factor multiplying $\exp(\delta E_f/kT)$ in equations 7.22 and 7.23.

Equation 5.54 was curvefitted to the experimental piezoresistivity, for $\chi = -2.5 \times 10^9$ dynes/cm^2, of sample CZ17A in the following way. The values of r_ℓ and r_t in equation 5.54 were presumed to be given by equations 7.18 and 7.19 respectively. The values of r_ℓ and r_t are essentially determined by the relative shift in energy with stress of the conduction band minima. For a given magnitude of stress, the relative shift in energy for a <110> stress is exactly one-half the relative shift for a <100> stress. Therefore, the r_ℓ and r_t for a <110> stress, $\chi = -2.5 \times 10^9$ dynes/cm^2, should equal the r_ℓ and r_t for <100> stress, for $\chi = -1.25 \times 10^9$ dynes/cm^2. Using equations 7.18 and 7.19 for r_ℓ and r_t in equation 5.54, and using r_t' as the unknown, the following result was obtained by curvefitting

$$r_t' = 0.3044 - (0.1977 \times 10^{-3}/^{\circ}K)\,T \qquad (\chi = -2.5 \times 10^9 \text{ dynes/cm}^2) \ .$$

However, this result is not precisely accurate, since according to this equation $r_t'/r_t = \langle \tau_t' \rangle / \langle \tau_t \rangle$ is less than unity, contrary to the theoretical predictions of chapter 4. The value of r_t'/r_t is about 0.87, and therefore r_t' is not too far off its predicted value. The fit obtained to the piezoresistivity of CZ17A (for $\chi = -2.5 \times 10^9$ dynes/cm^2) with r_t' given by the above equation is indicated in Figure 7.12.

Since the doping concentrations of sample D-1 were not known, no attempts were made to fit theory to the experimental results obtained on this sample.

7.4 Empirically Derived Mobility and Conduction Band Electron Concentration

The conduction band carrier concentration (for zero applied stress), as a function of temperature, was calculated for samples CZ7B, CZ17A, and CZ12B. Equation 7.14, with the appropriate values for N_D, N_A, and N_E for each sample, was used in these calculations. The results are given in Figure 7.16.

Using these calculated values for the conduction band electron concentration, n_{c_o}, the conduction mobility (for zero stress), μ_o, was determined by

$$\mu_o = \frac{1}{q n_{c_o} \rho_o} \quad ,$$

where ρ_o is the experimental resistivity. The results of these computations are given in Figure 7.17.

Two observations may be made from Figure 7.17. First of all, the mobilities of all three irradiated samples differ from the empirically derived mobility of the unirradiated sample CZ4B by at most 10 percent. The second observation is that the mobility of each of the irradiated samples is larger than the mobility of the unirradiated sample. This was unexpected, however this result is consistent with theory if it is assumed that the only ionized scattering centers in the irradiated samples are ionized phosphorus donors,

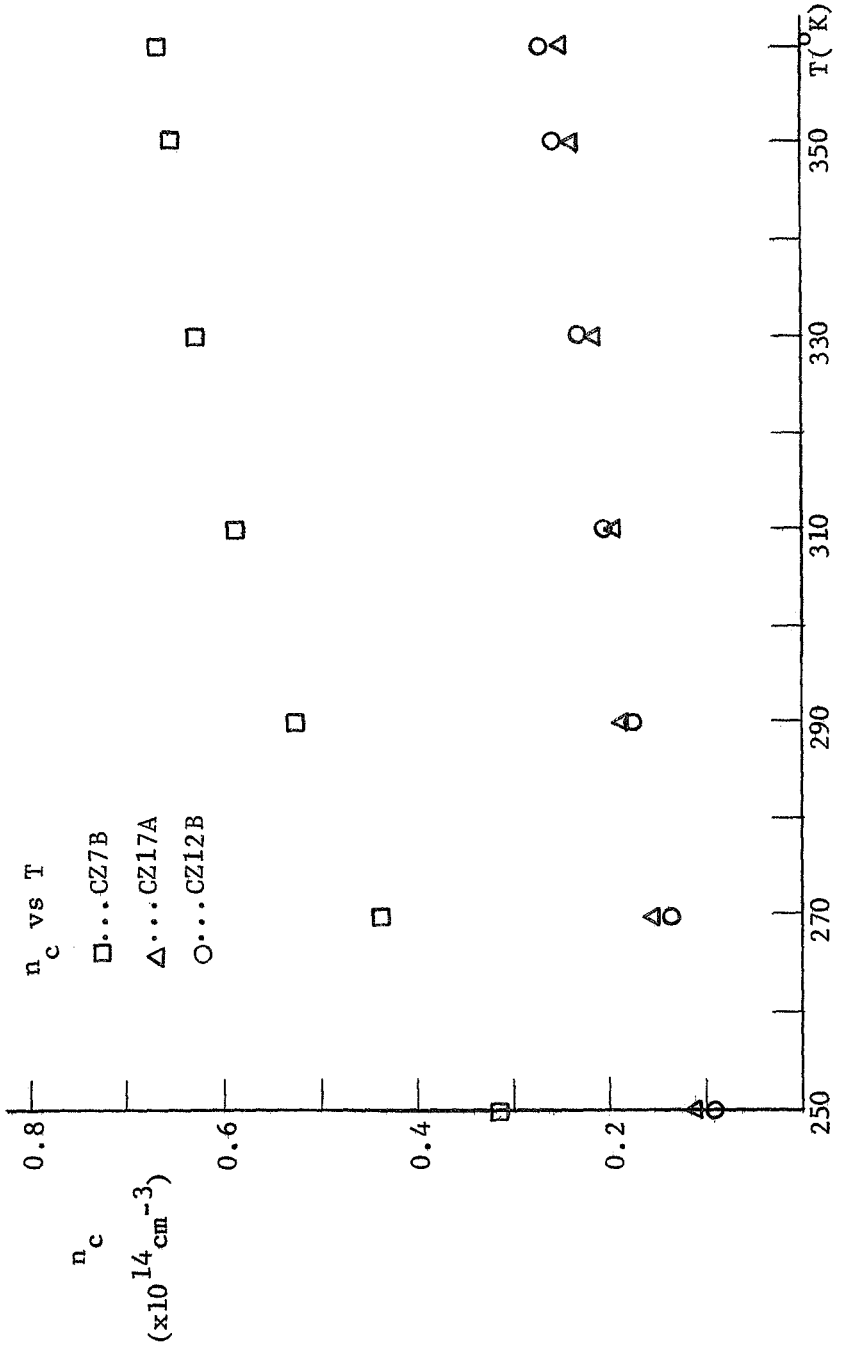

Figure 7.16 Conduction band electron concentration versus temperature for samples CZ7B, CZ12B, and CZ17A

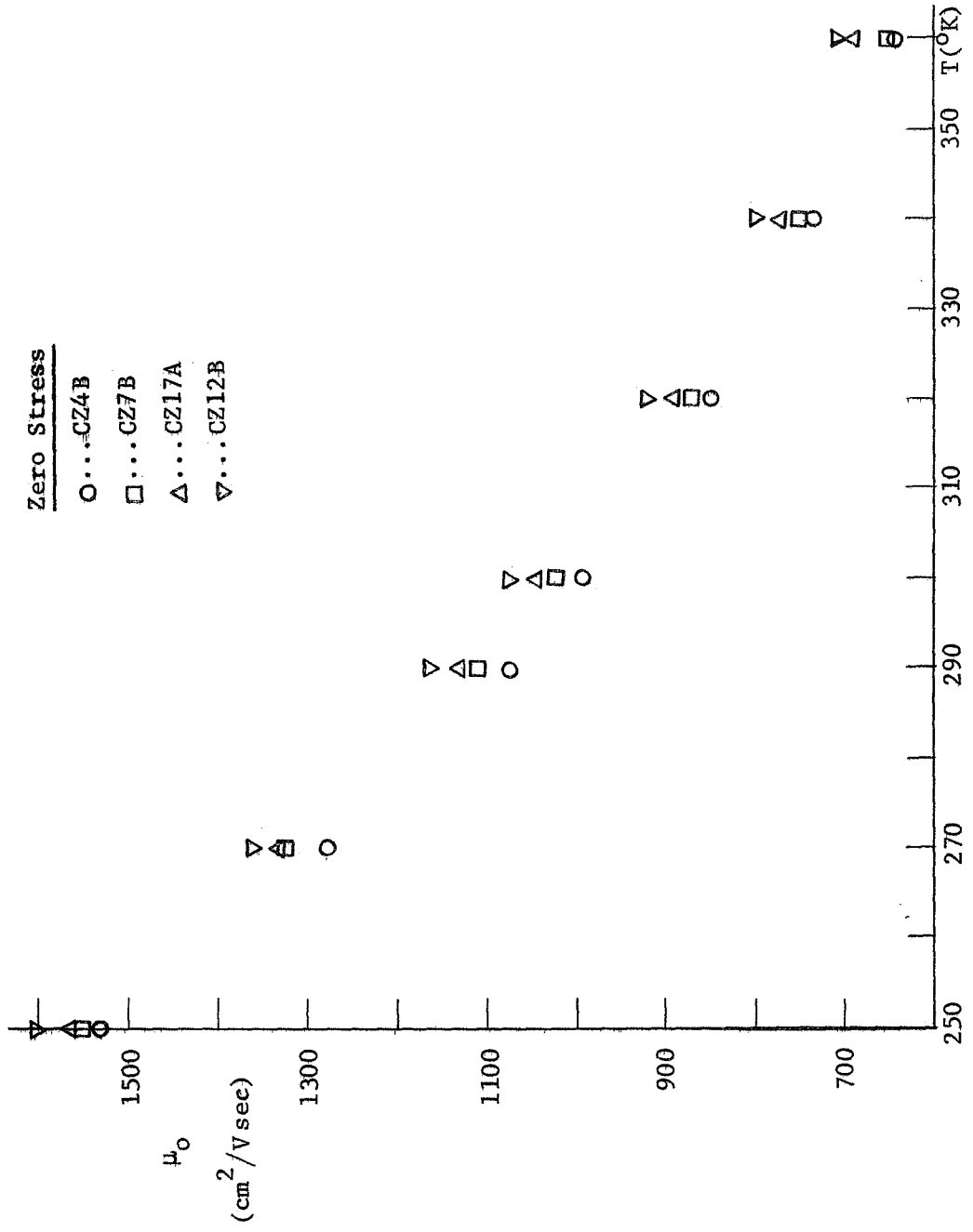

Figure 7.17 Mobility versus temperature for samples CZ4B, CZ7B, CZ12B, and CZ17A

ionized A-center acceptors, and ionized E-center acceptors. For if this hypothesis is true, there are more ionized scattering centers in the unirradiated sample than there are in either of the irradiated samples.

With this hypothesis, the maximum concentration of ionized impurity scattering centers in an irradiated sample is $2N_D$. At very high temperatures, this concentration will decrease to N_D. Comparing the hypothetical maximum ionized impurity concentration of each irradiated sample with the ionized impurity concentration of unirradiated sample CZ4B, we find

$$2N_D = 1.606 \times 10^{15} \text{ cm}^{-3} \qquad \text{(CZ7B)}$$

$$2N_D = 0.882 \times 10^{15} \text{ cm}^{-3} \qquad \text{(CZ17A)}$$

$$2N_D = 0.778 \times 10^{15} \text{ cm}^{-3} \qquad \text{(CZ12B)}$$

$$N_D = 1.72 \times 10^{15} \text{ cm}^{-3} . \qquad \text{(CZ4B)}$$

According to these values, the mobilities of these four samples should obey

$$\mu_o\big|_{CZ12B} > \mu_o\big|_{CZ17A} > \mu_o\big|_{CZ7B} > \mu_o\big|_{CZ4B} ,$$

at any temperature, due to the effect of ionized impurity scattering. This prediction, concerning the relative mobilities of the four samples, is borne out by the results shown in Figure 7.17, lending support to the analysis just presented.

The model for relaxation times proposed by Long (1960) (discussed in chapter 4), was fitted to the mobility of sample CZ4B by a parameter study method. The equations used were

$$\mu_o = \frac{q}{3m_\ell}\left\{ <\tau_{\ell_o}> + 2\,\frac{m_\ell}{m_t}\,<\tau_{t_o}> \right\} \quad , \tag{7.25}$$

with

$$\frac{1}{\tau_{\ell_o,t_o}} = W_{A_{\ell,t}}\left(\frac{T}{T_o}\right)\left(\frac{E}{KT_o}\right)^{\frac{1}{2}} + W_1\left(\frac{T_{c_1}}{T_o}\right)\left\{\frac{((E/KT_{c_1})+1)^{\frac{1}{2}}}{\exp(T_{c_1}/T)-1}\right.$$

$$\left. - \frac{(E/KT_{c_1}-1)^{\frac{1}{2}} \text{ or } 0}{1-\exp(-T_{c_1}/T)}\right\} + W_2\left(\frac{T_{c_2}}{T_o}\right)\left\{\frac{((E/KT_{c_2})+1)^{\frac{1}{2}}}{\exp(T_{c_1}/T)-1}\right.$$

$$\left. - \frac{((E/KT_{c_2})-1)^{\frac{1}{2}} \text{ or } 0}{1-\exp(-T_{c_2}/T)}\right\}$$

$$+ W_{I_{\ell,t}} N_i E^{-3/2}\left\{ \ln(1+2b) - \frac{2b}{1+2b}\right\} . \tag{7.26}$$

In these equations, $T_o = 300^oK$, $T_{c_1} = 190^oK$, $T_{c_2} = 630^oK$, and T is the sample temperature. For a definition of the other quantities in these equations, see chapter 4. Using Long's value (0.67) for $\tau_{A_\ell}/\tau_{A_t} = W_{A_t}/W_{A_\ell}$, the best fit to the mobility of CZ4B was obtained with

$$W_1/W_{A_\ell} = 0.075$$

$$W_2/W_{A_\ell} = 1.8$$

$$W_{I_\ell}/W_{A_\ell} = 0.0001$$

$$W_{I_t}/W_{A_\ell} = 0.0004$$

$$q/(3m_\ell W_{A_\ell}) = 256.1 \ .$$

The theoretical mobility predicted by equation 7.25 using these values is compared to the empirical mobility of sample CZ4B in Figure 7.18.

Although a good fit was obtained to zero stress mobility, this model, with the appropriate modifications (see chapter 4), failed to give results consistent with experimental observations for the stressed mobilities. This might be expected, as the model is a two phonon approximation to the real situation in which seven (or possibly eight) phonons of different energies are involved (see chapter 4). Finally it might be noted that Long's model predicts that

$$K_{T_o} = 0.85$$

at $T = 300^oK$.

7.5 Effect of Electron Irradiation on the Phosphorus Donor Concentration

Shown in Table 7.1 are the preirradiated resistivities, sample resistances, as well as the concentration of phosphorus donors before and after electron irradiation for samples CZ4B, CZ7B, CZ17A, and CA12B. The resistivities in this table were computed from the formula

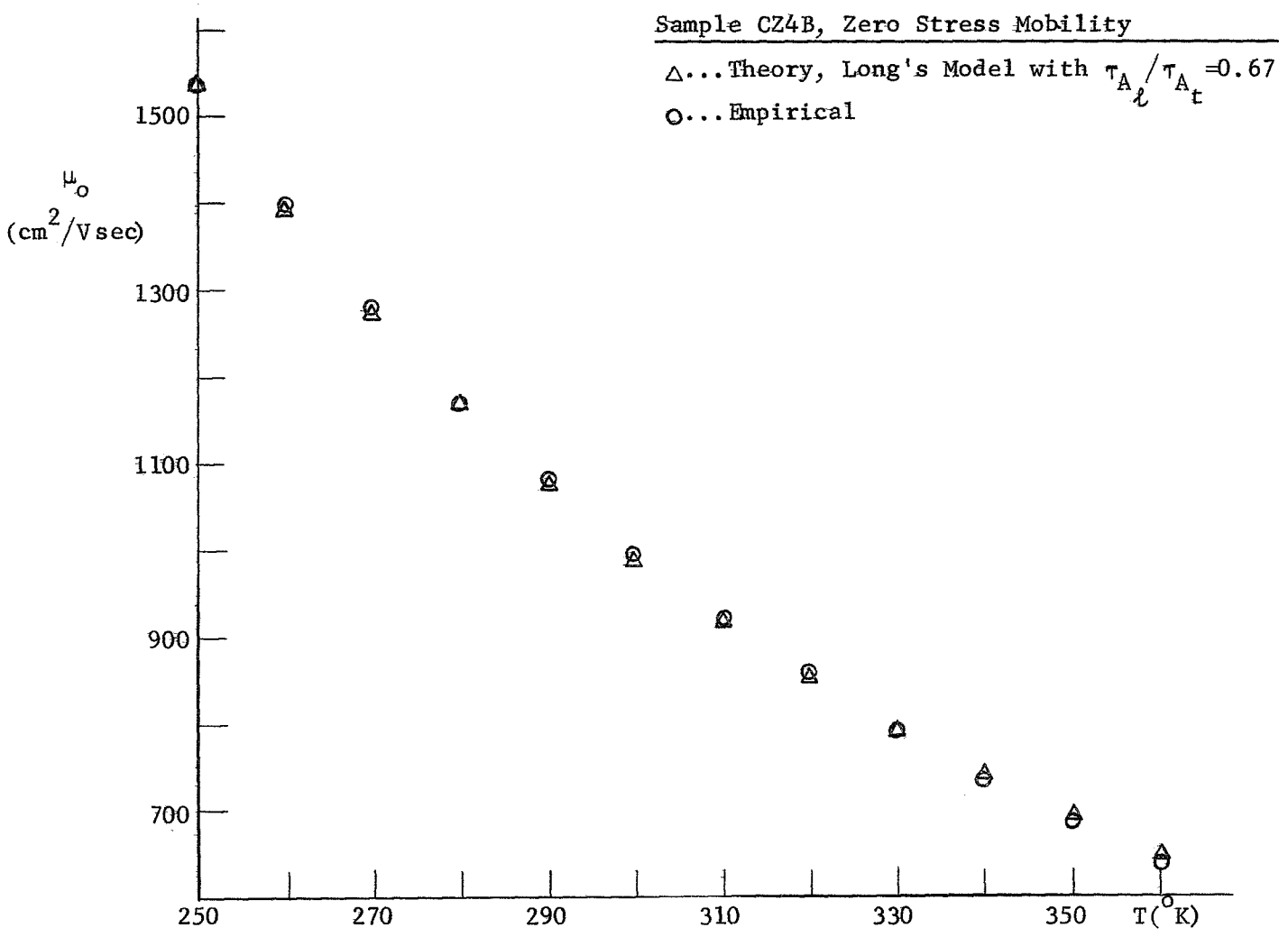

Figure 7.18 Zero stress mobility of sample CZ4B

Table 7.1 Effect of irradiation on the donor concentration

Sample	Before Electron Irradiation			After Electron Irradiation and Annealing	
	$\rho(300^{o}K)$	$R_{sample}(300^{o}K)$	N_D	Radiation Dosage	N_D
	Ωcm	Ω	($x10^{15}cm^{-3}$)	(electrons/cm^2)	($x10^{15}cm^{-3}$
CZ4B	3.7	150	1.73	0	-
CZ12B	3.4	140	1.90	$x10^{16}$	0.39
CZ17A	2.7	108	2.4	$x10^{16}$	0.44
CZ7B	2.3	95	2.7	$x10^{16}$	0.80

$$\rho_{sample} = \rho_{CZ4B} \times \frac{R_{sample}}{R_{CZ4B}} = (3.7\Omega cm) \times \frac{R_{sample}}{150\Omega} \quad ,$$

where the resistivity of sample CZ4B was measured as 3.7 Ωcm at $T = 300^{o}K$, and the room temperature sample resistance (measured between sample current contacts 1 and 2) was 150 Ω. This formula is valid as all samples had the same dimensions, to within less than 5 percent. The room temperature sample resistance of each of the irradiated samples was measured immediately prior to irradiation.

The preirradiated donor concentrations were determined from

$$N_{D_{sample}} = N_{D_{CZ4B}} \times \frac{\rho_{CZ4B}}{\rho_{sample}} = (1.73 \times 10^{15} cm^{-3}) \times \frac{3.7\Omega cm}{\rho_{sample}} \quad ,$$

where N_D for CZ4B was determined directly from Hall coefficient data. This equation implies that the mobilities of the two samples are exactly equal, while this is not precisely accurate. However the values determined in this way are sufficiently accurate for the present analysis.

A study of Table 7.1 reveals that some of the phosphorus donors of each irradiated sample have apparently disappeared after electron irradiation and annealing. Some of these missing phosphorus atoms are accounted for by the concentration of Si-E centers formed by electron irradiation. Each Si-E center has, as a part of its structure (see chapter 3), a phosphorus atom. Then the total concentration of phosphorus atoms that are accounted for, including the ones in the Si-E center complexes, for each irradiated sample is

$$N_D + N_E = 0.91 \times 10^{15} \text{ cm}^{-3} \qquad \text{(CZ7B)}$$

$$N_D + N_E = 0.63 \times 10^{15} \text{ cm}^{-3} \qquad \text{(CZ17A)}$$

$$N_D + N_E = 0.56 \times 10^{15} \text{ cm}^{-3} . \qquad \text{(CZ12B)}$$

According to these results, a very large number of phosphorus atoms are transformed from donors to nondonors by electron irradiation and annealing, assuming that the values deduced for N_D, N_A, and N_E for the irradiated samples are reasonably accurate.

7.6 Summary

Experimental data obtained on four irradiated samples, and one unirradiated sample was presented and analyzed. The resistivity and Hall coefficient as a function of temperature of these samples was discussed first. This was followed by an analysis of the piezoresistivities and electron mobilities of the five samples. Finally data was presented that showed that electron irradiation and annealing apparently have an effect on the phosphorus donor concentration.

8. CONCLUSIONS AND RECOMMENDATIONS FOR FURTHER STUDY

Based on the analysis of experimental results in chapter 7 and the theoretical observations made in chapter 5, several conclusions may be reached concerning the effect of electron irradiation damage on the electrical properties of n-type silicon. The first and most important conclusion is that the donor compensation that is present in electron irradiated samples completely alters the temperature characteristics of both the resistivity and piezoresistivity of these samples. The effect that this irradiation produced donor compensation has on the piezoresistivity of a sample was noted to depend upon radiation dosage and sample orientation.

The experimentally observed resistivities and Hall coefficients were found to be consistent with a model that includes the influence of both the Si-A center and Si-E center on the conduction band electron concentration. In this connection, it must be concluded that the Si-E center was not completely removed by annealing, contrary to the anticipated results.

The comparison of the empirical zero stress mobilities of the irradiated samples with the mobility of the unirradiated sample, cut from the same ingot as the irradiated samples, indicated that these particular irradiated samples all had mobilities larger than the mobility of the unirradiated sample. This surprising result, together with the analysis performed in section 7.5, leads to the conclusion that the mobilities of these samples were slightly enhanced by electron irradiation and annealing. This conclusion is in agreement

with section 7.4, in which the effect of electron irradiation damage on electron mobility is discussed.

During the course of this research, as attempts were made to fit theoretical expressions for piezoresistivity to experimental data, it became clear that the effect of stress on the relaxation times of a conduction electron could not be neglected in analyzing piezoresistivity. This conclusion was borne out by results discussed in section 7.3. Most of these results were consistent with the theoretical observations of chapter 4.

The detailed splitting of the Si-A center acceptor level with stress was also found to be important in determining piezoresistivity, particularly when the Fermi energy is near the Si-A center energy. The Si-A center acceptor level, as described by the model of Watkins and Corbett (1961), was found to be a unique defect due to its behavior in the presence of an applied stress. Watkins' and Corbett's model for the Si-A center gave good agreement to the experimental piezoresistivity results.

Some of the experimental and empirically derived results obtained here require further study to provide confirmation or refutation. One such result is the empirically obtained, apparent decrease in the phosphorus donor concentration with irradiation. The doping parameters of a sample like D-1, that exhibits a piezoresistivity almost independent of temperature, needs to be determined.

The effect of donor compensation on samples of orientations other than the three sample orientations studied here could be examined. The effect of acceptor compensation on the properties of p-type silicon is also a subject for further study.

A further study, both theoretical and experimental, of the effect of stress on the relaxation times of a conduction electron needs to be made. In connection with this, it may be possible to develop a model for the relaxation times, τ_ℓ and τ_t, that includes all seven (or eight) intervalley phonons. The model for the Si-A center, developed by Watkins and Corbett, needs to be extended to the case for which $N_A \sim N_D$, as this is the situation that obtains for a sample exhibiting a piezoresistivity nearly constant with temperature.

9. LIST OF REFERENCES

ASTM Standards. 1969. F76-68 method for measuring Hall mobility in extrinsic semiconductor single crystals. ASTM Standards, Part B, November 1969:719-737.

Aubrey, J. E., W. Gubler, T. Henningsen, and S. H. Koenig. 1963. Piezoresistance and piezo-Hall-effect in n-type silicon. Phys. Rev. 130:1667-1670.

Ballhausen, C. J. and H. B. Gray. 1964. Molecular Orbital Theory. W. A. Benjamin, Inc., New York, New York.

Balslev, I. 1966. Influence of uniaxial stress on the indirect absorption edge in silicon and germanium. Phys. Rev. 143: 636-647.

Bemski, G., G. Feher and E. Gere. 1958. Spin resonance in electron irradiated silicon. Bull. Am. Phys. Soc. 3:135.

Brockhouse, B. N. 1959. Lattice vibrations in silicon and germanium. Phys. Rev. Letters 2:256-258.

Corbett, J. W. 1966. Electron Radiation Damage in Semiconductors and Metals. Academic Press, New York, New York, and London, England.

Cresswell, M. W. and D. R. Muss. 1967. Effects of uniaxial stress on silicon and germanium. Document No. AD816146, Defense Documentation Center, Cameron Station, Alexandria, Virginia.

Fritzsche, H. 1959. Piezoresistance of n-type germanium. Phys. Rev. 115:336-345.

Gross, C. 1967. A radiation method of improving the temperature characteristics of silicon semiconductor strain gages. 22nd Annual ISA Conference Proceedings, Vol. 22, Part 2.

Hall, John J. 1967. Electronic effects in the elastic constants of n-type silicon. Phys. Rev. 161:756-761.

Ham, Frank S. 1955. Ionized impurity scattering in semiconductors. Phys. Rev. 100:1251.

Herring, Conyers. 1955. Transport properties of a many-valley semiconductor. The Bell System Technical Journal 34:237-290.

Herring, Conyers and Erich Vogt. 1956. Transport and deformation potential theory for many-valley semiconductors with anisotropic scattering. Phys. Rev. 101:944-961.

Hill, D. E. 1959. Electron bombardment of silicon. Phys. Rev. 114: 1414-1420.

Ito, R., H. Kawamura and M. Fukai. 1964. Anisotropic phonon scattering of electrons in germanium and silicon. Phys. Letters 13: 26-27.

Kanda, Yozo. 1967. Effect of stress on germanium and silicon p-n junctions. Jap. J. Appl. Phys. 4:475-486.

Kleimnan, L. 1962. Deformation potentials in silicon. I. Uniaxial strain. Phys. Rev. 128:2614-2621.

Long, Donald. 1960. Scattering of conduction electrons by lattice vibrations in silicon. Phys. Rev. 120:2024-2032.

Long, Donald and John Myers. 1959. Hall effect and impurity levels in phosphorus-doped silicon. Phys. Rev. 115:1119-1121.

Long, Donald and John Myers. 1960. Scattering anisotropies in n-type silicon. Phys. Rev. 120:39-44.

Ludwig, G. W. and R. L. Watters. 1956. Drift and conductivity mobility in silicon. Phys. Rev. 101:1699-1701.

Marquardt, D. W. 1963. An algorithm for least-squares estimation of nonlinear parameters. J. Soc. Indust. Appl. Math. 11:431-441.

Morin, F. J., T. H. Geballe and C. Herring. 1957. Temperature dependence of the piezoresistance of high-purity silicon and germanium. Phys. Rev. 105:525-539.

Price, P. J. 1956. Theory of transport effects in semiconductors: thermoelectricity. Phys. Rev. 104:1223-1239.

Rauch, C. J., J. J. Stickler, H. J. Zeigler and G. S. Heller. 1960. Millimeter cyclotron resonance in silicon. Phys. Rev. Letters 4:64-66.

Smith, C. S. 1954. Piezoresistance in silicon and germanium. Phys. Rev. 92:42-49.

Sullivan, N. V. and J. H. Eigler. 1957. Electroless nickel plating for making ohmic contacts to silicon. J. Electrochem. Soc. 104(4):226-229.

Wang, Shyh. 1966. Solid State Electronics. McGraw-Hill, New York, New York.

Watkins, G. D. and J. W. Corbett. 1961. Defects in silicon. I. Electron spin resonance of the silicon A center. Phys. Rev. 121:1001-1014.

Watkins, G. D. and J. W. Corbett. 1964. Defects in irradiated silicon: electron paramagnetic resonance and electron-nuclear double resonance of the Si-E center. Phys. Rev. 134:A1359-A1377.

Watkins, G. D., J. W. Corbett and R. M. Walker. 1959. Spin resonance in electron irradiated silicon at low temperatures. Bull. Am. Phys. Soc. 4:159.

Wertheim, G. K. 1957. Energy levels in electron-bombarded silicon. Phys. Rev. 105:1730-1735.

Wortman, J. J. 1964. Effect of mechanical strain on p-n junctions. Unpublished PhD thesis, Department of Electrical Engineering, Duke University, Durham, N. C. University Microfilms, Ann Arbor, Michigan.

Wortman, J. J. and R. A. Evans. 1965. Young's modulus, shear modulus, and Poisson's ratio in silicon and germanium. J. Appl. Phys. 36:153-156.

10. APPENDICES

10.1 Calculation of the Stress-Induced Energy Shifts of the Conduction Band Minima of Silicon for <100>, <110>, and <111> Applied Stresses

Hooke's law states that strain is directly proportional to stress for small deformations. The statement of this law for silicon has the form

$$\begin{bmatrix} e_1 \\ e_2 \\ e_3 \\ e_4 \\ e_5 \\ e_6 \end{bmatrix} = \begin{bmatrix} s_{11} & s_{12} & s_{12} & 0 & 0 & 0 \\ s_{12} & s_{11} & s_{12} & 0 & 0 & 0 \\ s_{12} & s_{12} & s_{11} & 0 & 0 & 0 \\ 0 & 0 & 0 & s_{44} & 0 & 0 \\ 0 & 0 & 0 & 0 & s_{44} & 0 \\ 0 & 0 & 0 & 0 & 0 & s_{44} \end{bmatrix} \begin{bmatrix} \sigma_1 \\ \sigma_2 \\ \sigma_3 \\ \sigma_4 \\ \sigma_5 \\ \sigma_6 \end{bmatrix} \tag{10.1}$$

when the strains and stresses are referred to silicon's crystal axes. The strain components, e_j, are related to conventional strains by

$$e_1 = e_{xx} \qquad e_4 = e_{yz}$$

$$e_2 = e_{yy} \qquad e_5 = e_{xz}$$

$$e_3 = e_{zz} \qquad e_6 = e_{xy} \ ,$$

with similar relations defining the stresses, σ_1, σ_2, etc. in terms of σ_{xx}, σ_{yy}, etc. The quantities s_{11}, s_{12}, and s_{44} are the elastic

compliance coefficients of silicon and have the values (see Wortman and Evans (1965))

$$s_{11} = 0.768 \times 10^{-12} \text{cm}^2/\text{dyne}$$

$$s_{12} = -0.214 \times 10^{-12} \text{cm}^2/\text{dyne}$$

$$s_{44} = 1.26 \times 10^{-12} \text{cm}^2/\text{dyne} \ .$$

The matrix of compliance coefficients, $[s_{jk}]$, has the simple form shown in equation 10.1 due to the restrictions imposed on the components of this matrix by the cubic symmetry of silicon's lattice structure.

For a stress of a general orientation, it is convenient to refer this stress to a new set of orthogonal axes, x', y', z' in which all the shear stresses are zero. It is found that it is always possible to find such a reference. The new reference is related to the crystal axes, x, y, z, by

$$\begin{bmatrix} x \\ y \\ z \end{bmatrix} = \begin{bmatrix} a_{11} & a_{12} & a_{13} \\ a_{21} & a_{22} & a_{23} \\ a_{31} & a_{32} & a_{33} \end{bmatrix} \begin{bmatrix} x' \\ y' \\ z' \end{bmatrix} \qquad (10.2)$$

where the a_{ij} are the direction cosines, e.g., a_{13} is the cosine of the angle between x and z'. Call the stress components in the x', y', z' system σ_1', σ_2', and σ_3'. Then in the x, y, z system the stresses may be written as

$$\sigma_1 = \sigma_1' a_{11}^2 + \sigma_2' a_{21}^2 + \sigma_3' a_{31}^2$$

$$\sigma_2 = \sigma_1' a_{12}^2 + \sigma_2' a_{22}^2 + \sigma_3' a_{32}^2$$

$$\sigma_3 = \sigma_1' a_{13}^2 + \sigma_2' a_{23}^2 + \sigma_3' a_{33}^2$$

$$\sigma_4 = \sigma_1' a_{12} a_{13} + \sigma_2' a_{22} a_{23} + \sigma_3' a_{32} a_{33}$$

$$\sigma_5 = \sigma_1' a_{11} a_{13} + \sigma_2' a_{21} a_{23} + \sigma_3' a_{31} a_{33}$$

$$\sigma_6 = \sigma_1' a_{11} a_{12} + \sigma_2' a_{21} a_{22} + \sigma_3' a_{31} a_{32} \quad .$$

These equations will now be used to compute the strains for $<100>$, $<110>$, and $<111>$ applied stresses.

First consider a $<100>$ applied stress χ. For this stress x', y', z' is x, y, z, and $\sigma' = \sigma_1 = \chi$, $\sigma_2 = \sigma_3 = \sigma_4 = \sigma_5 = \sigma_6 = 0$. Then from equation 10.1

$$e_1 = s_{11}\chi$$

$$e_2 = s_{12}\chi$$

$$e_3 = s_{12}\chi$$

and $e_4 = e_5 = e_6 = 0$. From equation 3.3, the energy shifts of valleys 1, 2, and 3 are

$$\Delta E_1 = \Xi_u e_1 = \Xi_u s_{11}\chi$$

$$\Delta E_2 = \Xi_u e_2 = \Xi_u s_{12}\chi$$

$$\Delta E_3 = \Xi_u e_3 = \Xi_u s_{12}\chi \, .$$

Thus the valley 1 (on the x axis) shifts by $\Xi_u s_{11} X$, while the valleys 2 and 3 (on axes y and z perpendicular to the stress X) both shift by an amount $\Xi_u s_{12} X$.

For a <110> stress X, the matrix of direction cosines has the components

$$\begin{bmatrix} \frac{1}{\sqrt{2}} & -\frac{1}{\sqrt{2}} & 0 \\ \frac{1}{\sqrt{2}} & \frac{1}{\sqrt{2}} & 0 \\ 0 & 0 & 1 \end{bmatrix}$$

It is found that

$$\sigma_1 = \sigma_2 = \sigma_6 = X/2$$

$$\sigma_3 = \sigma_4 = \sigma_5 = 0 \ ,$$

and it follows that

$$e_1 = e_2 = (s_{11} + s_{12})\ X/2$$

$$e_3 = s_{12} X$$

$$e_4 = e_5 = 0$$

$$e_6 = s_{44}\ X/2 \ .$$

Then for a <110> stress

$$\Delta E_1 = \Delta E_2 = \Xi_u(s_{11} + s_{12})\ X/2$$

$$\Delta E_3 = \Xi_u s_{12}\ X$$

For a <111> stress X, it is found that

$$e_1 = e_2 = e_3 = (s_{11} + 2s_{12})\ X/3$$

$$e_4 = e_5 = e_6 = s_{44}\ X/3\ ,$$

so that all valleys are shifted by an equal amount

$$\Delta E = \Xi_u(s_{11} + 2s_{12})\ X/3$$

by a <111> stress. Since only relative shifts in the valley energies are presumed to be important here, for a <111> stress

$$\Delta E_1 = \Delta E_2 = \Delta E_3 = 0$$

was used in this work.

The equations presented in this section may be used to calculate the strains and conduction band energy shifts resulting from an applied stress of any orientation.

10.2 Single Valley Mobility in a General Lattice Direction

Consider Figure 10.1. Illustrated in this figure is a constant energy surface of a conduction band minimum in silicon. Referred to the coordinate axes (x_1, x_2, and x_3) shown in this figure, the mobility tensor of this particular conduction band minimum is

$$\bar{\bar{\mu}} = \begin{bmatrix} \mu_\ell & 0 & 0 \\ 0 & \mu_t & 0 \\ 0 & 0 & \mu_t \end{bmatrix} , \qquad (10.3)$$

where $\mu_\ell = q \frac{\langle \tau_\ell \rangle}{m_\ell}$, and $\mu_t = \frac{q \langle \tau_t \rangle}{m_t}$. In direction x_1, the electrons in this minimum have a mobility μ_ℓ, while in directions x_2 and x_3 they have a mobility μ_t.

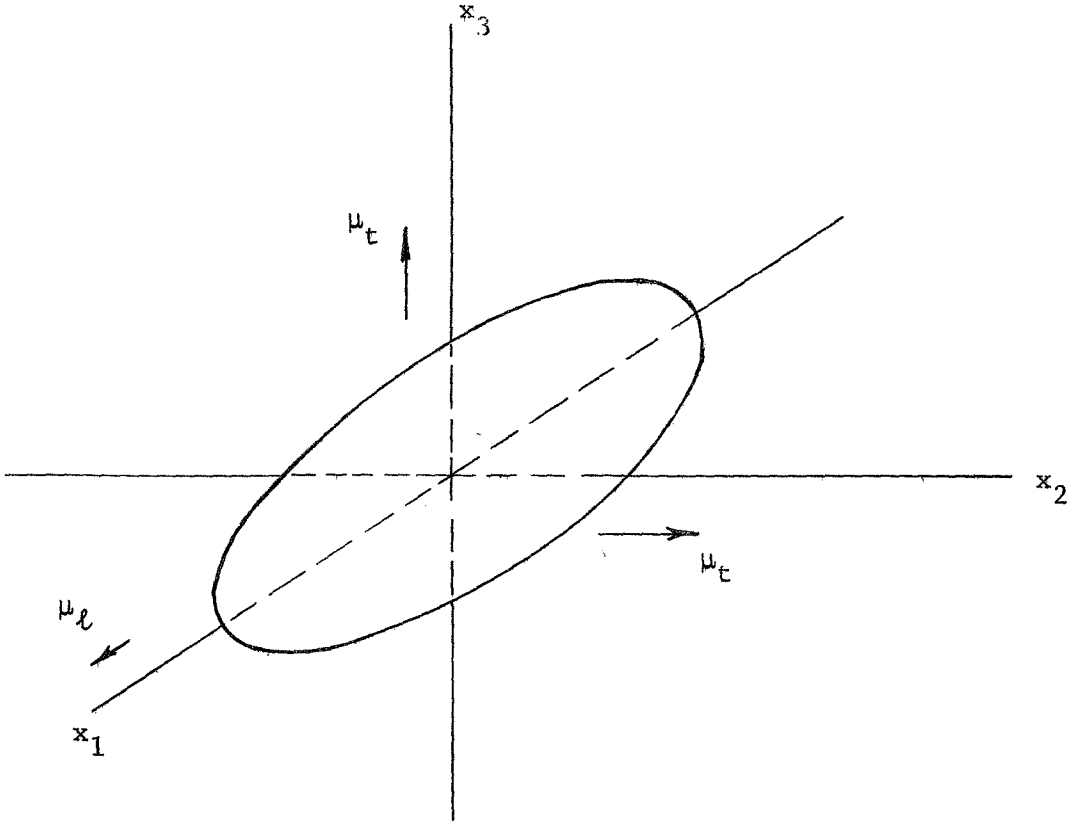

Figure 10.1 Constant energy surface for a conduction band minimum

For mobilities in directions other than the 1, 2, or 3 directions in Figure 10.1, say in the 1', 2', and 3' directions, the mobility tensor must be transformed by

$$\bar{\bar{\mu}}' = \bar{\bar{A}}\ \bar{\bar{\mu}}\ (\bar{\bar{A}})^{-1} \ , \tag{10.4}$$

where A defines the transformation from the unprimed to primed coordinates

$$\vec{r} = \bar{\bar{A}}\ \vec{r}' \ . \tag{10.5}$$

Figure 10.2 shows the three nonequivalent minima of silicon, each with its particular coordinate system. Also shown in this figure are the coordinate axes of a sample of a general orientation. Let x_1^s be the longitudinal axis of the sample. In the formulation of the (longitudinal) piezoresistivity of a sample of this orientation, it is necessary to know the mobility of the electrons in each of the three conduction band minima in the direction x_1^s. These mobilities may be calculated in terms of μ_ℓ and μ_t by equation 10.4.

For the case of a $<110>$ stress, the mobility of the electrons in conduction band minimum 1 in the direction, x_1^s of the applied stress is found to be

$$\mu^{(1)} = \frac{\mu_\ell + \mu_t'}{2} = \frac{q}{2}\left\{\frac{<\tau_\ell>}{m_\ell} + \frac{<\tau_t'>}{m_t}\right\} \ . \tag{10.6}$$

While for minima 2 and 3

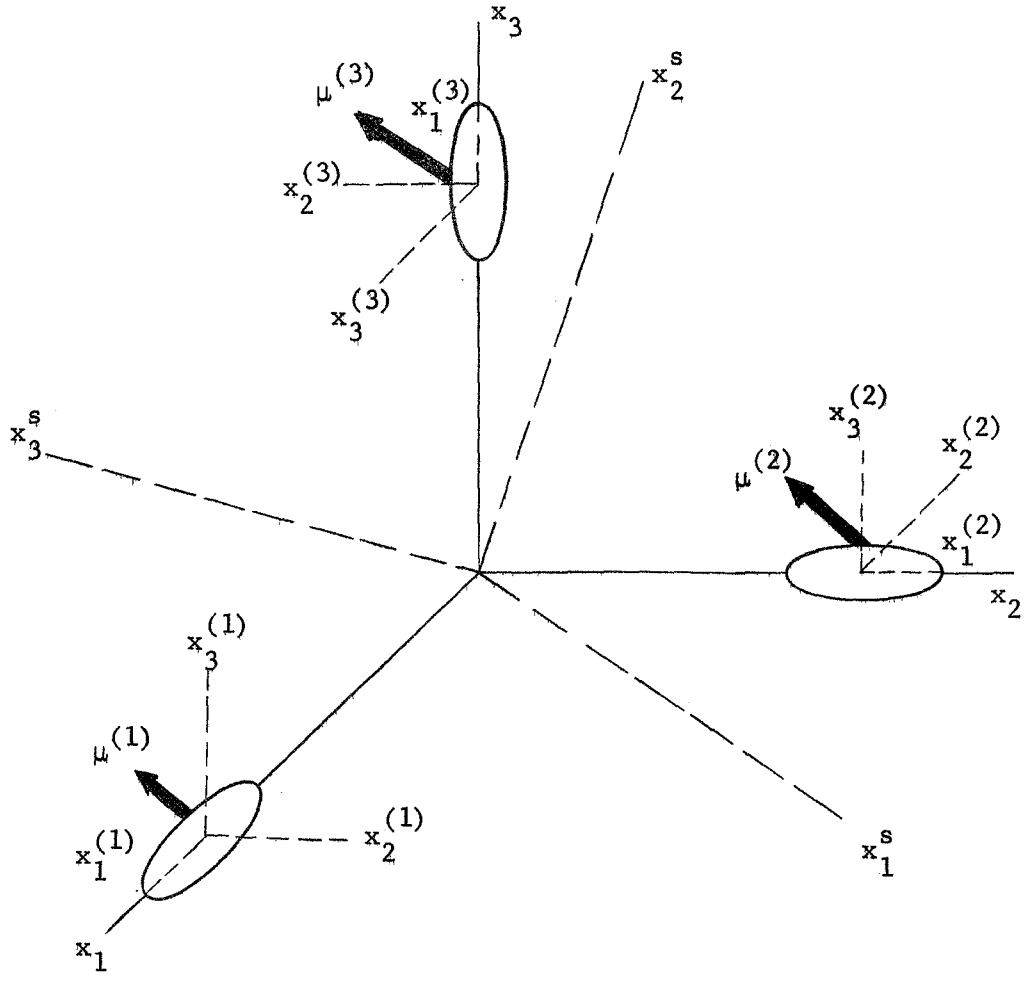

Figure 10.2 The individual coordinate systems of the three nonequivalent conduction band minima of silicon

$$\mu^{(2)} = \frac{\mu_\ell + \mu_t'}{2} = \frac{q}{2}\left\{\frac{\langle \tau_\ell \rangle}{m_\ell} + \frac{\langle \tau_t' \rangle}{m_t}\right\} \tag{10.7}$$

$$\mu^{(3)} = \mu_t = \frac{q\langle \tau_t \rangle}{m_t} \tag{10.8}$$

The prime on the μ_t' of minima 1 and 2 is necessary to distinguish this mobility from the μ_t of minimum 3. As is pointed out in chapter 4, for a $<110>$ stress, τ_t' of minima 1 and 2 differs from the τ_t of minimum 3 due to a difference in intervalley scattering rates.

10.3 Extraction of Values for N_D, N_A, and N_E from Hall Coefficient Data

Assume that the curve shown in Figure 10.3 represents experimental Hall coefficient versus temperature data. Values for N_D, N_A, and N_E may be determined accurately from this curve if the value of the Hall factor r, as a function of temperature, is known.

The Hall coefficient for zero stress, $R_H^{(o)}$, is related to the total conduction band electron concentration, n_c, by

$$R_H^{(o)} = -\frac{r}{qn_c} \quad . \tag{10.9}$$

The value used here for r is

$$r = 0.83 + (0.0011/^oK)\ T \ , \tag{10.10}$$

which was determined from the Hall coefficient data of sample CZ4B.

Choose three points on the $R_H^{(o)}$ versus T curve. Then for point (1)

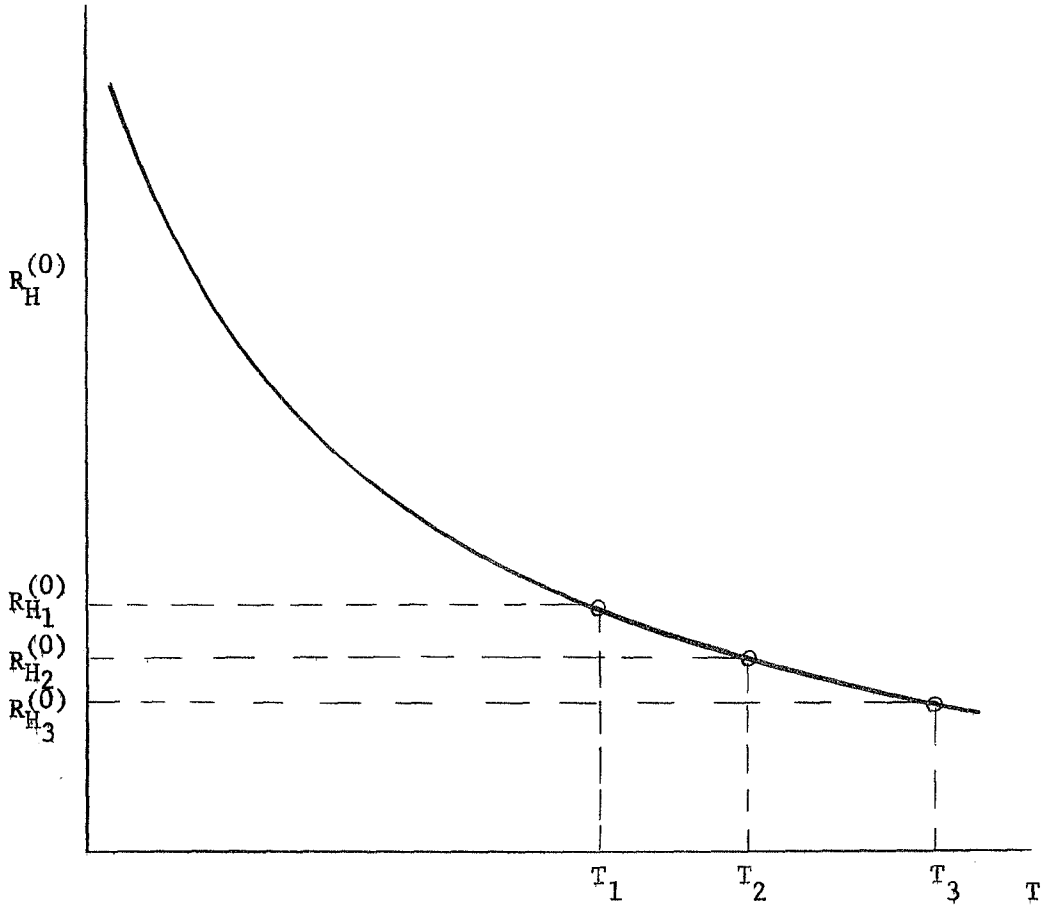

Figure 10.3 Zero stress Hall coefficient versus temperature

$$n_{c_1} = N_{c_1} \exp(E_{f_1}/kT_1) = -\frac{r_1}{qR_{H_1}^{(o)}} \tag{10.11}$$

and

$$n_{c_1} = N_D - \frac{N_A}{1 + 2\exp(-.17\text{eV}/kT_1)\exp(-E_{f_1}/kT_1)}$$

$$- \frac{N_E}{1 + \exp(-.40\text{eV}/kT_1)\exp(-E_{f_1}/kT_1)} \quad . \tag{10.12}$$

The quantity N_{c_1} is the effective density of states in the conduction band (assuming Boltzmann statistics describe occupancy of conduction

states) at the temperature T_1 and has the value

$$N_{c_1} = (5.278 \times 10^{15}(^{o}K)^{-3/2}) \times T_1^{3/2} \text{ cm}^{-3} . \qquad (10.13)$$

Now both n_{c_1} and $\exp(-E_{f_1}/kT_1)$ can be determined from equation 10.11. By similar equations n_{c_2}, n_{c_3}, $\exp(-E_{f_2}/kT_2)$, and $\exp(-E_{f_3}/kT_3)$ may be determined from the values of r and $R_H^{(o)}$ at points 2 and 3. Thus the three equations

$$n_{c_1} = N_D - \left[\frac{1}{1 + \alpha_1\lambda_1} \right] N_A - \left[\frac{1}{1 + \eta_1\lambda_1} \right] N_E \qquad (10.14a)$$

$$n_{c_2} = N_D - \left[\frac{1}{1 + \alpha_2\lambda_2} \right] N_A - \left[\frac{1}{1 + \eta_2\lambda_2} \right] N_E \qquad (10.14b)$$

$$n_{c_3} = N_D - \left[\frac{1}{1 + \alpha_3\lambda_3} \right] N_A - \left[\frac{1}{1 + \eta_3\lambda_3} \right] N_E \qquad (10.14c)$$

may be written, where

$$\alpha_i = 2 \exp(-.17 \text{ eV}/kT_i) \qquad (i = 1,2,3)$$

$$\lambda_i = \exp(-E_{f_1}/kT_i) \qquad (i = 1,2,3)$$

$$\eta_i = \exp(-.40\text{eV}/kT_i) , \qquad (i = 1,2,3)$$

where k is Boltzmann's constant and has the value 8.616×10^{-5} eV/^{o}K. Equations 10.14 are three equations in three unknowns, since n_{c_1}, n_{c_2}, n_{c_3}, as well as the coefficients of N_A and N_E in each equation are known. Solution of these equations yields the values of N_D, N_A, and N_E.